University of Stavanger

Faculty of Science and Technology

MASTER'S THESIS

Study program/ Specialization: Offshore Technology-Subsea and Marine technology	Spring semester, 2015 **<u>Open</u>** / Restricted access
Writer: **Jarand Hornseth Pollestad**	…… (Writer's signature)
Faculty supervisor: **Ove Tobias Gudmestad**	
Thesis title: **Investigation of Suction Anchor Pullout Capacity under Undrained Conditions**	
Credits (ECTS):30	
Key words: Suction anchor. Undrained conditions. Pullout capacity. Failure mechanism.	Pages: 109 + enclosure: 5 Stavanger, 15.06.2015 Date/year

Investigation of Suction Anchor Pullout Capacity under Undrained Conditions

Jarand Hornseth Pollestad

This dissertation is submitted for the degree of

Master of Science

June 2015

I would like to dedicate this thesis to my loving parents ...

Acknowledgements

And I would like to acknowledge professor Ove Tobias Gudmestad at the University of Stavanger for suggesting the thesis topic and providing guidance and support during the writing.

This thesis has been written as a finalisation of my master's degree in offshore technology with specialisation in marine-and subsea technology. The work related to this thesis has been done in the spring semester of 2015.

Abstract

Floating units are dependent on reliable mooring systems to ensure safety during marine operations. Suction anchors have proved to be a technologically viable and cost-effective concept. They are capable of precision installation, re-use, and provide large resistive capacity. This thesis investigates load capacity and failure modes of suction anchors subjected to vertical, horizontal (lateral), and incline loading. Suction anchor design considerations, installation procedure, and associated challenges are discussed before reviewing analytical methods for calculating holding / pullout capacity. Analytical results are compared with solutions obtained from finite element analyses conducted with PLAXIS 2D. A Mohr-Coulomb failure envelope with undrained total stress parameters was used. The thesis is limited to loading conditions in undrained soil with a linear strength development. The soil characteristics correspond to clay in the Troll field, North Sea. Finite element analyses indicate that vertical loading of suction anchors in undrained soil will result in a reverse end bearing failure. They also indicate that the horizontal holding capacity is primarily a function of caisson vertical cross-sectional area and the soil strength profile. It was found that the mooring line attachment point greatly impacts the capacity of suction anchors in all load cases investigated.

Table of contents

List of figures

List of tables

Chapter 1

Introduction

1.1 Background

Global consumption of oil and gas retain a large share of the worlds primary energy consumption. To satisfy the demand it is necessary to expand our resource base by conducting petroleum exploration-and production in increasingly deeper water. At certain depths fixed structures are neither technologically nor economically feasible. The use of floating units are prevalent in these situations. Floating units vary considerably in configuration. Design is directed by the need to meet functional requirements while staying within the project schedule and the cost limitations necessary to achieve satisfactory project economics, i.e. a positive return on the investments. The common denominator for floating units is the need for cost effective and reliable station keeping. To ensure safe operation it is desirable to employ reliable mooring systems. These mooring systems have to resist uplift and large lateral forces created by displacement of the structure. They will also have to withstand cyclic loading through the entire life cycle of the project.

The use of suction anchors for mooring applications have gained widespread use in the last few decades. It is a flexible concept which can be modified to provide large holding capacities against vertical, horizontal, and incline loads. Suction anchors have been proved cost efficient and reliable through use in major offshore developments in Brazil, North Sea, Norwegian Sea, Gulf of Mexico, West Africa and west of Shetland.

1.2 Thesis objectives

- Analyse vertical, horizontal, and incline capacities of suction anchors in undrained clay using the finite element method
- Evaluate the use of the Mohr-Coulomb model with total stress parameters against established analytical methods
- Assess how the aspect ratio (length to diameter ratio) of the suction anchor caisson affect anchor capacity
- Assess how mooring line connection point (padeye location) affect anchor capacity
- Study the development of stress and failure mechanism during vertical, horizontal, and incline loading of suction anchors

1.3 Organization of thesis

This thesis is composed of 9 chapters. A brief outline of each chapter is given below:

Chapter 2 contains a description of mooring systems, commonly used anchor types in marine operations, and field experiences with suction anchors.

Chapter 3 outlines suction anchor design considerations. This includes suction anchor design loads, functional requirements, engineering activities, and geometry.

Chapter 4 describes the suction anchor installation procedure. There is also discussion of resistive forces and limiting factors.

Chapter 5 is a study of established analytical methods for calculating vertical, horizontal, and incline capacity of suction anchors.

Chapter 6 contains a description of the finite element model, the selected soil parameters, and the failure criterion used to determine maximum holding / pullout capacity.

Chapter 7 presents the results obtained with finite element analysis. This includes maximum holding / pullout capacities against vertical, horizontal, and incline loading, as well as the development of stresses and failure mechanisms during loading.

Chapter 8 evaluates the results. A parameter analysis is done to investigate uncertainties.

Chapter 9 describes the primary findings and suggestions for future work.

1.4 Limitations of thesis

The soil is modelled with undrained total stress parameters. This was done to prevent overestimation of shear strength in the Mohr-Coulomb model. However, this results in no excess pore water pressure being generated, and therefore no distinction can be made between excess pore water pressures and effective stresses.

The suction anchor caisson is modelled into the soil, or "wished in place". The initial stresses that are created during installation is therefore not considered. It can be compared to assuming that the remoulded soil has regained its full strength.

The caisson geometry is simplified. It is modelled as a hollow cylinder open in one end. In reality there are protrusions, e.g. padeye and stiffeners, which affect operations.

The derived load capacities are with regards to a single static load. Cyclic loads are not taken into consideration.

Chapter 2

Mooring systems

Mooring systems are composed of anchors, mooring lines, fairleads, and winches. The mooring lines are composed of either chains, wires, synthetic fibres, or a combination of these. The arrangement of the lines differ depending on the requirements of the vessel they are keeping in position. The mooring lines are either taut, semi-taut, or catenary.

Catenary mooring lines assume a catenary shape, see figure 2.1, due to its weight and slack suspension. Because of this shape the forces on the anchors are primarily horizontal, and most of the restoring forces are generated by the weight of the mooring line itself as the grounded line is lifted when the vessel is displaced.

Taut mooring lines are pre-tensioned, see figure 2.1, creating a steep angle between the mooring line and the seabed. This results in a far greater vertical load component on the anchor. This configuration allows for more accurate control over vessel displacement, and shorter mooring lines. When the vessel is displaced the restoring forces are governed by the stiffness of the material (Randolph and Gourvenec, 2009). The mooring lines are connected to the anchor embedded in the seabed. Selection of anchor type depends on water depth, soil properties, required load capacity, cost- and availability of installation equipment.

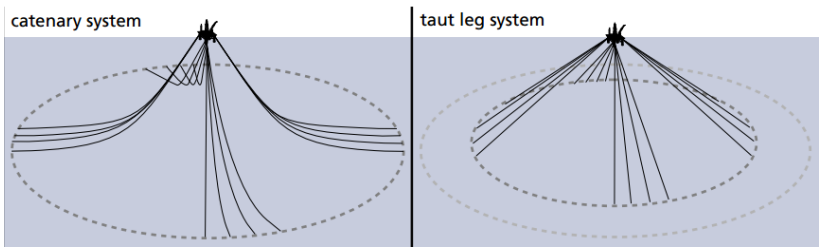

Fig. 2.1 Catenary-and taut mooring line configuration, Vryhof Anchors B.V. (2010)

2.1 Anchor types

2.1.1 Surface gravity anchors

These anchors are located on the seabed and resistance against uplift and lateral displacement is created by the weight of the anchor and friction forces against the seabed. An example is a box anchor, see figure 2.2, which is a container filled with some heavy material, typically rocks. One limitation of surface gravity anchors is that their size must be massive to provide sufficient holding capacity.

2.1.2 Drag anchors

A drag anchor consists primarily of a shank and a fluke, see figure 2.2. The mooring line is connected to the shank. When the anchor is dragged along the seabed the fluke digs into the soil. This configuration creates a large holding capacity against horizontal loads.

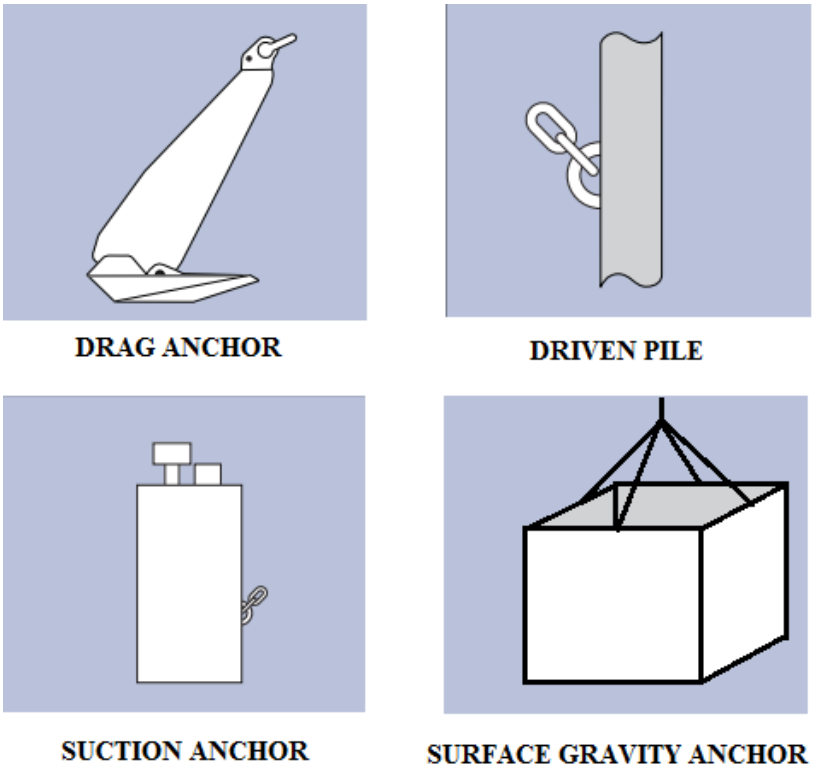

Fig. 2.2 Commonly used anchor types, Vryhof Anchors B.V. (2010)

2.1.3 Driven piles

These are cylindrical and hollow steel pipes with a large length to diameter ratio, see figure 2.2. They are drilled or driven into the seabed. The holding capacity of driven piles is generated by friction forces along the length of the pile, and soil resistance. Installing piles require specialised vessels and is complicated at large depths.

2.1.4 Dynamically penetrating anchors

These are torpedo or rocket shaped anchors lowered to a specified distance above seabed by an installation vessel. When the position is acceptable the anchor is released. It obtains a speed of 25-35 m/s before penetrating the seabed and embedding itself to depths of two or three times the anchor length (Randolph and Gourvenec, 2009).

Suction anchors

A suction anchor is a cylindrical and hollow steel segment (reinforced concrete in some instances) open at the bottom and closed at the top with a mooring line attached, see figure 2.2. In this thesis the word caisson, or suction caisson, refers to the cylindrical segment, and suction anchor refers to a caisson with a mooring line attached. The mooring line is connected to a padeye. It is critical that the padeye is located at a depth where overturning of the caisson during lateral loading can be avoided.

A suction anchor has a smaller length to diameter ratio than the driven pile. The installation procedure consists of two main steps. First, the anchor is lowered down to the correct location where the initial seabed penetration is caused by the self-weight of the caisson. Secondly, water is pumped out from the top of the caisson. By pumping out water a differential pressure is created between the pressure within the caisson and the surrounding hydrostatic pressure. The differential pressure creates a net downward force which cause further embedment in the soil.

Suction anchors are able to produce a large amount of holding capacity in horizontal, inclined, and vertical direction. The simple geometry results in low material usage and fabrication cost. Installation is simple and a high degree of accuracy can be obtained with respect to positioning. This makes it possible to use in complex mooring configurations. By reversing the pump it is simple to remove the anchor when necessary.

The suction anchor concept is sensitive to soil conditions. Soil samples from installation location should be collected and analysed prior to installation. The caissons are heavy and large. Multiple trips to shore may be required.

2.2 Field experiences with suction anchors

The first reported experimental study on the feasibility of vacuum anchorage in soil was by Goodman et al. (1961). The purpose was to investigate more efficient anchoring solutions for military equipment than what was provided by conventional solutions.

Hogervorst (1980) conducted full scale testing of suction anchors in the Netherlands at inshore locations with sandy soils, layered soils, and with overconsolidated clays. He found that the self-weight penetration phase provides sufficient sealing for the subsequent suction phase. Installation of piles through suction was found to be feasible.

The first commercial application of suction piles as anchors is reported by Senpere and Auvergne (1982). Twelve large capacity suction anchors were installed in the North Sea. They were designed to anchor two Catenary Anchor Leg Mooring (CALM) buoys in the Gorm field in the Danish sector. It was found that suction anchors are a viable alternative to conventional driven- or drilled piles. One reason for this is that the anchors can be installed using smaller vessels, and because the design can be adapted to a wide range of soil profiles.

Tjelta et al. (1986) reported the installation of a 360 tonnes heavy test unit in the Gullfaks Field, North Sea. The water depth is more than 200 m, and at the time it was the largest offshore soil penetration test ever undertaken. The test unit was composed of two steel suction caissons, both 23 m long and with a diameter of 6,5 m, mounted next to each other. The objective of the test was to observe and analyse soil reactions during installation through suction.

The Snorre tension leg platform (TLP) was the first TLP to use suction anchors (Fines et al., 1991). The mooring system consists of 16 tethers arranged in groups of 4 (1 group in each corner of the TLP). Each group is attached to one suction anchor. This project verified that suction anchors are applicable for the load conditions created by TLPs.

The Europipe 16/11-E (Draupner) jacket platform in the North Sea was the first jacket platform to use suction caissons as foundations instead of the more conventional driven piles (Tjelta, 1994).

It was first in the late 80's and early 90's that the use of suction anchors became a serious contender to conventional anchors. Table 2.1 is an excerpt from Tjelta (2001) listing some of the suction anchors used in mooring systems in the 90's.

A growing interest in using wind as an energy source have initiated investigations for alternatives to the conventional pile- and gravity foundations of offshore wind turbine masts. Even though the wind turbine masts are light they produce large time-varying horizontal loads causing large overturning moments on the foundation. The recent trend of increasing mast sizes will require excessively large pile-and gravity foundations. The low-cost and manageable suction caissons are therefore being investigated as an alternative.

The general experience is that both fabrication- and installation costs are less for suction anchors than for driven piles. The difference may be marginal depending on the market situation (Andersen and Jostad, 1999). The total cost savings associated with the suction anchor solution on the NKossa processing barge was estimated to be around 20 percent of the construction-and installation cost of the whole mooring system.

Table 2.1 Summary of key data for suction anchors used in major permanent mooring systems 1995-2000, Tjelta (2001). Notes: [1] Without top lid, [2] Including ballast, [3] Anchor top 2,5 m below mudline, and [4] Including protruding fins.

Field name	Year	Water depth [m]	Number of anchors	Anchor length [m]	Anchor diameter [m]	Weight [ton]
Nkossa production barge (Elf)	-95	180	14	12,5	4,5-5	40 [1]
Harding FPSO (BP)	-95	110	8	8-10	5	40
YME FPSO (Statoil)	-95	100	8	7	5	40
Nome FPSO (Statoil)	-96	350	12	10	5	-
Balder FPSO (Esso)	-97	350	8	7	5	100 [2]
Njord Semi/FPU (Hydro)	-97	330	20	7-11	5	40
Curlew FPSU (Shell)	-97	90	9	9-12	5-7	60-80
Marlim P-19/26 (Petrobras)	-97	700-1000	32	13	4,7	80 [2]
Schiehallion FPSO (BP)	-97	350	12	12	6,5	130
Visund Semi (Hydro)	-97	350	16	11 [3]	5[4]	50
Lufeng FPSO (Statoil)	-97	-	8	10	5	40
Aquila FPSO (Agip)	-97	850	9	16	5	70
Laminaria FPSO (Woodside)	-98	400	9	13	5,5	-
Marlim P-33/35 (Petrobras)	-98	600	16	17	4,7	75
Åsgard A FPSO (Statoil)	-98	350	12	11	5	-
Troll C Semi (Hydro)	-98	330	16	15	5	70
Åsgard B (Statoil)	-99	350	16	-	-	-
Åsgard C (Statoil)	-99	350	9	-	-	-
Siri (Statoil)	-99	70	1	-	-	-
Diana (Exxon)	-99	1450	12	30,5	6,4	250
Kuito FPSO (Chevron)	-00	430	12	-	-	-

Chapter 3

Suction Anchor Design Considerations

There is no real consensus in the industry today concerning specific design practices for suction anchors. The most promising is perhaps a comprehensive report created in a joint venture between the American Petroleum Institute (API) and DeepStar which was incorporated into API RP-2SK (2005).

The design of suction anchors today depends on the intended use and current best practice: 1. A suction anchor intended for mooring of a TLP must be able to resist large vertical uplift forces; 2. The mooring lines of a floating production unit (FPU) or similar usually has a catenary shape resulting in large inclined-and lateral loads on the anchor; and 3. If the anchors are to serve as foundations they will be subjected to large, compressive forces. The load conditions acting on the suction anchor during operation can be divided into three types (Clukey et al., 1995):

- Permanent (static) forces; These are loads that are applied permanently to the anchor such as pre-tensioning in a TLP tether.
- Low frequency cyclic loads; Oscillatory loads applied over a duration of several hours/days, e.g. mean wind or loop currents displacing the vessel resulting in cyclic loads on the anchors. These loads are sometimes referred to as quasi-static.
- High frequency cyclic loads; Oscillatory loads that are applied within seconds or minutes, e.g. hurricane- or storm wave loads acting upon the vessel thus transferring high frequency loads to the anchors.

Design loads to consider according to Bai and Bai (2010):

- *Maximum loads applied and equilibrated by the soil reactions.*
- *Maximum negative pressure (underpressure) required for pile embedment.*
- *Maximum internal pressure (overpressure) required for pile extraction.*
- *Maximum loads imposed on the pile during lifting, handling, launching, lowering, operation, and recovery.*

ExxonMobil Development Company (2000) lists the following functional requirements as a basis and methodology for the design of suction:

- *Must withstand long-term static and dynamic loading.*
- *Capacities shall be degraded as appropriate for (a) cyclic degradation of soil strength, (b) creep, and (c) pile-soil setup for the initial loading history of the piles.*
- *Analysis shall reflect positioning tolerances for installation.*
- *Suction-installed anchor piles shall be designed for the same in-place suite of global load conditions as the component that it supports.*

ExxonMobil Development Company (2000) also list the engineering activities which they want to be included in the design process:

- *Global sizing of the suction pile based on soil strength properties.*
- *Global sizing of the suction pile to ensure that the pump-in suction pressure is acceptable for the available soil strength (i.e. soil plug stability check).*
- *Global sizing of the suction pile to ensure that the pump-out pressure is acceptable for the available soil strength, in case that anchor removal is necessary.*
- *Structural design for maximum installed loads and soil reactions, including detailed design of the padeye area for the local stresses due to the mooring line loads and the padeye castings.*
- *Structural design for pump-in operation and, if applicable, for pump-out/pull-out operation.*
- *Design of appurtenances and pile top configuration for installation and for recovery.*

3.1 Stiffeners

Suction anchor walls are often no more than 4-5 cm thick. It is therefore necessary to include some external- or internal structure to strengthen the structural integrity of the design. This is usually done with internal ring stiffeners. These reduce the risk of buckling and reinforce the structure around the padeye where the mooring line is connected. Ring stiffeners may influence the anchor installation because the caisson penetration resistance is increased due to the bearing capacity of the rings (Andersen and Jostad, 2004).

According to DNV (2005) it is important during installation to control if the soil deforms back to the walls after passing the stiffeners. Any gaps filled with water will reduce the holding capacity of the anchor. Buckling is not considered a concern in operating conditions because the soil is supporting the structure. However, it is a concern during the installation phase when a differential pressure is created to embed the anchor. Hydrostatic buckling calculations should therefore be performed to verify the design.

3.2 Aspect ratio

The aspect ratio, which is the relationship between the length and the diameter of the caisson (L/d), greatly impacts the capacity of the anchor. There are some general guidelines for selecting aspect ratio depending on soil conditions.

In sand or hard clays it is common to use caissons with a low aspect ratio. This will make it easier to penetrate the resisting soil as well as reduce the amount of suction needed due to the large horizontal cross-sectional area. In very dense sands it is recommended to have an aspect ratio of 1,5 or less (Tjelta, 2001).

In softer clays a caisson with a larger aspect ratio can be used. This is because the soil is easier to penetrate and it is desirable to reach stronger layers of clay (assuming that soil strength increases with depth). The limiting factor for large aspect ratios is penetration refusal caused by large friction forces, and the inflow of displaced soil into the caisson.

3.3 Weight

Depending on the soil conditions it might be necessary to use ballast weight if the submerged weight of the anchor is insufficient to reach a satisfactory embedment depth before the suction phase can commence. In cases where the anchor is principally subjected to lateral loads, which is common in catenary mooring line configurations, the top cap of the suction anchor is sometimes retrieved and possibly reused. The mooring system used at the NKossa field in the Gulf of New Guinea was installed using only two top caps for the fourteen anchors (Colliat et al., 1996). This approach gave large savings in steel. The downside is that removing the top cap complicates retrieval of the anchor.

3.4 Water injection devices

Using ballast or increasing the self-weight of the anchor is not always practical as this demands more from the installation equipment. The suction forces that can be applied are not limitless. This will be discussed in chapter 4. Caissons are therefore sometimes equipped with water injection devices on the skirt / caisson tip. During penetration this system pumps water through tubes along the caisson tip which flushes the soil and reduce the soil resistance. The effectiveness of this method was verified by Tjelta et al. (1986) in a large scale penetration test.

The injection process differs from jetting where high pressure water jets are used to physically move the soil particles. The objective with the water injection is to modify the soil pore water pressure to manipulate the effective pressures and thereby alter the soil shear strength (Cotter, 2009). However, the effect of water injection on the long term holding capacity of the anchor is not fully understood. Simultaneous injection and suction of water might also seem counter-productive from an engineering standpoint.

3.5 Optimal load attachment point

A critical part of the anchor design is the location of the padeye (load attachment point). The optimum load attachment point is where forces from the mooring line is transferred to the caisson without rotating it. Any rotation will reduce the pullout capacity. Calculations have to be conducted so the resulting overturning moment at the centre line of the anchor tip is approximately zero (DNV, 2005). In a soil with constant strength this will result in a padeye location just below the middle; for a soil with linearly increasing strength the optimal

location will be approximately 2/3 below the surface (Tjelta (2001) and Ahn et al. (2013)). The precise position depends not only on the soil strength profile, but also on the load angle of the mooring line.

3.6 Profile of embedded mooring lines

When the mooring line for a vessel is laid it will assume a catenary shape unless it is pre-tensioned or equipped with buoyancy elements. A portion of the line will rest on the seabed where frictional forces between the line and soil will carry some of the load caused by displacement of the vessel. Because the padeye is located below the seabed a part of the mooring line close to the anchor will be embedded into the soil where it assumes a reverse catenary shape, see figure 3.1.

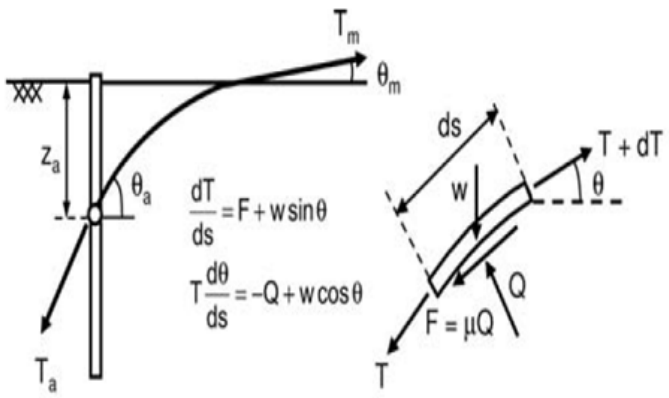

Fig. 3.1 Inverse catenary shape of an embedded mooring line, Neubecker and Randolph (1995)

where:

T_m = Tension in the anchor line at mudline
T_a = Tension in the anchor line at the anchor attachment point (padeye)
θ_a = Inclination of the anchor line at attachment point (measured from the horizontal)
θ_m = Inclination of the anchor line at the mudline (measured from the horizontal)
θ = Orientation of the anchor line element
Q = Normal force transmitted to the anchor line from the soil
F = Frictional force acting on the anchor line
μ = Friction coefficient between chain and soil
z_a = Depth to padeye
w = Self weight of the anchor line

As can be seen from figure 3.1 this reverse catenary shape results in a vertical force component on the caisson. Neubecker and Randolph (1995) developed an analytical solution for the mooring line angle at the padeye, θ_a. This is a simplified solution based on the assumption that the self-weight of the mooring line is negligible at greater embedment depths, see equation 3.1:

$$-\frac{T_a}{1+\mu^2}[\exp^{\mu(\theta_a-\theta)}(\cos\theta+\mu\sin\theta)]_{\theta_a}^{\theta}=\int_z^D Q dz \tag{3.1}$$

For the common case when the line angle at the mudline, θ_m is zero equation 3.1 can be written as:

$$\theta_a=\sqrt{\frac{2z_aQ_{av}}{T_a}} \tag{3.2}$$

3.7 Factor of safety

A useful method to ensure that the suction anchors design is sufficiently reliable is to employ a safety factor. The factor of safety is a design margin that allows for uncertainties in the theoretical design loads. Preliminary results from a reliability study of suction anchors in deepwater applications indicate that a factor of safety of 2,0 results in a lifetime (20-years) probability of failure between $1,4*10^{-2}$ and $1,8*10^{-2}$ (Clukey, 2000).

Chapter 4

Suction Anchor Installation Procedure

General installation procedure for suction anchors:

1. Transport of suction caissons and mooring lines to installation location using derrick barges, or cargo barges with a separate crane vessel, see figure 4.1.

2. Preparation of equipment before the lifting operation in accordance with predefined lifting procedures. Attach mooring line.

3. Lowering of suction anchor down to seabed with vent cap open, see figure 4.2. This allows air to escape the caisson.

4. A work Remote Operated Vehicle (ROV) is often employed to ensure accurate positioning of anchor prior to seabed penetration.

5. Self-weight penetration in seabed.

6. The vent cap is closed and water is pumped out from the caisson. This is done with either a ROV mounted pump, see figure 4.3, or a separate pump system operated from the surface. The pressure drawdown further penetrate the anchor to a predetermined depth, see figure 4.4.

7. The free end of the mooring line is suspended from a buoy to allow for retrieval followed by connection to structure and tensioning.

8. Repeat process until mooring configuration is completed.

Fig. 4.1 Transport of suction anchors to location

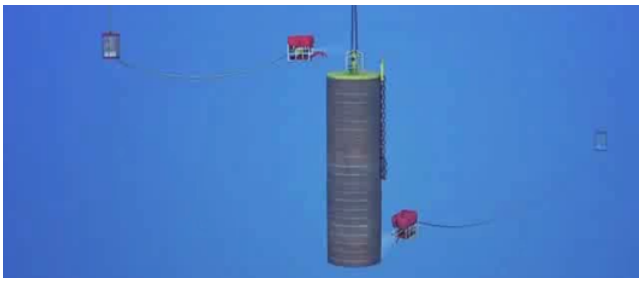

Fig. 4.2 Lowering of suction anchor to seabed. ROV's are employed to monitor the operation

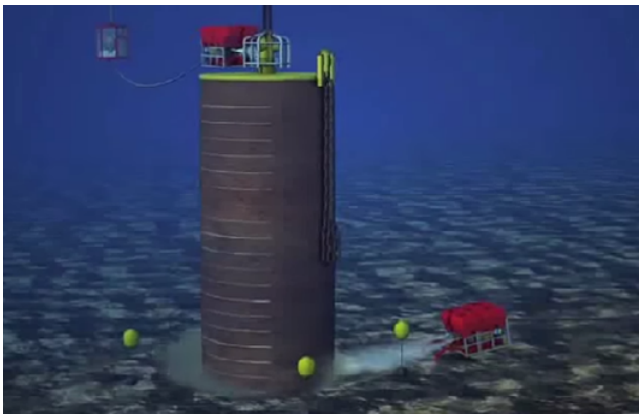

Fig. 4.3 A pressure drawdown is created by pumping water out from the caisson.

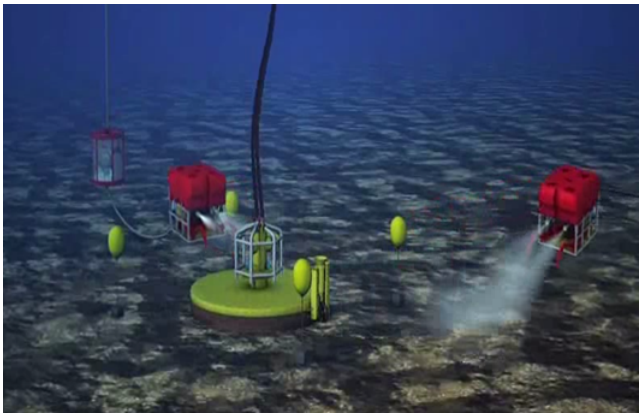

Fig. 4.4 The suction anchor is installed

4.1 Parameters influencing installation

We can divide the installation procedure into two main phases. The self-weight penetration phase comprise the period between contact with the seabed and until soil resistance along the caisson walls and caisson tip are equal to the submerged weight of the anchor, thereby halting penetration (Cao et al., 2002). The second phase is the suction phase where a downward force is created by pumping out water from the caisson. The controlling parameters of object penetration in the ocean bottom can according to Schmid (1969) be summarized as:

- Impact velocity
- Mass, geometry, and structure of the penetrating object
- The impact configuration (i.e. impact trajectory and geometry)
- Soil properties

Of the aforementioned parameters, soil properties is the primary uncertainty of penetration calculations. Soil resistance against penetration is composed of (Houlsby and Byrne, 2004):

- Friction along the outside of the caisson
- Friction along the inside of the caisson
- Friction along plate-or ring stiffeners (if any)
- End bearing on caisson tip and any protruding parts (e.g. plate-or ring stiffeners and padeyes), see figure 4.5

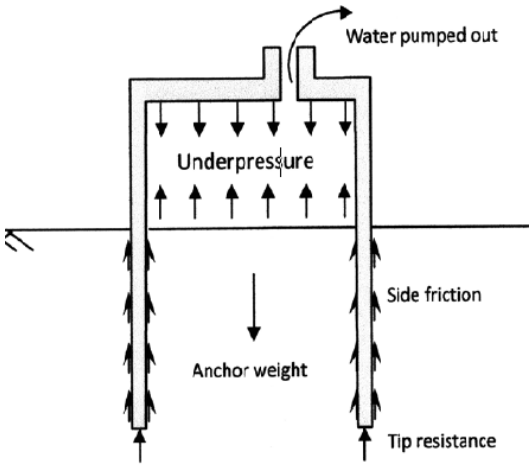

Fig. 4.5 Forces acting on the caisson during suction installation phase

4.1.1 Soil penetration resistance

DNV (1992) proposed a method for calculating soil resistance against penetration with skirted foundations (caissons). This method is applicable to the self-weight penetration phase of suction anchors. In accordance with DNV (1992), calculation of soil penetration resistance should be based on real data collected from location, and from relevant laboratory experiments.

The most commonly used technique for measuring penetration resistance is Cone Penetration Tests (CPT's). The very basic version of CPT is to drive an instrumented cone into the soil at a constant rate, while producing a computerized log of parameters of interest, e.g. tip resistance, sleeve resistance, and friction ratio. Friction ratio is the ratio between tip resistance and sleeve resistance given in percent. This information is sufficient to deduce the soil type and liquefaction resistance.

Scaling of this information to calculate suction anchor penetration resistance is complicated. This is because there are uncertainties linked to the effect of changes in penetration rate and possible excess pore pressure.

There is also the issue of inhomogeneous soil properties with varying degree of strength over the penetration area. This may not be reflected in CPT's due to the relatively small scale compared to suction anchors. DNV suggests to conduct two sets of calculations to deal with these challenges. One set with the most probable penetration resistance, and one set with the largest expected penetration resistance. The latter will be used to determine required ballast during installation. Reasonable design criteria should be created based on these two sets of calculations.

DNV algorithm for assessing soil strength and resulting penetration resistance (DNV, 1992):

1. Identify soil borings and CPT's
2. Determine for each CPT an average cone penetration resistance, $q_{c,av}$, at even intervals, for example 0.2 m
3. Determine for each CPT an average cone penetration resistance, termed $\bar{q}_c$, of a selected number of individual $q_{c,av}$ representing certain identified layers of soil

The penetration resistance can then be derived from equation 4.1

$$R = k_p(L)A_p\bar{q}_c(L) + A_s\int_0^L k_f(z)dz \tag{4.1}$$

where:

R = penetration resistance
L = depth of tip of penetrating member
$k_p(z)$ = empirical coefficient relating q_c to end resistance
$k_f(z)$ = empirical coefficient relating q_c to skin friction
$\bar{q}_c(z)$ = average cone resistance at depth z
A_p = tip area of penetrating member
A_s = side area of penetrating member, per unit penetration depth

The coefficients k_p and k_f greatly influence the magnitude of the resistance and must therefore be selected with care. DNV suggests the values presented in table 4.1 for suction anchors with steel caissons.

Table 4.1 Numerical values of coefficients k_p and k_f in sand and clay, North Sea conditions, DNV (1992)

Type of soil	**Most probable**		**Largest expected**	
	k_p	k_f	k_p	k_f
Clay	0,4	0,03	0,6	0,05
Sand	0,3	0,001	0,6	0,003

4.1.2 Self-weight installation in clay

Houlsby and Byrne (2004) assume that the strength of clay (undrained) increase linearly with depth, and derive the simplified equation 4.2. Undrained soils denote fine grained soils like silts and clays. These soils have small, and often not continuous, void spaces which results in low permeability. Drained soils like sands and gravels have large and continuous void spaces which allow water to flow freely.

$$\acute{W} = \alpha_0 z \pi D_0 s_{u_1} + \alpha_i z \pi D_i s_{u_1} + (\acute{\gamma} z + s_{u_2} N_c)(\pi D t) \tag{4.2}$$

where:

$\acute{W}$ = buoyant weight of the anchor
α_0 = friction factor for the outside caisson wall
α_i = friction factor for the inside caisson wall
D_0 and D_i = outer and inner diameter of the caisson respectively
s_{u_1} = average undrained strength between mudline and depth, z
s_{u_2} = average undrained strength at depth, z
$\acute{\gamma}$ = effective unit weight of soil
N_c = bearing capacity factor
D = $\frac{D_0 - D_i}{2}$
t = wall thickness
z = skirt penetration depth

Self-weight penetration will continue until the right hand of the equation, which is the mobilised soil resistance, is equal to the buoyant weight of the anchor. A similar method can be seen in Andersen and Jostad (1999) with the exception that only one friction factor is used, see equation 4.3. Neither of these equations takes into account stiffeners or other protruding parts like padeyes. Bearing and friction terms for these will have to be added.

$$Q_{tot} = Q_{side} + Q_{tip} = A_{wall} \alpha s_u^{D\bar{S}S} + (N_c s_{u,tip}^{av} + \acute{\gamma} z) A_{tip} \tag{4.3}$$

where:

Q_{tot} = total penetration resistance
Q_{side} = resistance from friction
Q_{tip} = tip resistance
A_{wall} = total surface area of the caisson walls
α = friction factor
$s_u^{D\bar{S}S}$ = Direct Simple Shear (DSS) strength over the penetration depth
$s_{u,tip}^{av}$ = average undrained strength at depth, h
A_{tip} = caisson tip bearing area

Bearing capacity factor

The selection of bearing capacity factor, N_c is not standardised. There is disunity concerning how the ratio between caisson wall thickness and caisson diameter affects the bearing capacity factor. The value also depends on soil type, loading conditions, and the depth of embedment to diameter ratio (Huang et al., 2003). DNV-RP-E303 suggests calculating the factor with Brinch-Hansen's bearing capacity equation, see equation 4.4. This will result in a bearing capacity factor ranging from approximately 6 at the mudline to 9 at depths greater than 4,5 times the diameter of the caisson. In Houlsby and Byrne (2004) it is stated that a bearing capacity factor of 9 can be adopted for suction anchor installation in clay as long as passive suction is in place, i.e. the top cap is sealed.

$$N_c = 6,2\left(1+0,34\arctan\left(\frac{z}{D}\right)\right) \tag{4.4}$$

Undrained shear strength

Undrained shear strength, s_u can be determined from CPT's through empirical correlations and / or theoretical solutions (Robertson and Mayne, 1998). Some typical values for s_u are presented in table 4.2.

Table 4.2 Undrained shear strength values for a selection of soils

S	s_u **(kPa)**
Very firm silty clays / clayey silts	> 150
Firm silty clays / clayey silts	75 - 150
Soft-firm silty clays / clayey silts	40 - 75
Soft silty / clayey silts	20 - 40
Very soft silty clays / clayey silts	< 20

Friction factor

Adhesion of soil to the caisson wall and wall roughness is described by a friction factor, α. The friction factor is often set to be equal to the inverse of the soil sensitivity. Sensitivity of soil is the ratio between the shear strength of undisturbed / intact soil and disturbed / remoulded soil (Bai and Bai, 2010).

Allowable self-weight penetration rate

During self-weight penetration the seawater within the caisson is discharged through open vent caps. If the vent caps does not allow the entrapped water to escape fast enough, then pressure will build up within the caisson. This pressure can, if large enough, compromise the seal created by the embedment of the caisson and create flow channels along the caisson walls (Huang et al., 2003). Water channels along the caisson walls will severely compromise the pullout strength of the anchor. It is especially important to be aware of the pressure within the caisson during the penetration of the first few meters. This is because the surrounding soil has little overburden pressure to strengthen the seal.

4.2 Suction assisted penetration in clay

4.2.1 Necessary suction pressure

After the self-weight penetration phase the caisson is sufficiently embedded into the soil to form a seal. This prevents inflow of seawater. Pumping seawater out from the caisson results in an additional vertical force acting in the same direction as the buoyant weight of the caisson. This force is equal to the differential pressure, ($s = p_{ambient} - p_{suction}$) times the horizontal cross-sectional area of the caisson. Using equation 4.2 we can add this force to the left hand side, see equation 4.5. Houlsby and Byrne (2004) state that when suction is applied it should be accounted for when calculating the end bearing term thereby reducing the amount of suction needed.

$$\acute{W} + s\left(\frac{\pi D_i^2}{4}\right) = \alpha_0 h \pi D_0 s_{u_1} + \alpha_i h \pi D_i s_{u_1} + (\acute{\gamma} z - s + s_{u_2} N_c)(\pi D t) \tag{4.5}$$

The applied suction required to cause soil penetration by the caisson is given by:

$$s_{required} = \frac{Q_{tot} - \acute{W}}{A_i} \tag{4.6}$$

Where:

Q_{tot} = soil resistance
$\acute{W}$ = submerged weight of the anchor
A_i = horizontal cross-sectional area of the caisson

4.2.2 Allowable suction

A greater suction pressure results in a larger differential pressure and therefore more vertical force. However, there are limitations to the amount of suction that can be applied. One is the pump capacity. The pump is often mounted on a ROV. This restricts pump weight and allowable energy consumption. Another issue is cavitation. If the ambient pressure is low, e.g. shallow water, then the pressure required inside the caisson to achieve the necessary differential pressure could potentially be below the cavitation pressure. The cavitation pressure mostly depends on the water depth and temperature and is typically a small fraction of atmospheric pressure. The risk of cavitation decrease as the ambient pressure increase, e.g. deeper water.

A more pressing issue regarding maximum allowable suction is the stability of the soil plug within the caisson and the structural integrity of the relatively thin steel walls. When suction is applied it creates a difference between vertical stresses on the inside and outside of the caisson. When this difference exceeds a certain value, especially along the tip of the caisson, it will cause local plastic failure. The soil plug then loses its stability and soil will flow into the caisson resulting in soil heave and halting further penetration. The required suction therefore has to be less than a specific value, named allowable suction.

To calculate the pressure differential over the soil plug required to lift it we can analyse the forces working on the soil plug in a state of equilibrium, see figure 4.6.

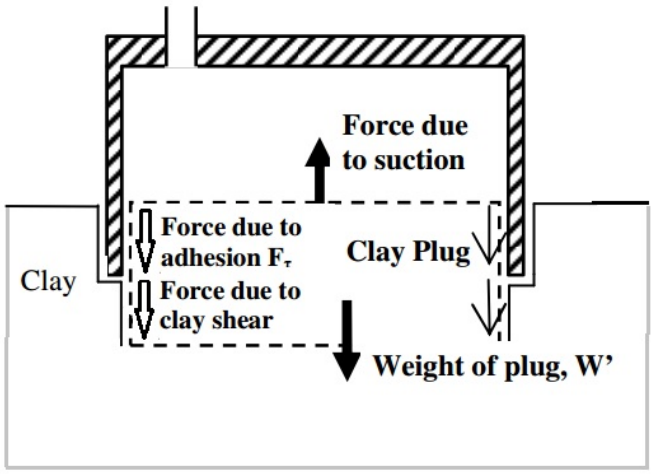

Fig. 4.6 Forces acting on the soil plug within the caisson, Cotter (2009)

Forces on the plug in equilibrium can be written as:

$$F_s = \acute{P} + F_\tau + F_{shear}$$

$$s_{plug}\left(\frac{\pi D_i^2}{4}\right) = \acute{\gamma_c} h_c \left(\frac{\pi D_i^2}{4}\right) + \alpha_i \pi D_i z s_u + \pi D_i (h_c - z) s_u \tag{4.7}$$

Where:

F_s = suction force
$\acute{P}$ = weight of plug
F_τ = friction forces
F_{shear} = force required to shear the clay plug
h_c = height of clay layer
$\acute{\gamma_c}$ = buoyant unit weight of clay
s_{plug} = $p_{suction} - p_{belowplug}$

If we assume that the suction anchor only penetrates a homogeneous layer of clay then equation 4.7 can be written as:

$$s_{plug} = \left(\acute{\gamma_c} + \frac{4\alpha_i s_u}{D_i}\right) z \tag{4.8}$$

If the differential pressure across the plug exceeds s_{plug} then the clay plug will be lifted and prevent further penetration. DNV (2005) gives an expression for allowable underpressure above the plug relative to the ambient hydrostatic pressure, and which also takes into account force required to shear the bottom of the soil plug, see equation 4.9

$$s_{allowable,DNV} = N_c s_{u,tip}^{LB} + \frac{A_{wall,inside} s_u^{D\bar{S}S}}{A_i} \tag{4.9}$$

Where:

$s_{u,tip}^{LB}$ = $2/3$ of the average of compression, extension, and DSS shear strengths at skirt tip level. $2/3$ is a safety factor.

Soil heave

Soil heave occurs inside the caisson because soil is displaced during penetration to accommodate the caisson walls. During self-weight penetration approximately 50 percent of the displaced soil enter the caisson; the remaining 50 percent is pushed outwards. During the suction phase almost 100 percent of the displaced soil flows into the caisson (Andersen and Jostad, 2004). The result is that along the segment of a suction caisson installed through suction, the effective stress in the soil is less on the outside than on the inside. This results in less friction on the outside.

Excessive soil plug heave often develops in practical engineering even though allowable suction is not exceeded. The cause of this, in addition to local plastic failure, is an increase in porosity of the soil due to pressure changes and / or possibly seepage liquefaction (Yang et al., 2003). Seepage liquefaction is the conversion of soil, or more specific granular aggregates, to fluid by flow through it (Leeder and Arlucea, 2009). The risk of seepage is larger in highly porous media, e.g. sands and gravels.

4.3 Soil strength after installation

Installation of a suction anchor will have negative effect on the shear strength of the soil adjacent to the installed caisson. The soil will be subject to plastic deformation, remoulding, and pore water pressure changes. The shear strength will be reduced to a remoulded shear strength. The remoulded shear strength value depends on the original shear strength and the sensitivity of the soil. This reduction in shear strength at the soil-caisson interface reduce the pullout capacity of the anchor.

Consolidation will take place when installation is completed. This is expulsion of excess pore water pressure from the soil. This consolidation is usually accompanied by an increase in shear strength (soil set-up). The set-up effect is caused by the aforementioned reduction in pore water pressure as well as increased horizontal normal effective stress and thixotropy. Thixotropy is the gaining of strength over time while at rest with constant water content and constant porosity (Mitchell, 1981).

According to Andersen and Jostad (1999) a suction anchor with an aspect ratio of 5 that has recently been installed in soil with a sensitivity of 4 will have a capacity that is 25-35 percent less that it will have in untouched soil. The set-up effect cause most of the shear

strength to be recovered after a certain period. The recovery is almost to full strength in the self-weight penetrated zone. In the suction installed zone the recovery will be a bit less.

Chapter 5

Pullout capacity

This chapter presents suggested analytical methods to calculate suction anchor capacity during vertical, horizontal, and lateral loading. These semi-empirical methods were derived through the limit equilibrium method or upper bound limit analysis.

Limit equilibrium method A simplified model is made of the physical problem and a failure mechanism is postulated. The load / stress distribution along the boundaries of the model is assumed, and an equilibrium equation is written to determine the unknown failure load. Soil kinematics is not taken into consideration for this method. The failure load is therefore not necessarily upper bound (maximum).

Upper bound limit analysis A failure mechanism has to be postulated. The solution is then optimized with respect to the parameters upon which the chosen failure mechanism depends. The objective is to find the upper bound (maximum) of the limiting parameter thereby finding the upper bound for the system as a whole.

Finite element method (FEM) As been made clear there is a need to assume a failure mechanism when using the limit equilibrium method or upper bound limit analysis. This is not necessary when using the FEM. During FEM the most probable failure mechanism is determined during calculation. It is also possible to assess the response of the model before failure has occurred.

5.1 Vertical capacity

Vertical load capacity of a suction anchor can be found by considering the probable failure modes during this load condition. These are (Randolph and Gourvenec, 2009):

- Reverse end bearing failure [1]
- Caisson pullout [2]
- Caisson- and soil plug pullout [3]

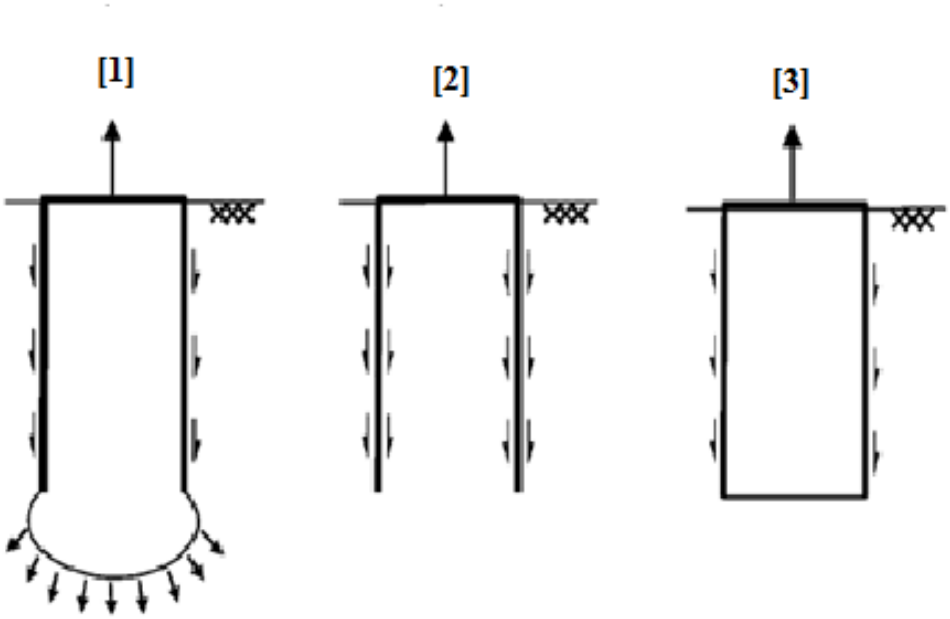

Fig. 5.1 Probable failure modes during vertical loading, Randolph and Gourvenec (2009)

Drainage conditions have great influence on which failure mode to expect. If the applied load rate is rapid, and the permeability of the soil is low, then there will be undrained conditions. Under these conditions the applied load rate is faster than the rate at which pore water is able to drain from the soil. This results in the development of negative changes in pore water pressure (passive suction) in the soil plug within the caisson and in the surrounding soil. The mobilisation of passive suction in adjacent soil opposes uplifting forces. This is referred to as reverse end bearing or reverse end bearing mechanism.

5.1.1 Randolph, M. and Gourvenec, S.

Randolph and Gourvenec (2009) argues that the ultimate vertical pullout capacity under undrained conditions, V_{ult} is governed by the submerged anchor weight, external friction, and the reversed end bearing capacity, see equation 5.1.

$$V_{ult} = \acute{W} + A_{wall,o}\alpha_o \bar{s_{u(t)}} + N_c s_u A_i \tag{5.1}$$

where:

$\bar{s_{u(t)}}$ = average undrained soil strength over the penetration depth at time, t after installation.

$A_{wall,o}$ = external surface area of the caisson

Note that the weight of the soil plug within the caisson is not included in equation 5.1 because:

> *The overburden from the soil column outside the caisson above tip level, and the weight of the soil plug within the caisson are equal and opposite and so their effect cancel out* (Randolph and Gourvenec, 2009)

If the applied load rate is very slow then the soil in the caisson may become fully drained. Water can then flow from adjacent soil into the caisson where it forms a water filled gap between the soil plug and the top cap, or in other locations in the soil plug. The water gap allows the caisson to displace.
For the caisson to displace further the water gap must increase, but the flow rate is restricted by the permeability of the soil. The velocity which the anchor can be pulled out is therefore restricted by, among other factors, the permeability of the soil. This makes the suction anchor design especially suited for low permeable soils like clay. Should the water filled gap become too large it is possible to pump water as was done during the installation.

Instead, consider a highly permeable soil like sand where water flow is almost unrestricted so that no passive suction will develop. This is comparable to a suction anchor without the top cap (Deng and Carter, 2000). The ultimate load capacity is then governed by internal- and external friction and anchor weight, see equation 5.2.

$$V_{ult} = \acute{W} + A_{wall,o}\alpha_o \bar{s_{u(t)}} + A_{wall,i}\alpha_i \bar{s_{u(t)}} \tag{5.2}$$

where:

$A_{wall,i}$ = internal surface area of the caisson

If the applied load rate is such that the soil is partially drained, meaning the excess pore water pressure has partly dissipated, then the ultimate capacity is determined by external friction, the anchor weight, and the amount of passive suction that could be generated. Partially drained conditions are to be expected during the life cycle of a suction anchor. The phenomena is not fully understood and it is complicated to calculate the capacity because the only deterministic value is the weight of the anchor. It is therefore normal to make estimations based on the two extremes, fully drained and fully undrained, and conduct further investigations using finite element analysis (FEA) if necessary.

Figure 5.2 contain plots of the vertical pullout capacity as a function of aspect ratio. Calculations are done using equation 5.1 and equation 5.2. The undrained capacity is primarily of interest, but drained capacity is plotted in this case to illustrate the large reduction in capacity for drained conditions. Multiple friction factors are used in this example to assess how they affect the capacity. The soil parameters used are listed in table 5.1. The strength values chosen are discussed in chapter 6. Note that the weight of the caisson is not taken into consideration in neither analytical nor FEA calculations. This is because it is simply a constant addition to the capacity and can be added at a later point if wanted.

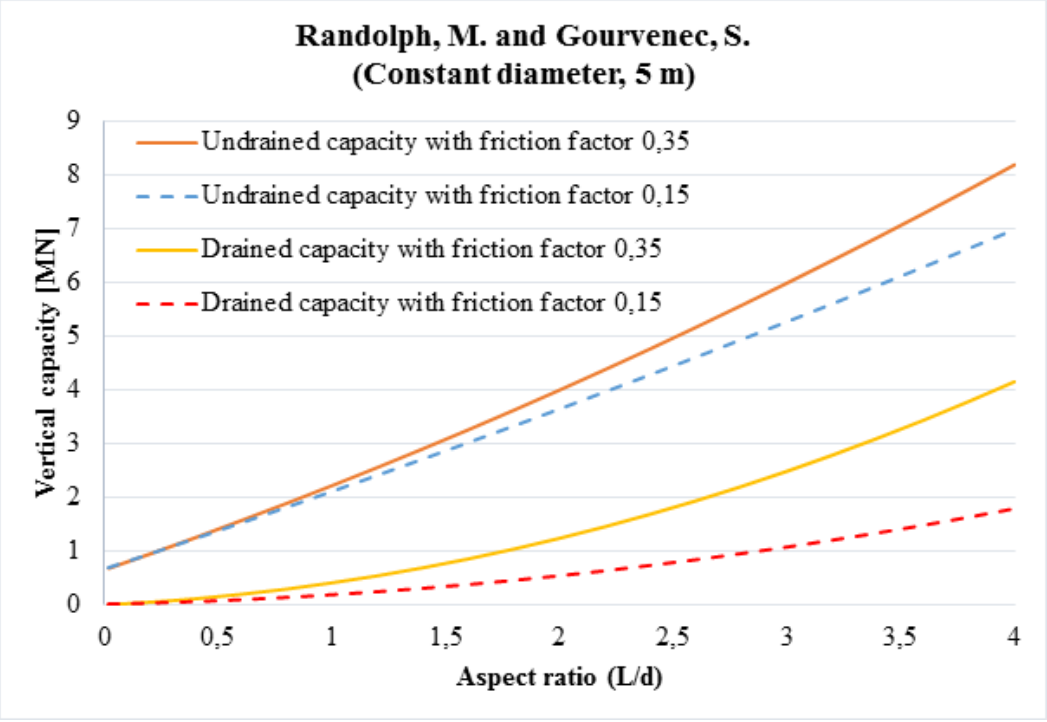

Fig. 5.2 Vertical pullout capacity calculated using equation 5.1 and 5.2. Diameter is held constant. The graphs illustrate the difference between drained and undrained capacity

Table 5.1 Soil parameters used in analytical calculations

Undrained shear strength, s_u	$3,68 + 1,54z$	kPa
Average undrained shear strength over caisson length, $s_{u,avg}$	$\frac{s_u(z) + s_u(0)}{2}$	kPa
Soil-steel friction coefficient, α	0,35	unless stated otherwise
Bearing capacity factor, N_c	9	unless stated otherwise
Unit weight of soil, γ	14	kN/m^3

The graphs in figure 5.2 are created using a constant diameter (5 m) and varying caisson lengths to obtain aspect ratios (L/d) between 0 and 4. It is clear that an increase in aspect ratio cause significant improvement in pullout capacity. The increase in this case is due to the shear strength which increases linearly with depth, and the growing surface area of the caisson which friction forces can act upon.

In figure 5.3 it is the length which is held constant (5 m). Because aspect ratio is defined as length over diameter this means that a decrease in aspect ratio signify a caisson with increased diameter (when length is constant). From equation 5.1 it can be seen that the pullout capacity in undrained soil is dependent on the horizontal cross-sectional area of the caisson. This explains the very large capacity for small aspect ratios in the case of constant length with varying diameter. The contribution from friction force is practically non-existent in comparison. This can be seen by observing the curves which are overlapping even though the friction coefficient for one curve is more than twice the magnitude of the other. Figure 5.4 and 5.5 show the relative contribution of different resistive forces to the total undrained capacity in the case of constant diameter and constant length respectively.

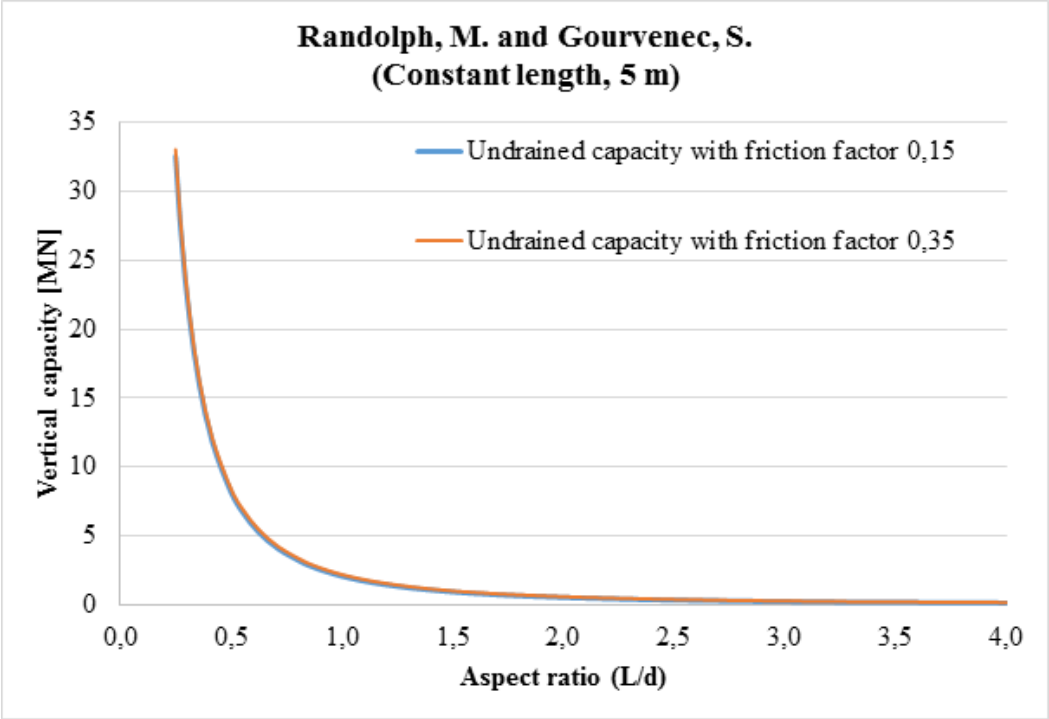

Fig. 5.3 Undrained vertical capacity calculated with equation 5.1. Caisson length is constant

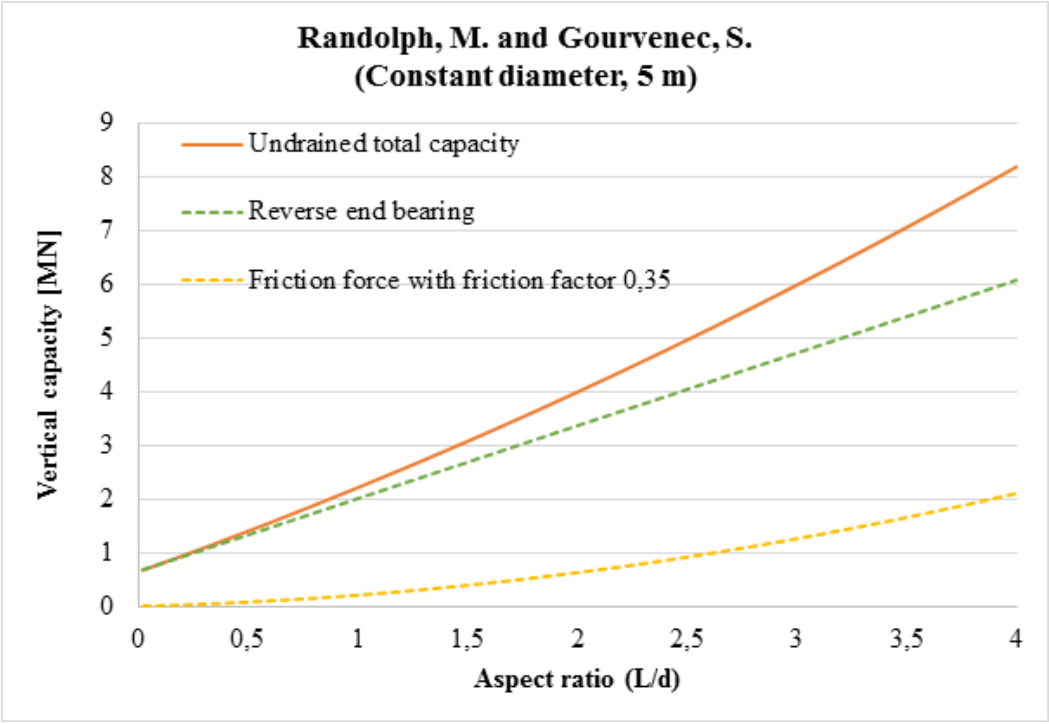

Fig. 5.4 Contribution from different resistive forces to the vertical capacity obtained with equation 5.1 when diameter is constant

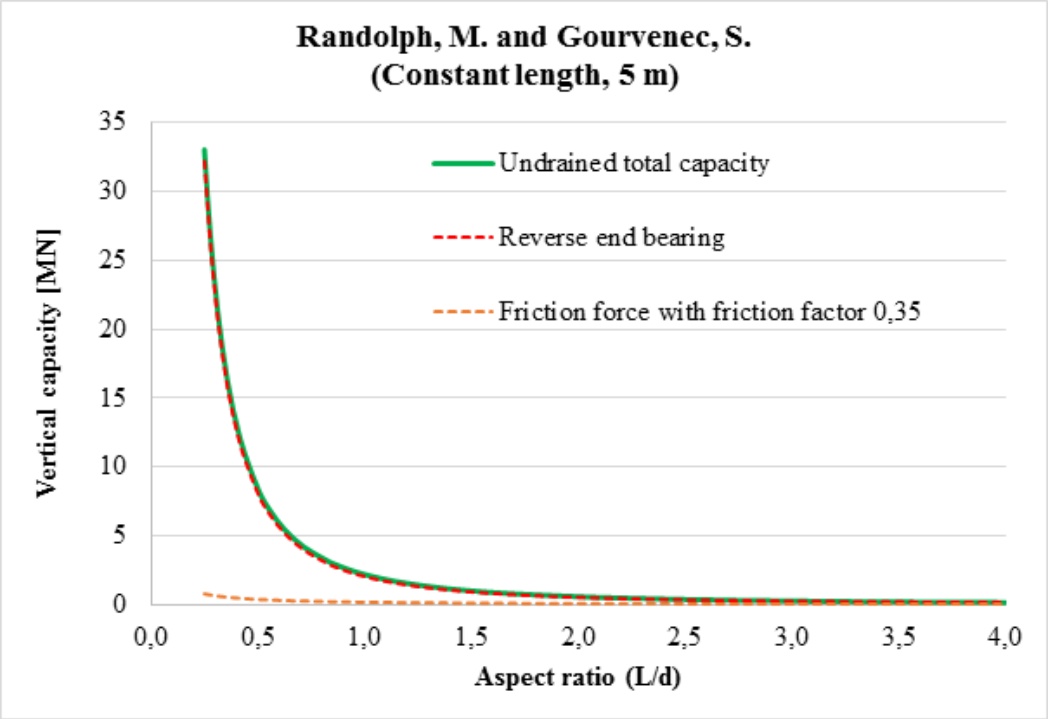

Fig. 5.5 Contribution from different resistive forces to the vertical capacity obtained with equation 5.1 when length is constant

5.1.2 Deng, W. and Carter, J.P.

Deng and Carter (2000) also advocate the use of bearing capacity theory to calculate undrained capacity. The pullout resistance is created by a combination of reversed end bearing capacity and friction forces, see equation 5.3. F_{ext} is the external friction forces, ζ_{ce} and ζ_{cs} is an embedment factor and shape factor respectively.

$$V_{ult} = \zeta_{ce}\zeta_{cs}N_c s_u A_i + F_{ext} \tag{5.3}$$

It is further stated that the friction forces can be expressed as proportional to the reversed end bearing using a proportionality factor, β.

$$F_{ext} = \beta\,\zeta_{ce}\zeta_{cs}N_c s_u A_i \tag{5.4}$$

Combining equation 5.3 and 5.4:

$$\begin{aligned} V_{ult} &= (N_c + \beta)\,\zeta_{ce}\zeta_{cs}s_u A_i \\ &= N_p \zeta_{ce}\zeta_{cs}s_u A_i \end{aligned} \tag{5.5}$$

where:

$\zeta_{ce} = 1 + 0,4\left(\frac{L}{d}\right)$
$\zeta_{cs} = 1,2$ for circular foundations

N_p which is a combination of a bearing capacity factor and a proportionality factor can according to finite element predictions be given as:

$$N_p = 7,9\left(\frac{L}{D}\right)^{-0,18} \tag{5.6}$$

The complete expression for vertical pullout capacity in undrained soil is then given by equation 5.7. Figure 5.6 and 5.7 show graphs created with equation 5.7 using the parameters in table 5.1.

$$V_{ult} = 7,9\left(\frac{L}{D}\right)^{-0,18} 1,2\left(1 + 0,4\left(\frac{L}{d}\right)\right) s_u A_i \tag{5.7}$$

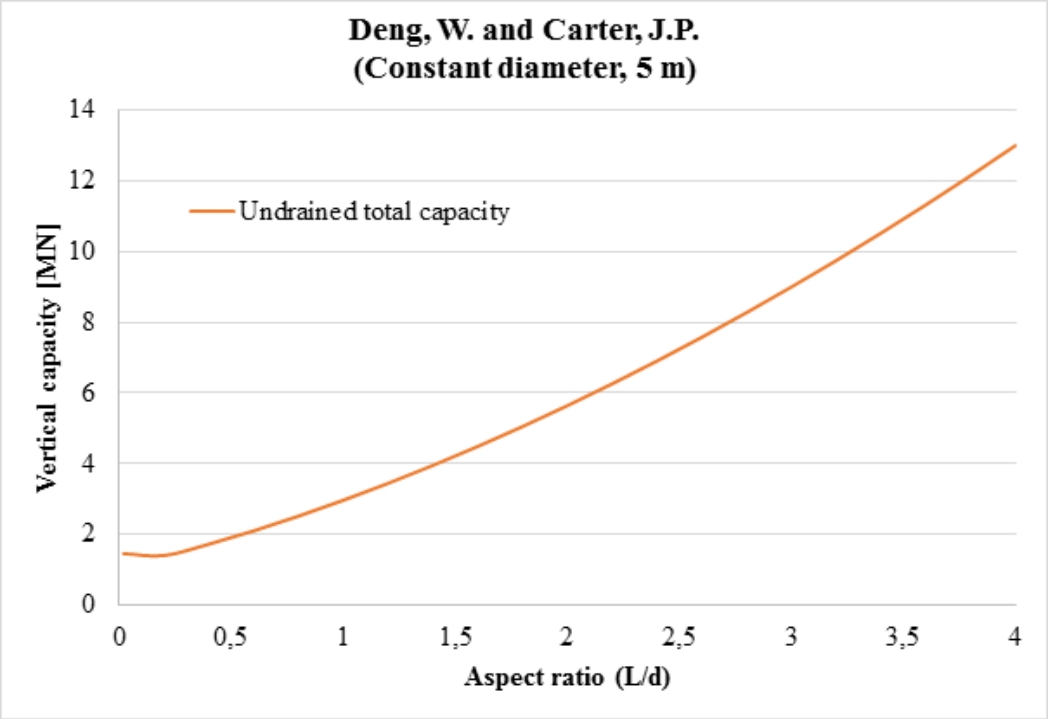

Fig. 5.6 Vertical pullout capacity calculated using equation 5.7 (constant caisson diameter)

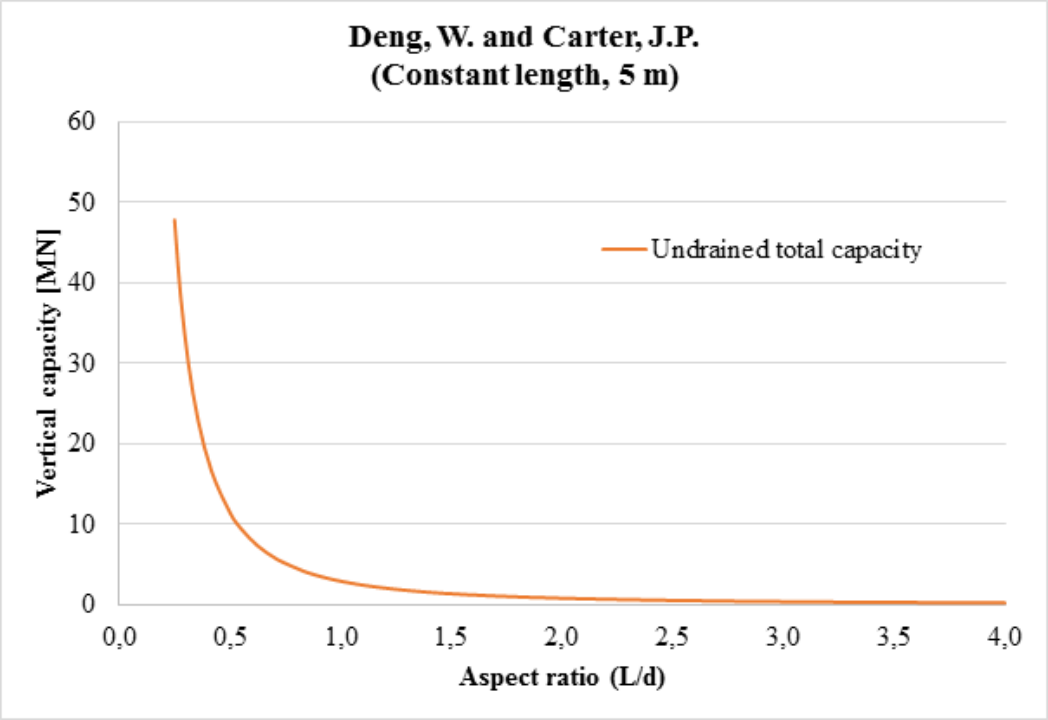

Fig. 5.7 Vertical pullout capacity calculated using equation 5.7 (constant caisson length)

5.1.3 Iskander, M., El-Gharbawy, S. and Olson, R.

Iskander et al. (2002) presents an equation which is essentially the same equation as presented by Randolph and Gourvenec (2009) with the exception of the added weight of the soil plug. This does however make a significant contribution to the total capacity, as can be seen in figure 5.8 and 5.9. Parameters are taken from table 5.1.

$$V_{ult} = V_{so} + V_b + \acute{P} \tag{5.8}$$

where:

$V_{so} = \int_0^H \alpha s_u \pi D_0 dz$

$V_b = s_u N_c f \left(\frac{\pi}{4}\right) D_0^2$

$\acute{P}$ = Weight of soil plug

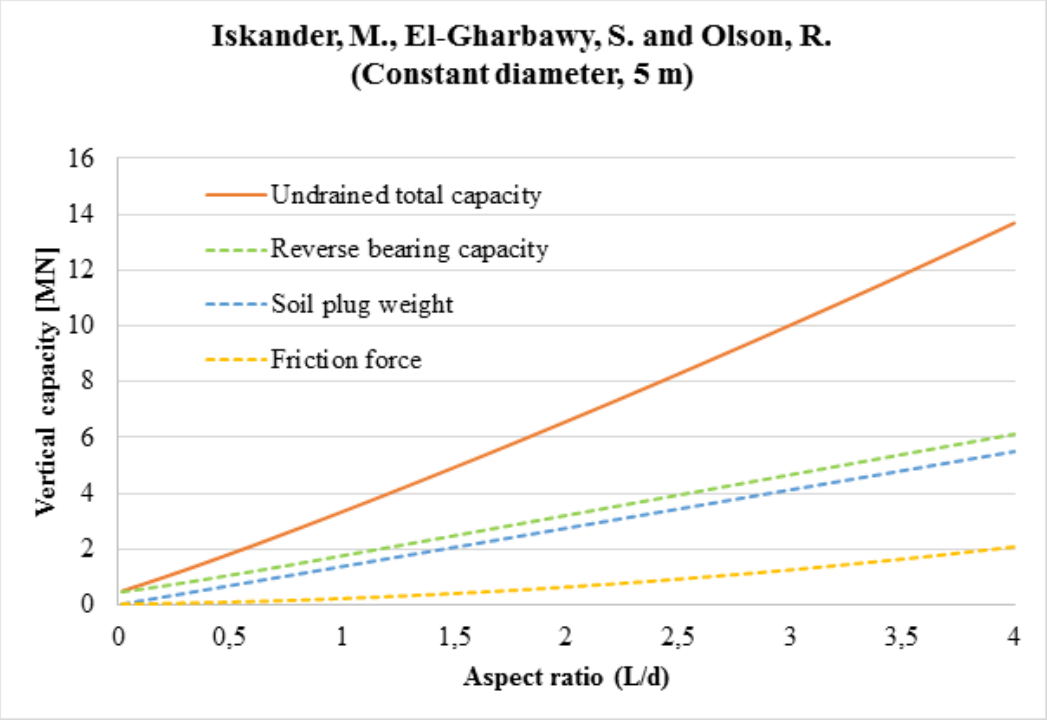

Fig. 5.8 Contribution of different resistive forces to the total undrained capacity using equation 5.8 when diameter is constant

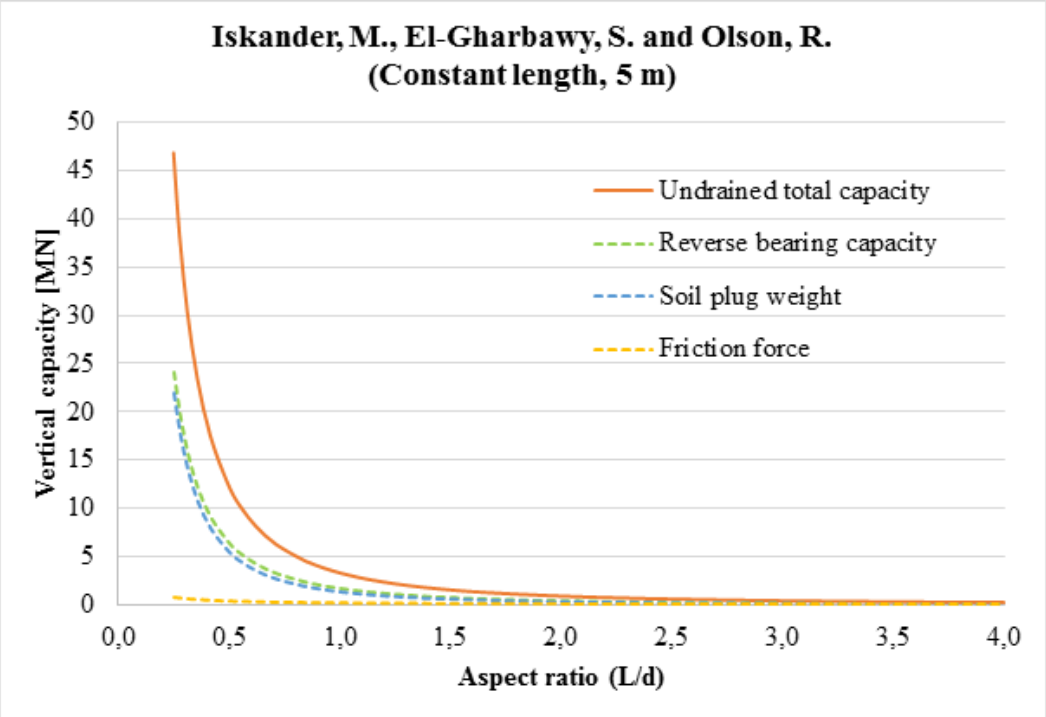

Fig. 5.9 Contribution of different resistive forces to the total undrained capacity using equation 5.8 when length is constant

5.1.4 Rahman, M.S., Wang, J., Deng, W. and Carter, J.P.

In an neural network model for uplift capacity of suction anchors Rahman et al. (2001) express the ultimate vertical capacity as uplift traction times the horizontal cross-sectional area of the caisson, see equation 5.9.

$$\begin{aligned} V_{ult} &= p_u A_i \\ &= (N_c d_c s_u + \bar{\gamma}_c L) A_i \end{aligned} \tag{5.9}$$

where:

$$N_c = 8 \left(\frac{L}{d}\right)^{-0,1833}$$

$$d_c = 1 + 0,4 \arctan\left(\frac{L}{d}\right)$$

Plots created with equation 5.9 using parameters from table 5.1 are shown in figure 5.10 and 5.11.

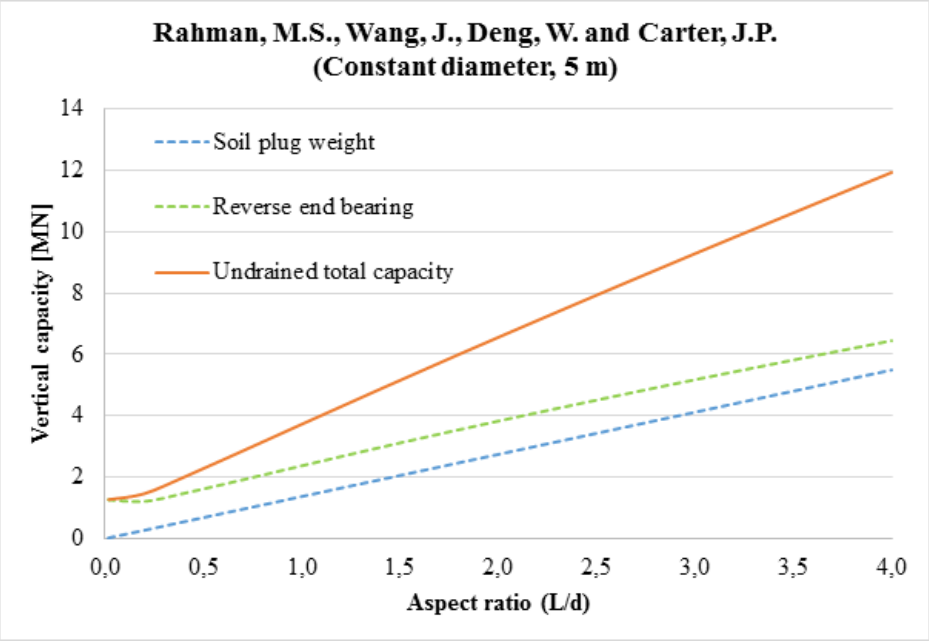

Fig. 5.10 Contribution of different resistive forces to the total undrained capacity using equation 5.9 when diameter is constant

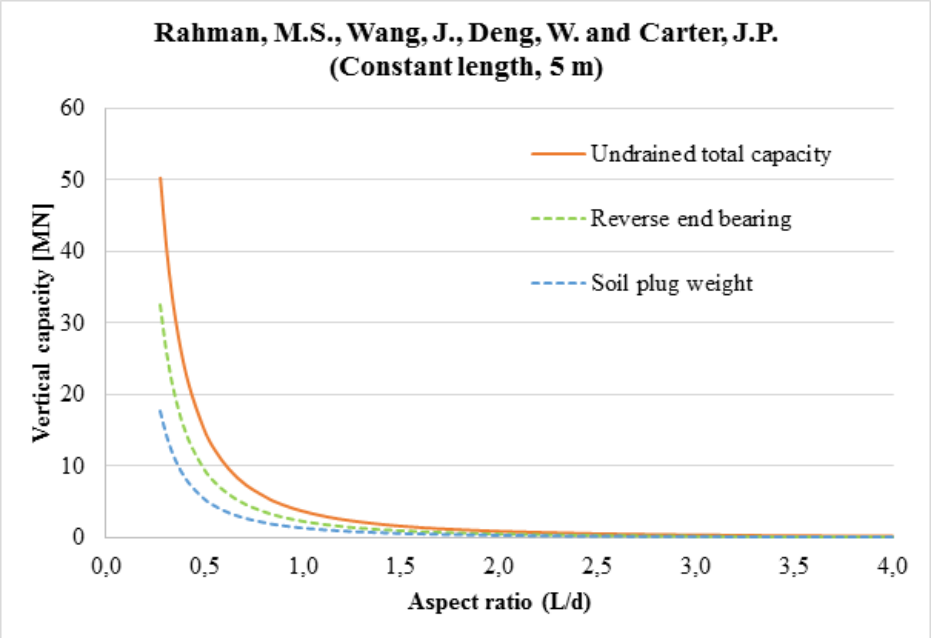

Fig. 5.11 Contribution of different resistive forces to the total undrained capacity using equation 5.9 when length is constant

The analytical solutions which are to be investigated can be seen relative to each other in figure 5.12 and 5.13.

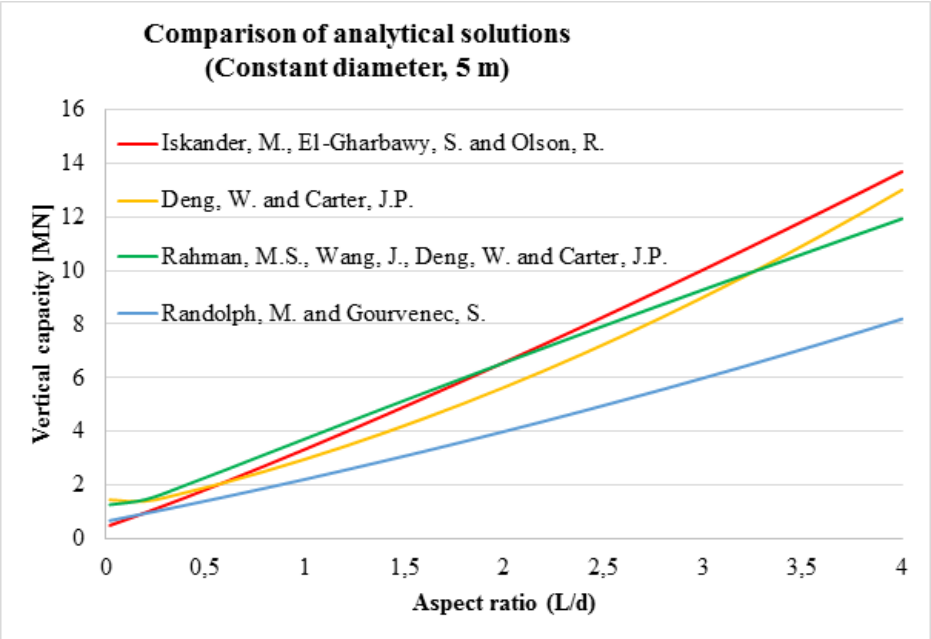

Fig. 5.12 Comparison of analytical solutions (constant caisson diameter)

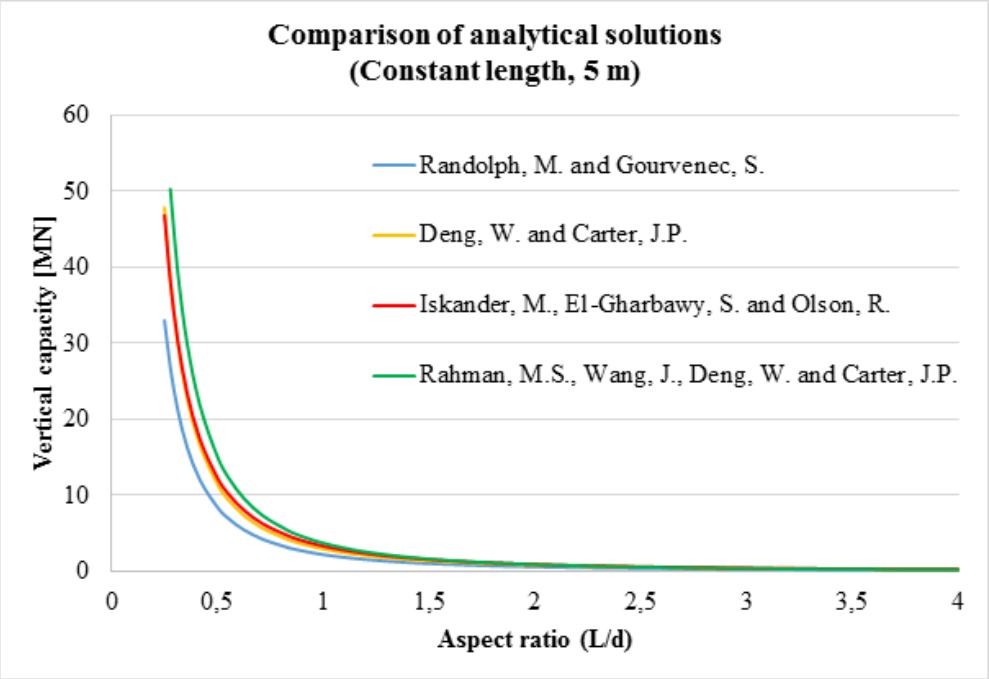

Fig. 5.13 Comparison of analytical solutions (constant caisson length)

5.2 Horizontal capacity

(Randolph, 2002) state that for a suction anchor subjected to a lateral load component there are three main regions where failure occurs.

- ***At shallow depths***. *The flow may be approximated by a conical wedge (figure 5.14) as suggested by Murff and Hamilton (1993) for lateral pile analysis.*

- ***Below the conical wedge***. *Constrained flow of soil around the caisson is assumed. The net pressure on the caisson in this region is taken as the limit pressure for a cylinder moving through soil (Randolph and Houlsby, 1984).*

- ***At the base of the caisson***. *The internal soil plug shears relative to the external soil along a spherical surface centred on the centre of rotation, see figure 5.15.*

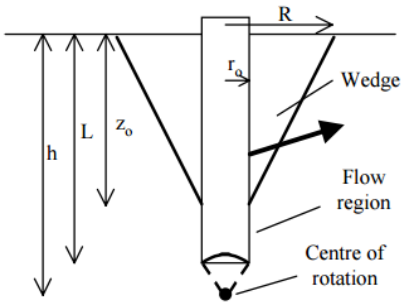

Fig. 5.14 Soil failure zones during horizontal loading, (Randolph, 2002)

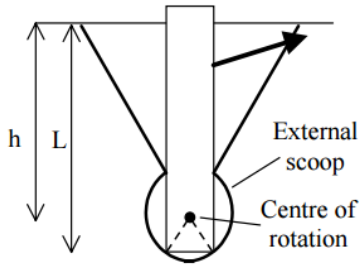

Fig. 5.15 Scooping of soil due to high center of rotation, (Randolph, 2002)

If the padeye is assumed to be located at the optimum depth then it can be considered a case of pure translation where no rotation of the caisson takes place. According to Broms (1964) the ultimate horizontal load capacity can be calculated as:

$$H_{ult} = LD_o N_p \bar{s_u} \tag{5.10}$$

where:

L = embedded length of the caisson
D_o = outer diameter of the caisson
N_p = lateral bearing capacity factor

Equation 5.10 was derived on the assumption that soil is linearly elastic. This is not a good assumption even at small strain rates. However, the equation is useful in establishing preliminary estimates. If more accurate estimates are required then a computer model with a non-linear soil model should be used. The value of N_p can be estimated analytically, see equation 5.11 (Aubeny and Murff, 2005).

$$N_p = N_1 - N_2 \exp^{-\frac{\eta z}{D_o}} \tag{5.11}$$

where:

$N_1 = 9,42 + 2,52\alpha$, $\alpha = 0 \Rightarrow$ perfectly smooth caisson, $\alpha = 1 \Rightarrow$ fully rough caisson
$N_2 = 7,42 + 1,7\alpha$
$\eta = 0,25 + 0,05\rho$, for $\rho < 6$
$\eta = 0,55$, for $\rho > 6$
$\rho = \frac{s_{u_o}}{s_{u_1} D_o}$
s_{u_o} = shear strength at seabed
s_{u_1} = incremental shear strength per unit depth

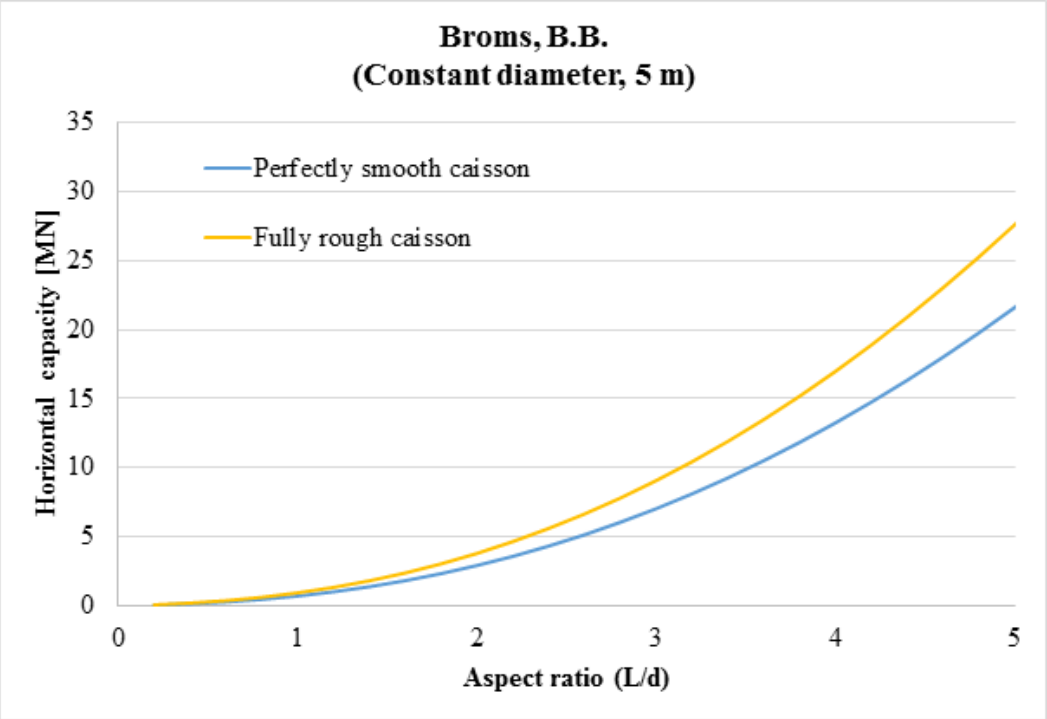

Fig. 5.16 Horizontal (lateral) capacity of suction caisson derived using equation 5.10 when diameter is constant. Soil strength values are taken from table 5.1

5.3 Inclined capacity

Future mooring systems tend towards taut- and semi-taut mooring lines. This will result in loading angles of 30 degrees or more (relative to the horizontal) on the anchors.
Supachawarote et al. (2004) used FEM to develop expressions describing the relationship between vertical- and horizontal load components for various cylinder aspect ratios (L/d). Equation 5.12 was developed for an embedded cylinder with aspect ratio 5. This equation does not take into consideration the bending moment created by the eccentricity between the vertical load component of an applied load, and the neutral axes of the caisson.

$$\left(\frac{H}{H_{ult}}\right)^{a} + \left(\frac{V}{V_{ult}}\right)^{b} = 1 \tag{5.12}$$

where:

H = Horizontal load component
V = Vertical load component
a = 3
b = 3

Chapter 6

Finite Element Model

The finite element method was employed to validate the analytical solutions and conduct a parameter study. The method generally consists of the steps seen in figure 6.1.

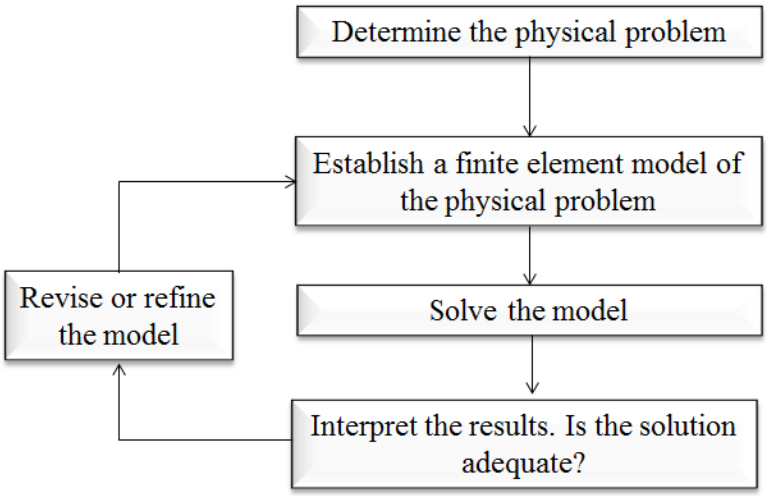

Fig. 6.1 Description of the finite element method (FEM)

The basic process applied when a model is to be established for a problem which is governed by a set of partial differential equations is to take the continuum, for example a structure, and idealize it as an assembly of elements. Each element consists of a number of nodes and lines. This discretization is done because obtaining the solution for a complex system using functions across the whole domain is difficult and even impossible in many cases.

By dividing the domain into elements (meshing) it is possible to approximate the solution for each single element and combine them to form the solution for the whole problem. A large amount of elements is usually needed to create an accurate response prediction. This requires a large number of equations to be solved. Computers are therefore necessary for most realistic problems.

6.1 PLAXIS 2D

The utilized software, Plaxis 2D, is a finite element software package created for conducting two-dimensional analyses of geotechnical problems. It was created at the Technical University of Delft, Netherlands.

6.1.1 Soil properties

The soil used in the model is a two-phase medium composed of a soil skeleton and the pore-fluid (water) it encompasses. It is represented using 15-node triangular elements, see figure 6.2.

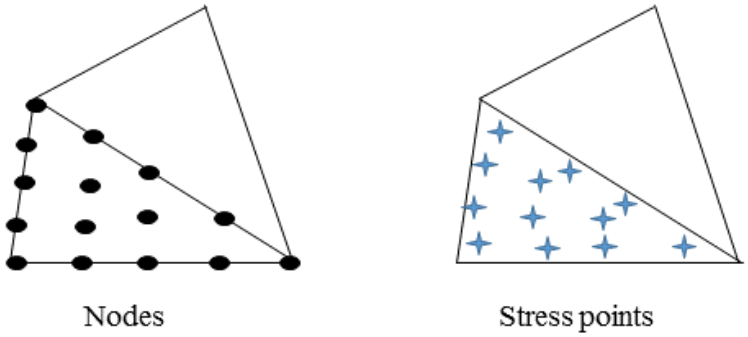

Fig. 6.2 15-node triangle, (PLAXIS, 2008)

The 15-node elements produce high-quality response predictions using quadratic interpolation, and it is a suitable alternative in analyses where the soil body is subjected to large deformations. Large deformations are expected when studying suction anchor capacity. The disadvantage of using a large number of nodes is the increased computational demand. During the analysis it is assumed that the soil is undrained and that the flow of fluid through the soil is governed by Darcy's law. It is further assumed that the Mohr-Coulomb elastic-perfectly plastic soil model is applicable for this problem.

Mohr-Coulomb

To understand the Mohr-Coulomb model it is advantageous to first discuss the principle of effective stress. Effective stress becomes important when analysing forces transmitted through the soil skeleton from particle to particle. The effective stress principle was presented by Karl Terzhagi in 1923 (Craig, 2004). It can be written as:

$$\sigma = \sigma' + u \tag{6.1}$$

Where:

σ = total normal stress acting on the specified soil area
u = pore water pressure (pressure of the water in the void space)
σ' = effective normal stress. This is the part of the total stress transmitted through the soil skeleton only

A useful illustration of the principle can be seen in figure 6.3. The plane XX is drawn at the interface between particles in a soil body. The XX plane is approximately straight due to the small size of the particles. The voids in between the particles are filled with water. When the normal force, P is applied to the soil body with area, A, it will be resisted by interparticle forces and pore water pressure, u. The interparticle forces can be decomposed into a tangential-and vertical component represented by T and N' respectively due to the curvature of the XX plane.

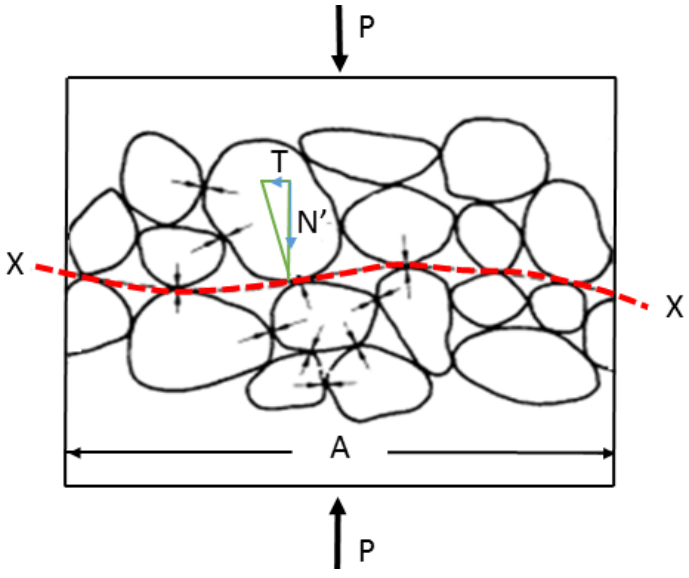

Fig. 6.3 Effective stress principle, Craig (2004)

Equilibrium in the normal direction can then be written as:

$$P = \sum N' + uA$$

$$\frac{P}{A} = \frac{\sum N'}{A} + u$$

$$\sigma = \sigma' + u \tag{6.2}$$

$$\sigma' = \frac{\sum N'}{A}$$

Note that the principle only applies to fully saturated soils because the presence of a compressible medium, e.g. air, complicates the problem. There is also a simplification done with regards to the contact surface between the particles, however the error is negligible (Craig, 2004). The shear strength of soil can now be approximated by a linear function, see equation 6.3

$$\tau = c' + \sigma' \tan \phi' \tag{6.3}$$

Where:

τ = shear strength (s_u).
c' = effective cohesion.
σ' = effective normal stress.
ϕ' = effective friction angle.

Effective cohesion and effective friction angle are named "effective" because they are based on the effective normal stress. Cohesion is used to describe the non-frictional part of shear resistance. It is caused mainly by electrostatic forces and chemical bonds (Lambe and Whitman, 1969). Cohesion is usually a very small component of the shear resistance, and is prone to sudden changes. Great caution should therefore be taken in relying upon the contribution of this parameter to shear resistance.

The effective friction angle is the angle measured between the normal force and the resultant force. It is closely related to the response angle which is the largest slope angle a granular material can sustain by itself. Internal friction angle is dependent on the degree of interlocking between particles. It can be illustrated as the angle of inclination relative to the horizontal axis in a Mohr-Coulomb circle, see figure 6.5. It is important to be aware that these parameters are simplified as mathematical constants created to define a linear relationship between shear strength and effective normal stress.

The reason why effective stresses are used and not total stresses is because only the soil skeleton, and not the pore water pressure, will resist shear forces. If the shear stress at any point on any plane within the soil mass becomes equal to the shear strength of the soil at this point, then failure will occur.

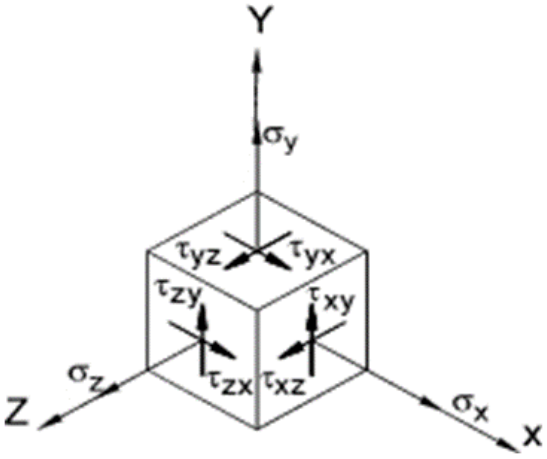

Fig. 6.4 Normal-and shear stresses working on an element, Beardmore (2011)

Consider now the general state of stress for a small element of a material, see figure 6.4. Each surface of this cube have one normal stress and two shear stresses acting upon it. In the case when a surface on the cube is exposed to normal stress only (shear stresses are zero) then the face is referred to as a principal plane. The normal stresses that act upon principal planes are called principal stresses. The largest principal stress on a surface is termed major principal stress, σ_1, while the smallest is termed minor principal stress, σ_3. The principal planes and principal stresses are useful because knowing these it is possible to calculate the stresses in any other direction. It is of interest to find which combination of σ_1 and σ_3 give rise to shear failure in the soil. One commonly used method is through graphical representation using a Mohr- Circle, see figure 6.5. In this figure σ_1 and σ_3 is represented by a circle while equation 6.3 forms a Mohr-Coulomb failure envelope. The combination

of stresses represented by the blue circle can according to the Mohr-circle be considered safe; the combination of stresses represented by the red circle result in failure. This is further shown in figure 6.6.

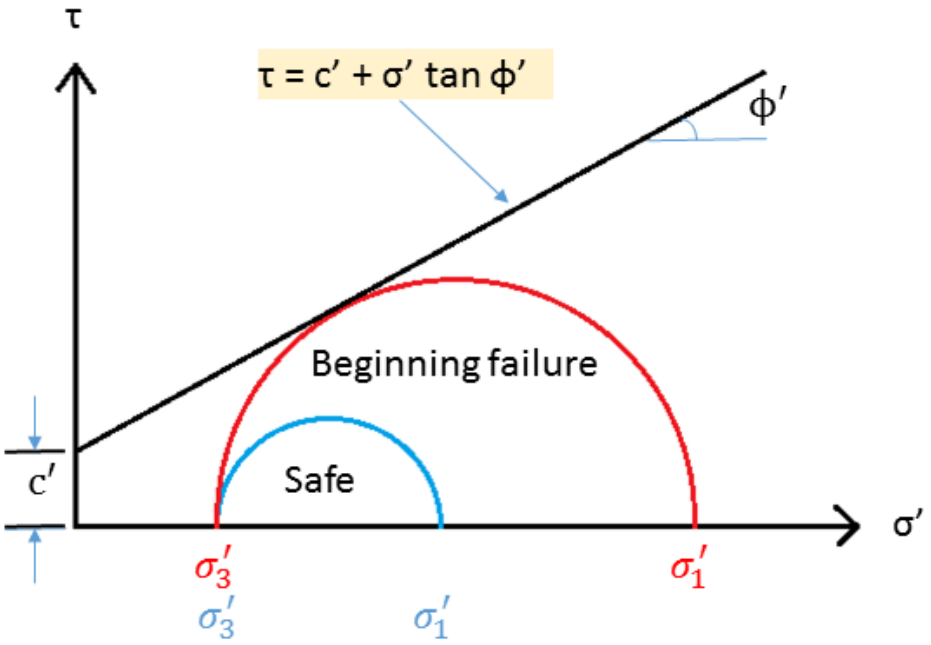

Fig. 6.5 Mohr circle and Mohr-Coulomb failure envelope

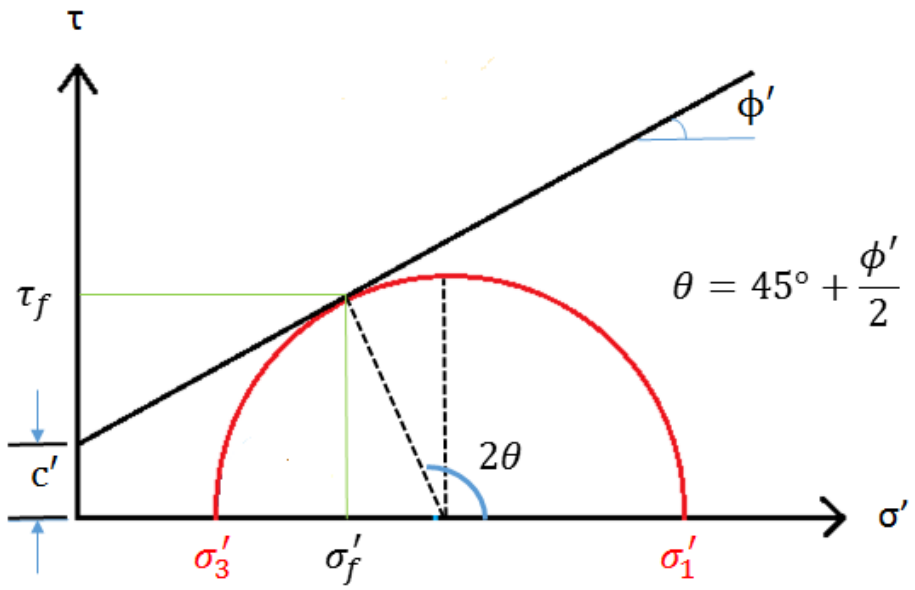

Fig. 6.6 θ is the theoretical angle between the major principal plane and the plane of failure, σ_f' is the effective normal stress at failure, and τ_f is the shear strength of the material for the given combination of stresses and angles.

From figure 6.6 it can be derived expressions for shear strength and effective normal stress as functions of principal stresses, see equation 6.4 and 6.5 (Craig, 2004):

$$\tau_f = \frac{1}{2}(\sigma_1' - \sigma_3')\sin 2\theta \tag{6.4}$$

$$\sigma_f' = \frac{1}{2}(\sigma_1' + \sigma_3') + \frac{1}{2}(\sigma_1' - \sigma_3')\cos 2\theta \tag{6.5}$$

$$\sin\phi' = \frac{\frac{1}{2}(\sigma_1' - \sigma_3')}{c'\cot\phi' + \frac{1}{2}(\sigma_1' + \sigma_3')}$$

$$(\sigma_1' - \sigma_3') = (\sigma_1' + \sigma_3')\sin\phi' + 2c'\cos\phi')$$

$$\sigma_1' = \sigma_3' \tan^2\left(45° + \frac{\phi'}{2}\right) + 2c'\tan\left(45° + \frac{\phi'}{2}\right) \tag{6.6}$$

Equation 6.6 is a version of the Mohr-Coulomb failure criterion. Given the effective confining (minor principal) stress, effective cohesion, and effective internal frictional angle the major principal stress at which failure occurs can be found. The complete representation of yield criteria for three-dimensional stress is given by six separate yield-criteria which can be illustrated as a hexagonal cone, see figure 6.7.

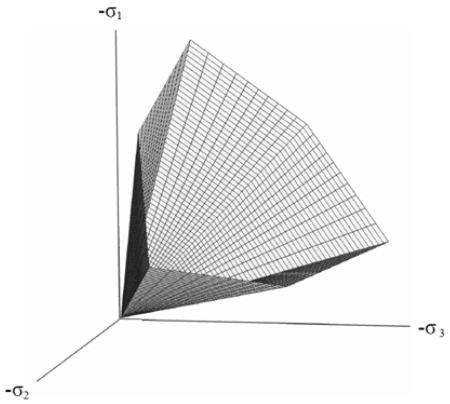

Fig. 6.7 3D representation of Mohr-Coulomb yield criteria, PLAXIS (2008)

Mohr-Coulomb parameters in PLAXIS

Effective Young's modulus, E': Young's modulus, or the modulus of elasticity, is a measure of stiffness. It is related to the ratio of stress over strain in the elastic range of a stress-strain diagram of a material. One weakness of the Mohr-Coulomb model is that stiffness is assumed to be linear elastic below the failure surface while in reality many soils show non-linear behaviour immediately when subjected to loads, see figure 6.8.

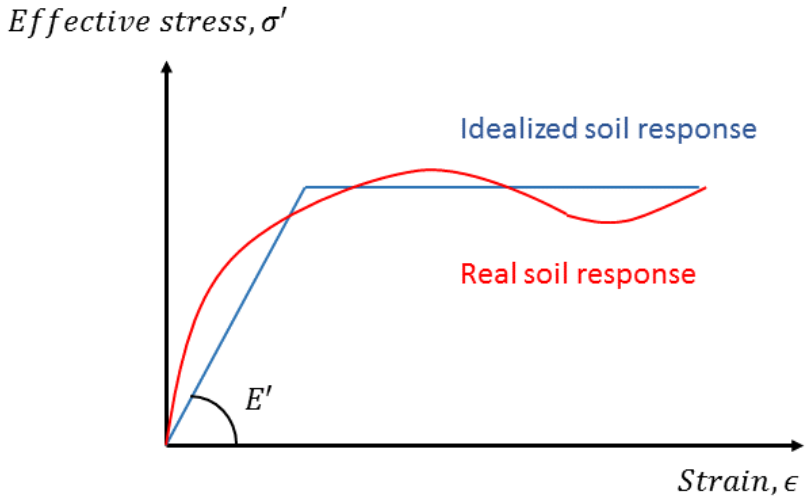

Fig. 6.8 Idealized-and real response of soil when subjected to stress

Poisson ratio, v: Poisson ratio is the negative of the ratio between lateral- and longitudinal strain in a material subjected to axial stress. A list of typical Poisson ratio values for different soils can be found in table 6.1.

Table 6.1 Poisson ratio for a selection of soils, Newcomb and Birgisson (1999)

Soil	Range
Untreated granular material	0,3-0,4
Cement-treated granular material	0,1-0,2
Cement-treated fine-grained material	0,15-0,35
Lime-stabilized material	0,1-0,25
Lime-flyash mixture	0,1-0,15
Loose sand or silty sand	0,2-0,4
Dense sand	0,3-0,45
Fine-grained soils	0,3-0,5
Saturated soft clays	**0,4-0,5**

Saturated and unsaturated unit weight (γ_{sat} and γ_{unsat}): The saturated and the unsaturated unit weight refers to the unit weight of saturated and unsaturated soil respectively. In PLAXIS the saturated unit weight applies to the soil beneath the phreatic level (water table) and unsaturated unit weight applies to the soil above the phreatic level.

Permeability (k_x and k_y): The permeability of a porous material is its ability to transport a fluid or a gas. It is a measure of the pore connectivity in the material. As discussed in chapter 5 it is the low permeability of clay that makes undrained loading a possibility.

Dilatancy angle (ψ): The angle of dilation refers to the positive change in volumetric strain, i.e. increase in volume, when the soil is sheared. This can be explained by densely packed soil grains rolling on top of each other thereby increasing the volume. Clays tend to show little to no dilatancy (PLAXIS, 2008).

Overestimation of shear strength

Caution must be taken when using *effective* stress parameters to model undrained behaviour of soil using the Mohr-Coulomb model. This model assumess elastic-perfectly plastic behaviour up until the point of failure. No volumetric change is allowed during undrained loading. This results in no excess pore water pressure being generated (Puzrin et al., 2010). From figure 6.6 it can be seen that this results in a vertical stress path to the point of failure. In reality there will be volumetric changes in the soil. Clays in particular have a tendency to contract during loading. Due to the low permeability of clay it will take time for water to dissipate, and the pore water pressure within the clay will therefore increase. Because the total stress remains constant it can be seen from equation 6.2 that the effective stress is reduced to compensate for the increasing pore water pressure. The real stress path will therefore curve left as the clay contracts and therefore reach the failure envelope at an earlier point, see figure 6.9.

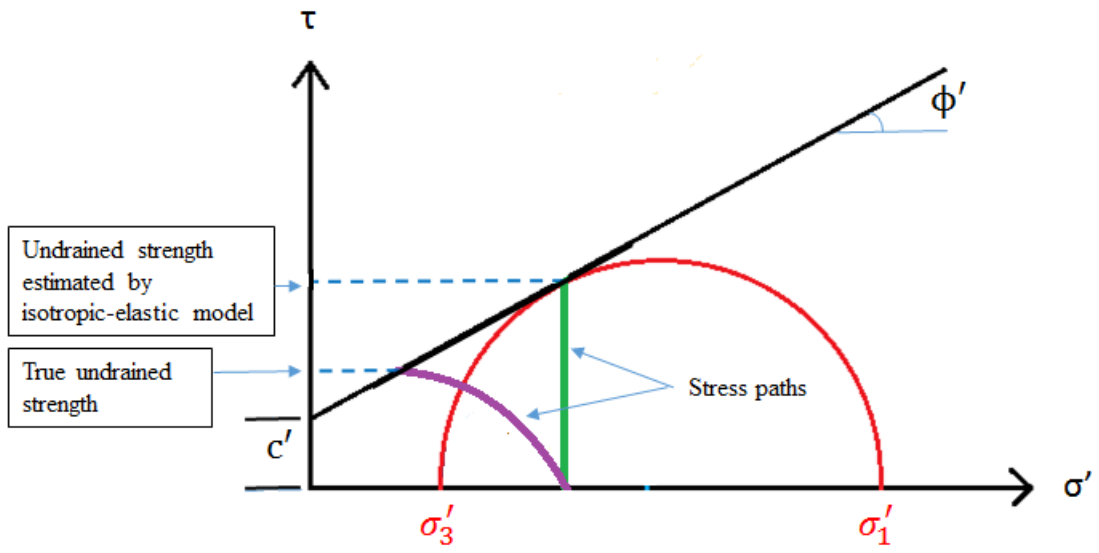

Fig. 6.9 Overestimation of shear strength when using effective stress parameters to model undrained conditions in the Mohr-Coulomb model

Depending on the deviance between the real and actual stress path it can be seen that the effective stress approach in Mohr-Coulomb models may lead to grossly overestimating the strength of the soil. This is not acceptable when the objective is to assess the capacity of suction anchors which is primarily dependent on the strength of the soil in which it resides. A bypass for this problem was to model the soil as a drained medium using undrained *total* stress parameters. Effective friction angle, ϕ' and the dilatancy angle, ψ is set to zero. As can be seen from equation 6.3 the cohesion parameter can be used to represent undrained shear strength. A drawback of this approach is that PLAXIS will make no distinction between effective stresses and pore pressures. All output values should therefore be interpreted as total stresses.

PLAXIS offer an option where incremental cohesion value can be entered as a function of depth, see equation 6.7. The soil model will therefore have a failure envelope which is independent of the stress path, and which increases with depth, see figure 6.10. An incremental value will also be added to the undrained stiffness parameter, E_u in order to achieve a more realistic model.

$$c'(y) = c'_{ref} + (y_{ref} - y)c'_{inc} \qquad y < y_{ref} \tag{6.7}$$

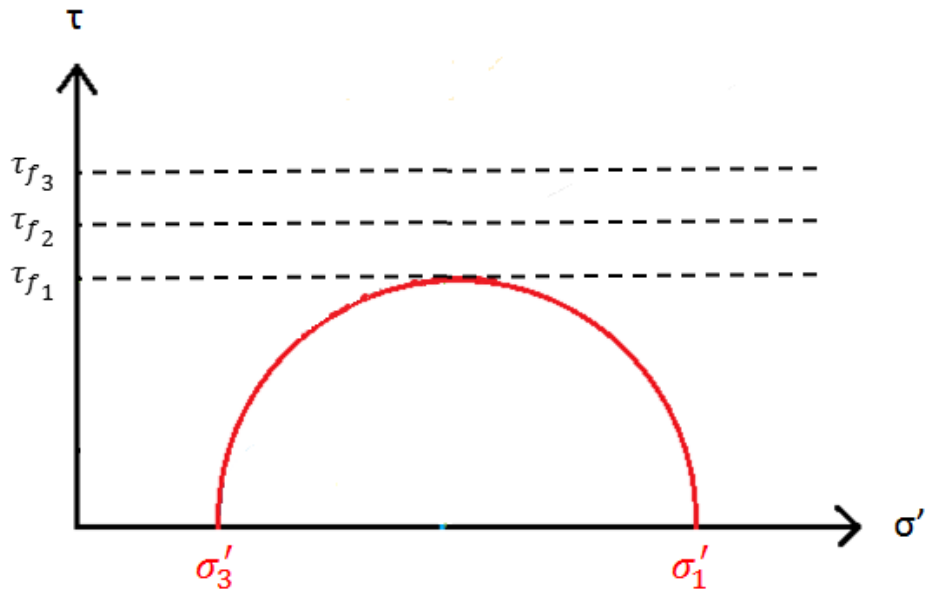

Fig. 6.10 Cohesion parameter used to define undrained shear strength as a function of depth

The undrained soil shear strength value, the incremental value, and the undrained Poisson ratio used in the model are based on values from clay at the Troll field, North Sea, Norway (Benz and Nordal, 2000). The overconsolidation ratio (OCR) and the plasticity index (PI) of Troll clay was found to be 1,5 and 20 percent respectively (Mayne, 2008). Table 6.2 was then used to derive the appropriate undrained stiffness, E_u to undrained shear strength, s_u relationship. A summary of undrained total stress parameters used in the base soil model can be seen in table 6.3.

Table 6.2 Relationship between undrained stiffness and undrained shear strength given the overconsolidation ratio and plasticity index, United States Naval Facilities Engineering Command (1982)

	E_u/s_u		
OCR	P I< 30	30 < PI < 50	PI > 50
< 3	**600**	300	125
3 - 5	400	200	75
> 5	150	75	50

Table 6.3 Soil parameters of base soil model in FEA

Soil parameters		
c_{ref}	3,68	kPa
c_{inc}	1,54 z	kPa
E_{ref}	2208	kPa
E_{incr}	924 z	kPa
k_x	0,0001	m^2
k_y	0,0001	m^2
ϕ'	0	$^\circ$
ψ	0	$^\circ$
γ_{unsat}	14	kN
γ_{sat}	16	kN
v_u	0,495	

6.1.2 Caisson material properties

The suction caisson itself is modelled as an axisymmetric problem using elastic 5-node plate elements, see figure 6.11 and 6.12. Plates in PLAXIS are composed of beam elements with three degrees of freedom per node (two for translation and one for rotation). The plate elements require input for flexural rigidity (EI), axial stiffness (EA), Poisson ratio (v), and weight (w). The thickness of the plate elements is obtained automatically as a function of EI and EA. Unrealistically large values for stiffness were used to ensure that the caisson remained rigid. Buckling of the caisson must be taken into consideration in a complete analysis as it may be the limiting factor for the load capacity.

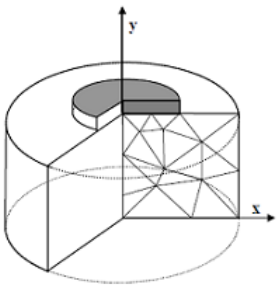

Fig. 6.11 Axisymmetric problem, PLAXIS (2008)

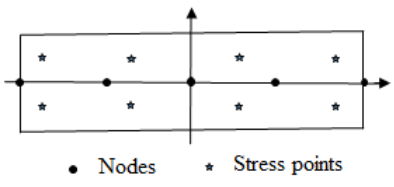

Fig. 6.12 5-node plate element

Interface elements are applied to the caisson-soil interface so that the interaction can be controlled. Without these elements the soil and the structure share nodes so that no relative displacement between the two is possible. A strength reduction factor, R_{inter} is used which relates the interface strength to the soil strength. R_{inter} is set to 0,5 which is a typical value for steel-clay interaction (Ou, 2006).

Note that the caisson self-weight is not taken into consideration in neither analytical calculations nor FEA. This is because the caisson weight is simply a constant addition to the capacity of the anchor. The magnitude of this addition naturally differs depending on the volume of the caisson. It is however not of interest when assessing the accuracy of presented analytical methods, or when analysing the parameters affecting the capacity. The weight can be added subsequently if desirable. Parameter values for the base plate model used for the caisson can be found in table 6.4.

Table 6.4 Material properties used for caisson in FEA

EA	1,40E+11	kN/m
EI	2,90E+07	kNm^2/m
d	0,05	m
v	0,15	

The soil volume used in the FEA was very large compared to the caisson itself. This was to minimize the influence from soil volume boundary conditions on deformations close to the caisson. Figure 6.13 show the model and mesh of a caisson with diameter 5 m (the model is axisymmetric) and length 10 m prior to load being applied. The geometry lines allow the mesh to be divided into zones. The global coarseness of the mesh is set to fine and the mesh quality is further refined in the vicinity of the caisson to increase the accuracy of the analysis.

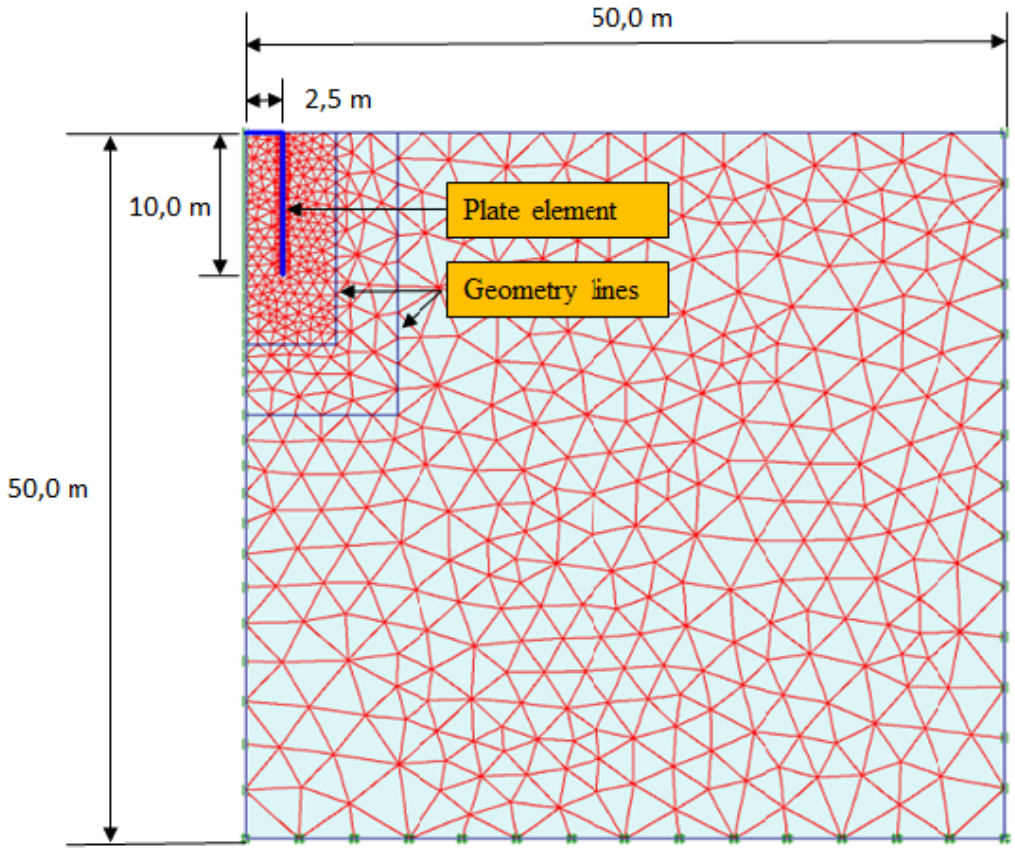

Fig. 6.13 Caisson and soil modelled in PLAXIS

Applied fixities and boundary conditions, PLAXIS (2008):

- Vertical geometry lines for which the x-coordinate is equal to the lowest or highest x-coordinate in the model obtain a horizontal fixity ($u_x = 0$).

- Horizontal geometry lines for which the y-coordinate is equal to the lowest y-coordinate in the model obtain a full fixity ($u_x = u_y = 0$).

- Plates that extend to the boundary of the geometry model obtain a fixed rotation in the point at the boundary ($\varphi_z = 0$) if at least one of the displacement directions of that point is fixed.

Failure criterion

The point at which many finite element analysis programs declare failure is when an infinitesimal load increment creates infinite displacement, in other words when the system is singular. However, this will require caisson displacement values greater than what is realistic. The chosen criterion was therefore to set the load capacity equal to the load applied at 2 meter displacement. This value was based on observations of load-displacement graphs which revealed that the yield plateau will in most cases be clearly defined by the time this displacement was reached, and therefore be close to the load singularity value within a satisfactory computation time.

Chapter 7

Results

7.1 Vertical uplift capacity

Figure 7.1 and 7.2 shows vertical pullout capacities of suction anchors obtained through FEM plotted against the analytical solutions derived in chapter 5. Key values are listed in table 7.1 and 7.2. An evaluation of the results can be found in chapter 8.

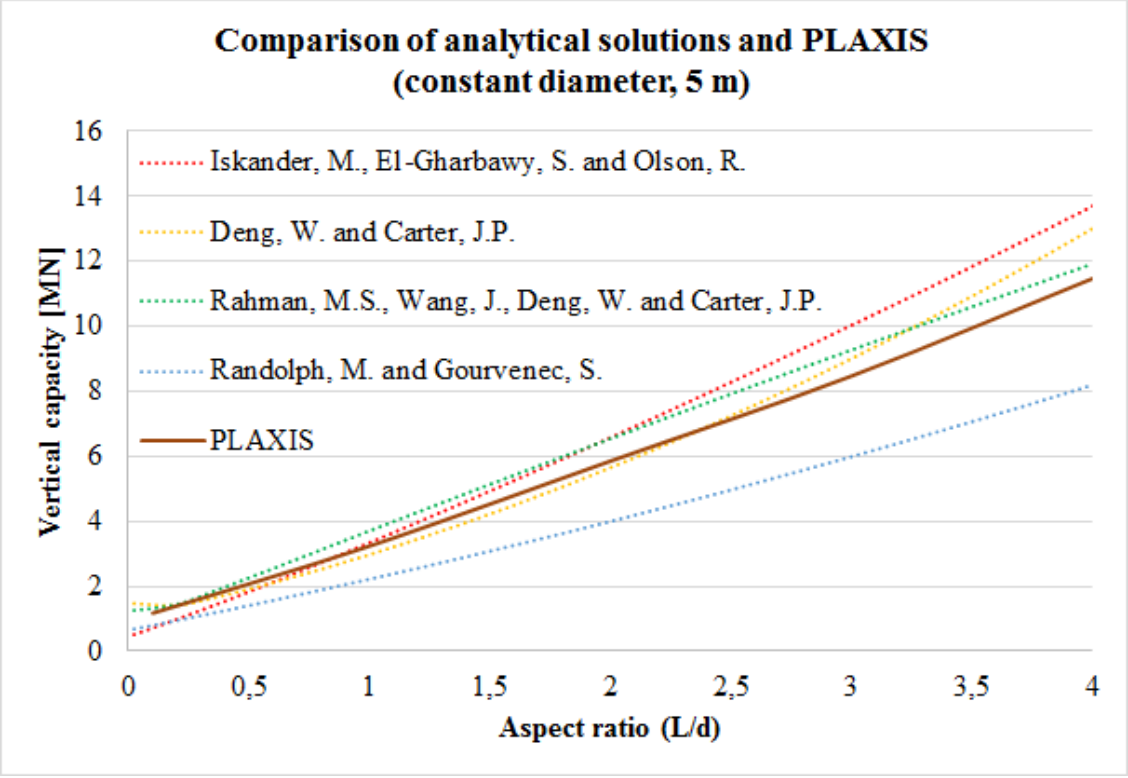

Fig. 7.1 Vertical pullout capacities of suction anchors obtained through FEM plotted against analytical solutions in the case of constant diameter, 5 m

Table 7.1 Key values from figure 7.1. Vertical capacities [MN] obtained through analytical solutions and FEM (PLAXIS) in the case of constant diameter, 5 m

Length [m]	Diameter [m]	Aspect ratio (L/d)	Randolph [MN]	Deng [MN]	Iskander [MN]	Rahman [MN]	PLAXIS [MN]
0,5	5	**0,1**	0,83	1,43	0,77	1,38	1,18
5	5	**1**	2,22	2,97	3,34	3,72	3,24
10	5	**2**	4,00	5,64	6,57	6,56	5,86
15	5	**3**	5,99	9,00	10,02	9,28	8,47
20	5	**4**	8,19	13,00	13,69	11,93	11,47

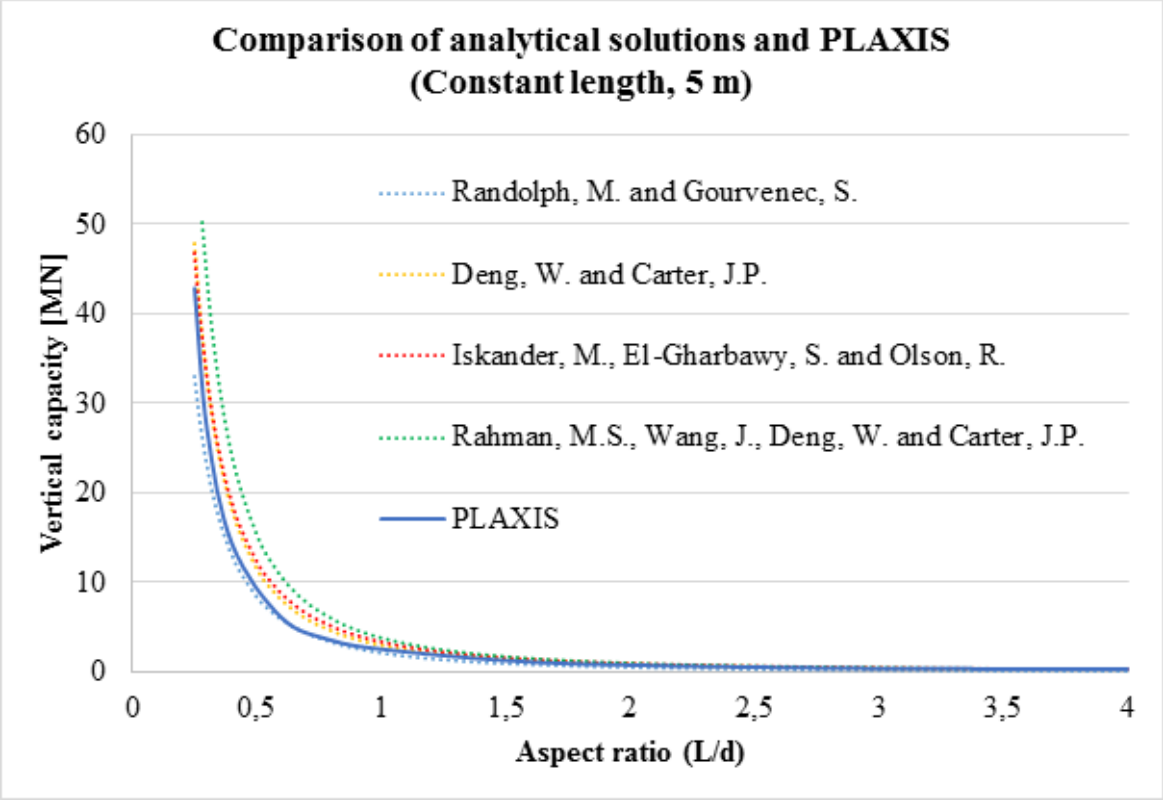

Fig. 7.2 Vertical pullout capacities of suction anchors obtained through FEM plotted against analytical solutions in the case of constant length, 5 m

Table 7.2 Key values from figure 7.2. Vertical capacities [MN] obtained through analytical solutions and FEM (PLAXIS) in the case of constant length, 5 m

Length [m]	**Diameter [m]**	**Aspect ratio (L/d)**	**Randolph [MN]**	**Deng [MN]**	**Iskander [MN]**	**Rahman [MN]**	**PLAXIS [MN]**
5	20,00	**0,25**	33,00	47,85	46,83	62,48	44,33
5	16,67	**0,3**	24,81	35,42	35,36	46,39	27,89
5	12,50	**0,4**	7,99	10,73	11,69	14,13	14,36
5	8,33	**0,6**	6,38	8,62	9,36	11,28	6,22
5	6,25	**0,8**	3,93	5,26	5,83	6,79	3,56
5	5,00	**1**	2,22	2,97	3,34	3,72	2,56
5	3,33	**1,5**	0,99	1,35	1,51	1,57	1,30
5	2,50	**2**	0,61	0,84	0,92	0,91	0,78
5	1,67	**3**	0,28	0,41	0,42	0,38	0,41
5	1,25	**4**	0,18	0,27	0,26	0,22	0,34

It is advantageous to study the development of the failure mechanism during loading to evaluate the plausibility of the results. A suction anchor with aspect ratio 3 (constant diameter, 5 m) is used for this purpose. The investigated loads can be seen on the load-displacement graph in figure 7.3, and the stress development in figure 7.4 and 7.5.

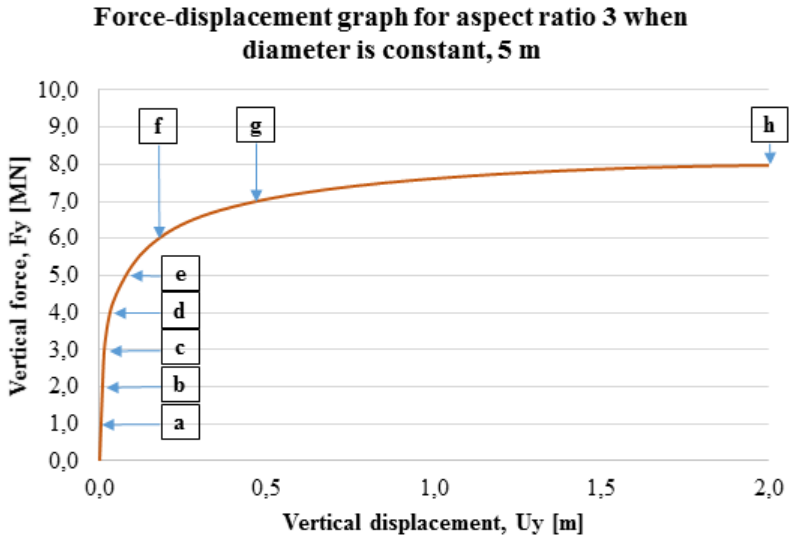

Fig. 7.3 Force-displacement graph for a caisson with aspect ratio 3 (constant diameter, 5 m). The figure also show stages during the load application which will be discussed in detail.

(a) $0,125 * F_{y,ult}$

The applied load is 12,5 % of the load applied at 2 m caisson displacement $(F_{y,ult})$. $F_{y,ult}$ is according to the established failure criteria the capacity of the anchor. At this applied load there is an upward displacement (fraction of a centimetre) of the soil within the caisson, and in the soil in immediate vicinity of the caisson external surface. Upward soil lift on the outside is caused by friction forces. The soil within the caisson is displaced approximately 25 % more than the soil outside. Mohr-Coulomb points, which indicate that stresses at this coordinate lies on the Mohr-Coulomb failure envelope, have started to form at the caisson tip, see figure 7.4. This can be attributed to stresses created by "soil flow" towards the bottom of the caisson as passive suction begins to mobilise, see figure 7.6.

(b) $0,25 * F_{y,ult}$

The number of Mohr-Coulomb points at the caisson tip have increased as more passive suction is mobilised. The total vertical displacement of the soil within the caisson and at the caisson tip equals that of the caisson itself. The vertical caisson displacement at point (b) is approximately 8,5 cm.

(c) $0,375 * F_{y,ult}$

The number of Mohr-Coulomb points at the caisson tip have grown and they have appeared along the entire length of the external caisson wall. This indicates that friction forces have developed to their maximum somewhere between point (b) and (c). The vertical caisson displacement at point (c) is approximately 14 cm.

(d) $0,5 * F_{y,ult}$

The Mohr-Coulomb cluster of failure points beneath the caisson tip starts to extend downwards and towards the centre of the caisson. The distance from the caisson at which soil is mobilised due to passive suction steadily increases. The load-displacement curve have at this load entered the elastic-plastic region.

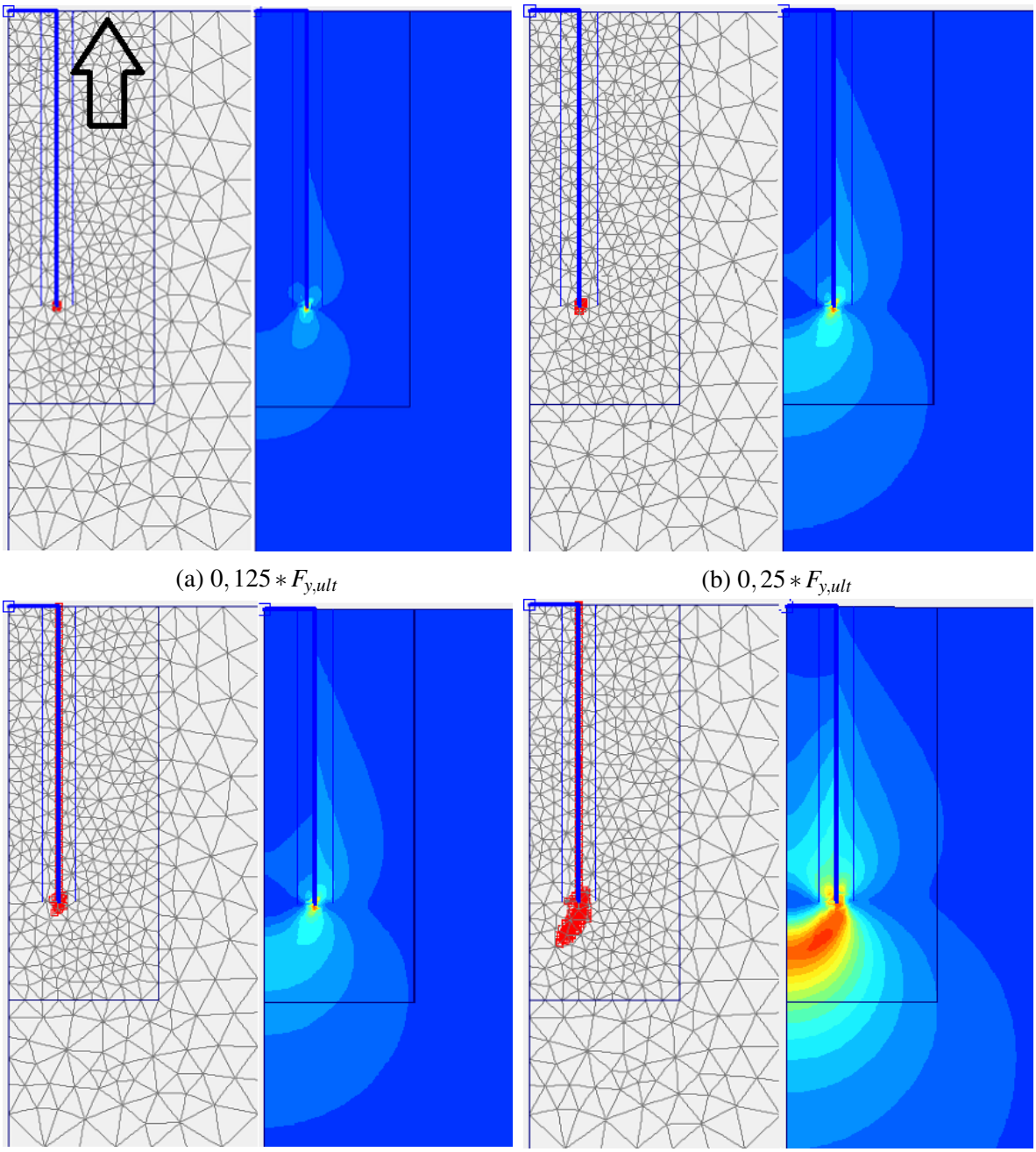

(a) $0,125 * F_{y,ult}$ (b) $0,25 * F_{y,ult}$

(c) $0,375 * F_{y,ult}$ (d) $0,5 * F_{y,ult}$

Fig. 7.4 Development of failure points and stress during vertical pullout, stages a-d

(e) $0,625 * F_{y,ult}$

As can be seen from figure 7.3 there is a significant increase in vertical caisson displacement from point (d) to (e) relative to earlier load increments. Mohr-Coulomb points form a half-sphere below the caisson. They have also appeared under the caisson top cap. The surrounding soil which is mobilised by the passive suction pulls on the soil column within the caisson. The soil column within the caisson is held in place by the suction force created by pumping water out from the top during installation. The weight of the soil and the applied suction have caused stresses to reach the failure envelope at the top of the caisson where the pressure differential is greatest, see figure 7.5.

(f) $0,75 * F_{y,ult}$

Increased mobilisation of soil have resulted in Mohr-Coulomb points developing further down the soil column within the caisson extending from the top cap. The half-sphere beneath the caisson has grown considerably. The passive suction have reached such a magnitude that soil close to the caisson, but above the tip, has started to displace downwards, see figure 7.7.

(g) $0,875 * F_{y,ult}$

Mohr-Coulomb points can now be found in the soil column at the entire length of the caisson. The half-sphere cluster of points have extended further above the caisson tip on the outside of the caisson. There is at this load a large relative displacement between the soil within- and outside the caisson. The passive suction now affects the soil all the way up to the mudline resulting in a very small downwards displacement of soil at the mudline (in the order of 10^{-6} m).

(h) $F_{y,ult}$

The ultimate vertical capacity of this anchor configuration has been reached according to the defined failure criterion. Figure 7.9 and 7.8 shows the displacement of the soil and the deformed mesh at this load stage. It can be seen from these figures that the tip of the caisson is a critical part of the caisson geometry with regards to soil failure. The number of Mohr-Coulomb points have increased dramatically and have appeared all the way up to the mudline.

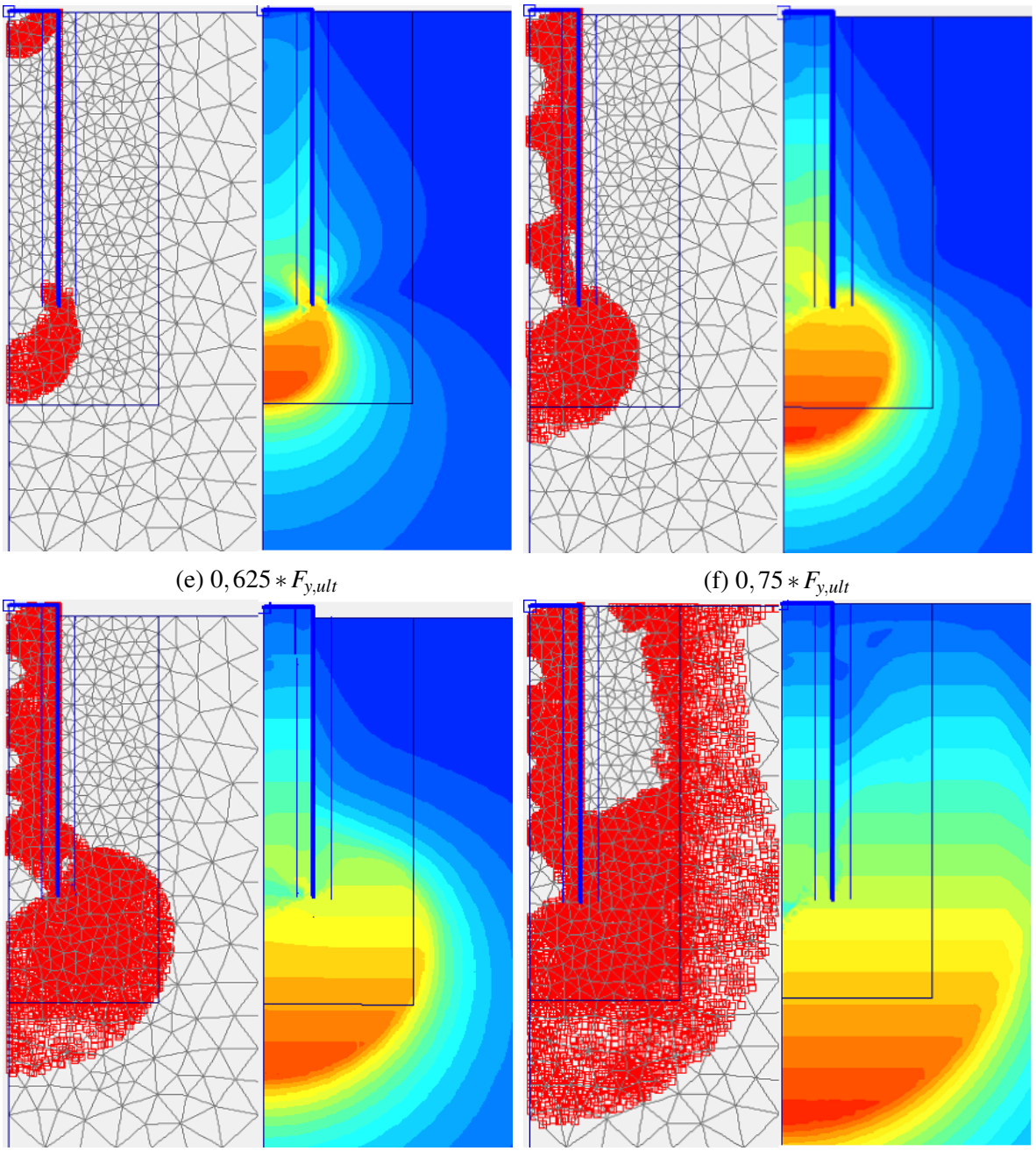

(e) $0,625 * F_{y,ult}$ (f) $0,75 * F_{y,ult}$

(g) $0,875 * F_{y,ult}$ (h) $F_{y,ult}$

Fig. 7.5 Development of failure points and stress during vertical pullout, stages e-h

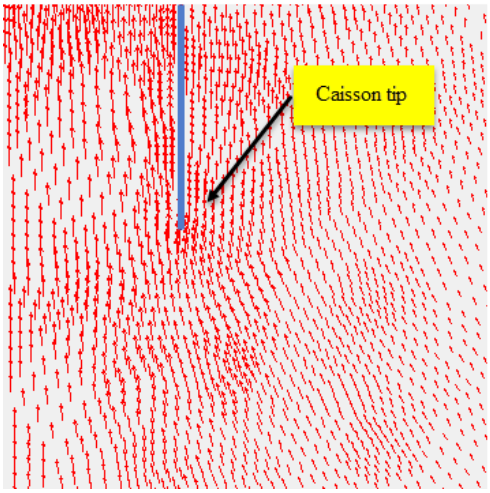

Fig. 7.6 Soil displacement around caisson tip at $0,125 * F_{y,ult}$

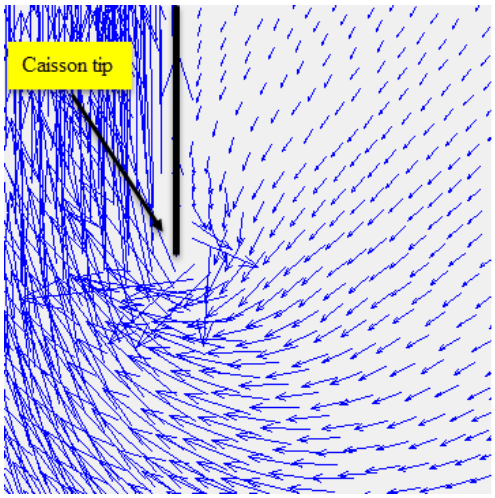

Fig. 7.7 Soil displacement around caisson tip at $0,75 * F_{y,ult}$

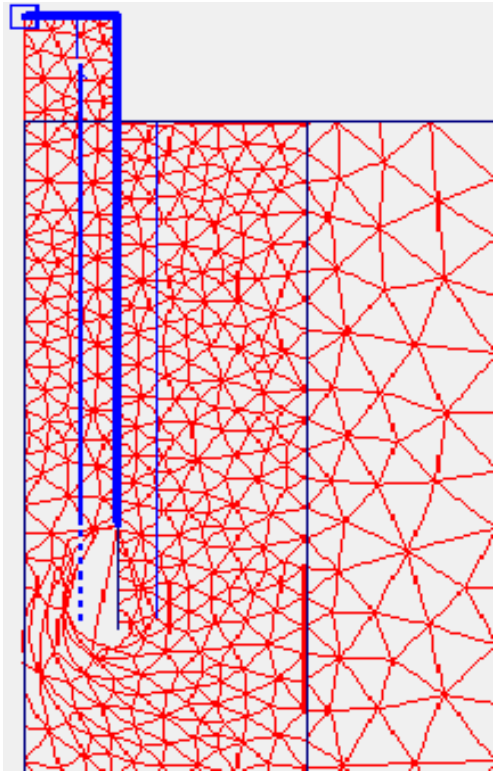

Fig. 7.8 Deformed mesh at 2 m vertical caisson displacement

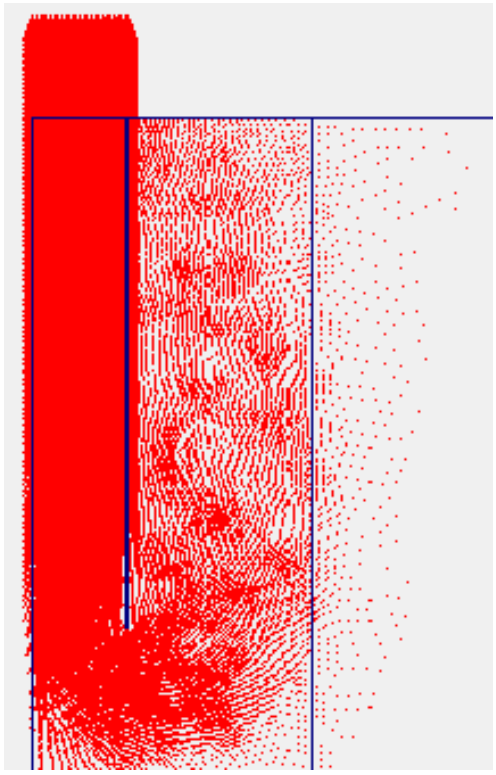

Fig. 7.9 Displacement of soil at 2 m vertical caisson displacement

7.2 Horizontal capacity

Figure 7.10 show horizontal (lateral) capacities of suction anchors obtained through FEM plotted against the analytical solutions derived in chapter 5. Key values are listed in table 7.3. An evaluation of the results can be found in chapter 8.

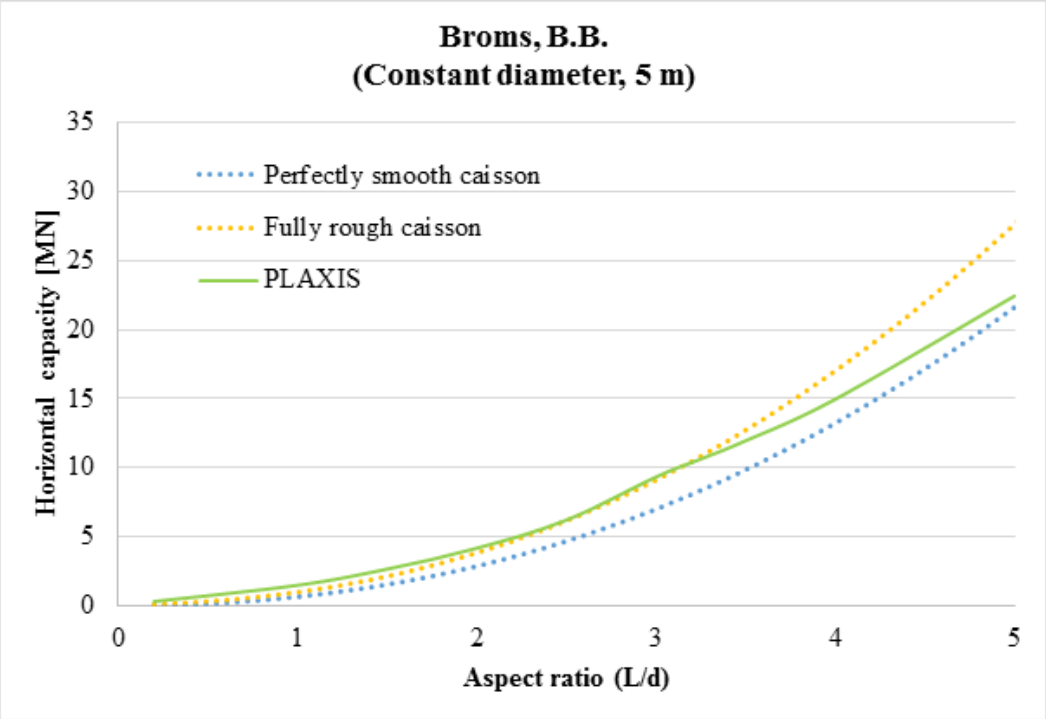

Fig. 7.10 Horizontal (lateral) capacities of suction anchors obtained through FEM plotted against analytical solutions in the case of constant diameter, 5 m

Table 7.3 Key values from figure 7.10. Horizontal (lateral) capacities [MN] obtained through analytical solutions and FEM (PLAXIS) in the case of constant diameter, 5 m

Length [m]	**Diameter** [m]	**Aspect ratio** (L/d)	**Broms (perfectly smooth caisson)** [MN]	**Broms (fully rough caisson)** [MN]	**PLAXIS** [MN]
1	5	**0,2**	0,05	0,07	0,32
5	5	**1**	0,71	0,94	1,50
10	5	**2**	2,92	3,79	4,17
15	5	**3**	7,03	9,06	9,10
20	5	**4**	13,24	16,96	15,34
25	5	**5**	21,59	27,58	22,43

It is advantageous to study the development of the failure mechanism during loading. Figure 7.12, 7.13, 7.14, and 7.15 shows the development of Mohr-Coulomb points (failure points) around a suction anchor caisson with diameter 5 m and length 25 m. It is subjected to fully horizontal loads towards the right. These loads are applied at two-thirds of the caisson length (at $z = 16,67m$).

$0,5 * F_{h,ult}$

Mohr-Coulomb points have appeared at the caisson tip and in the immediate vicinity of the upper part of the caisson wall. Stresses are greater on the side of the caisson at which the load is applied (frontside). Total displacements are at this point in the order of $10^{-3}m$.

$0,75 * F_{h,ult}$

Mohr-Coulomb points extend down the entire length of the caisson wall. They also extend from the caisson tip and outwards to a distance of approximately twice the caisson diameter.

$0,9 * F_{h,ult}$

Mohr-Coulomb points on the frontside have extended all the way to the surface. As can be seen from figure 7.11 there is a slight upwards displacement of the soil on the frontside, and a slight downwards displacement of the soil on the backside.

$F_{h,ult}$

Mohr-Coulomb points have reached the surface on both sides of the caisson, and complete failure has occurred. It is worth noting that the largest soil displacement is still in the order of $10^{-3}m$.

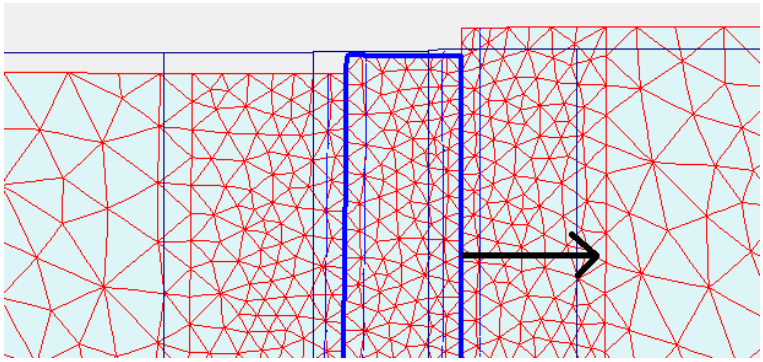

Fig. 7.11 Displacement of soil when $0,9 * F_{h,ult}$ is applied. Displacement are scaled up 15 times

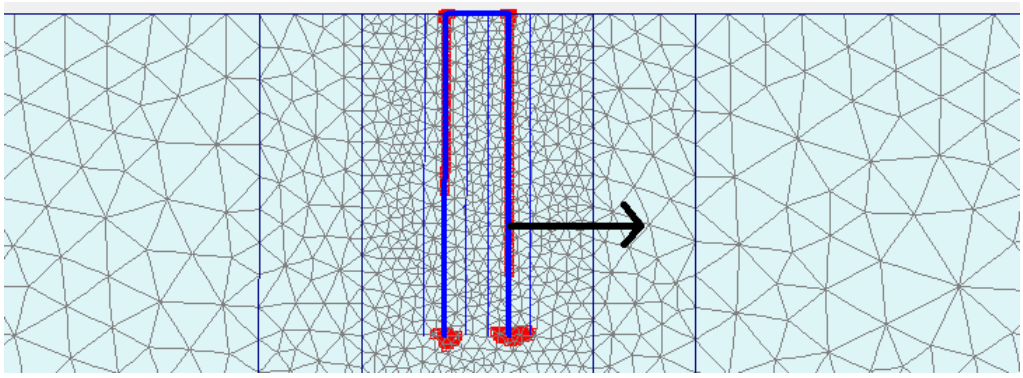

Fig. 7.12 Failure points caused by $0,5 * F_{h,ult}$ applied load

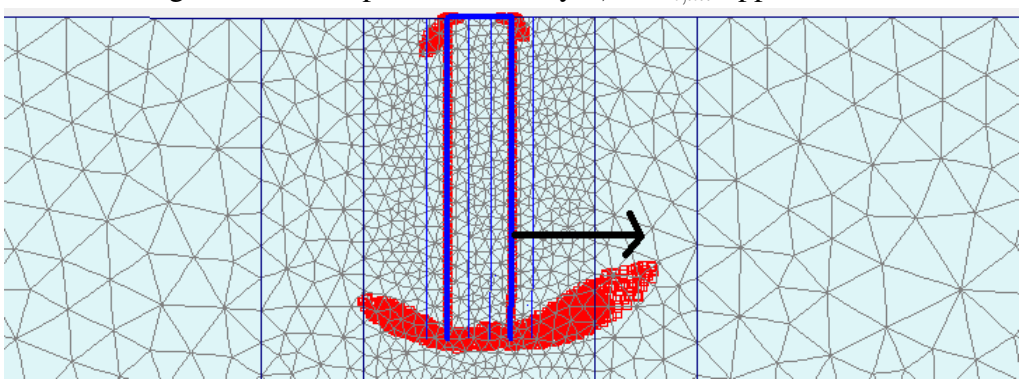

Fig. 7.13 Failure points caused by $0,75 * F_{h,ult}$ applied load

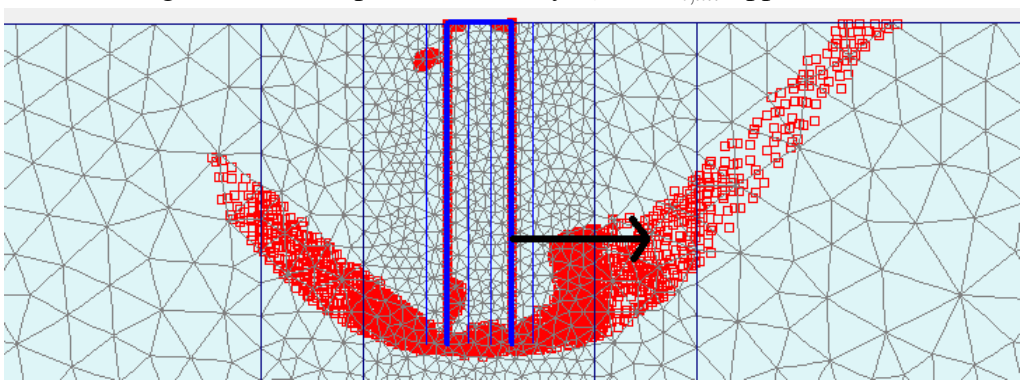

Fig. 7.14 Failure points caused by $0,9 * F_{h,ult}$ applied load

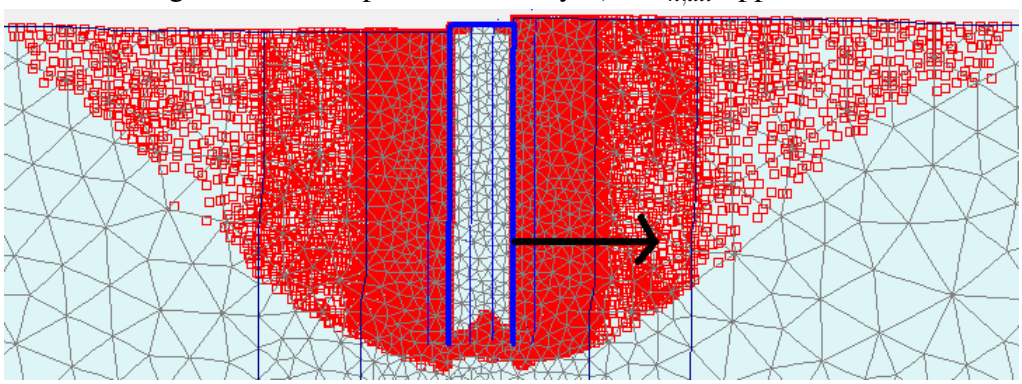

Fig. 7.15 Failure points caused by $F_{h,ult}$ applied load

7.3 Inclined capacity

It is first assumed that the optimum padeye location (load attachment point) of a suction anchor subjected to incline loading is at 2/3 of the total caisson length (2/3 L), i.e. on a 15 m long caisson the load should be attached 10 m from the top. Simulations were conducted to assess the optimal padeye location relative to the vertical centreline of the caisson. More precisely, should the load "centre of attack" be at 2/3 L of the vertical caisson centreline regardless of load angle, see figure 7.16, or at 2/3 L of the caisson wall, see figure 7.17.

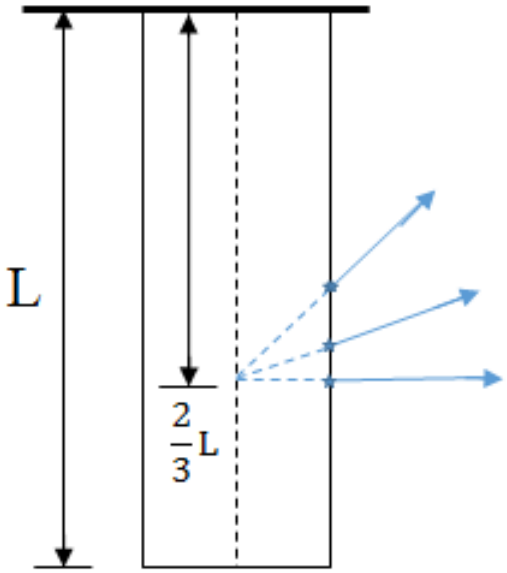

Fig. 7.16 Padeye located at 2/3 of the vertical caisson centreline regardless of load angle

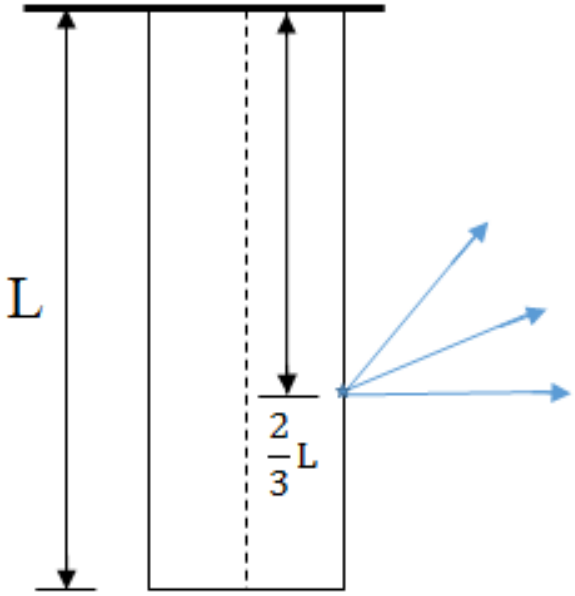

Fig. 7.17 Padeye located at 2/3 of the caisson wall

A caisson with aspect ratio 3 (diameter 5 m) was used for the simulations. Loads were applied in the two configurations seen in figure 7.16 and 7.17. The failure loads (taken as maximum anchor capacity) can be seen in figure 7.18 plotted in a horizontal-vertical (HV) load space. The results indicate a larger capacity at most load angles when the load "centre of attack" is at 2/3 L of the vertical caisson centreline regardless of load angle.

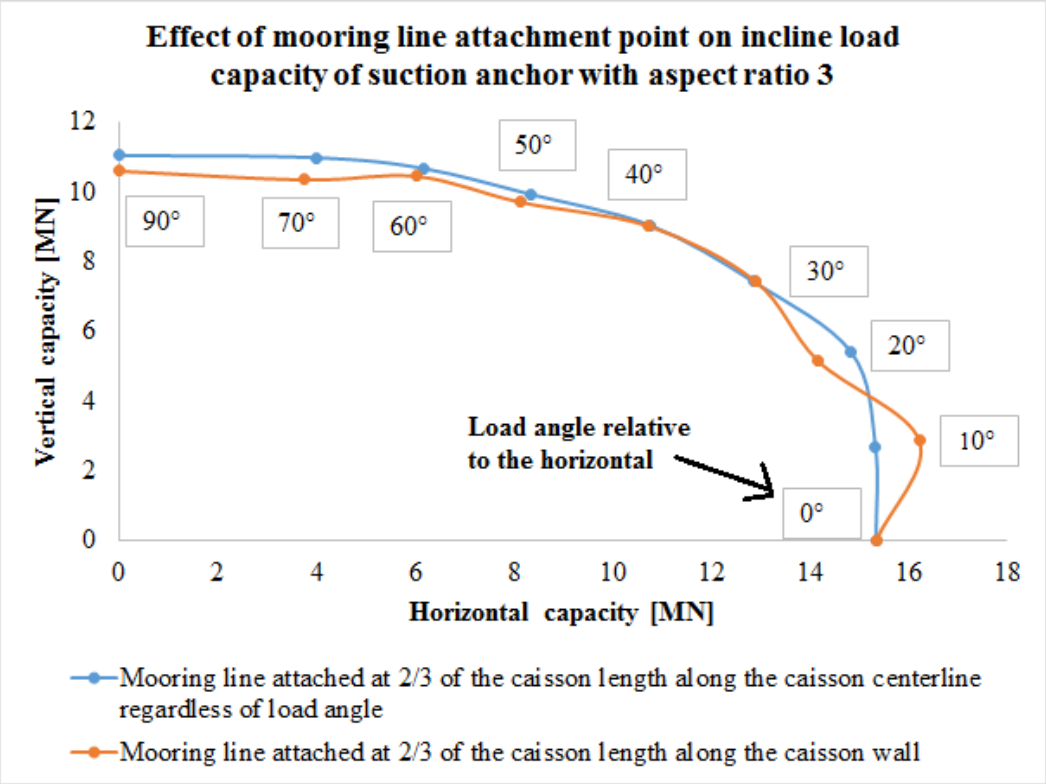

Fig. 7.18 Comparison of capacities obtained when padeye location is held constant with respect to caisson vertical centreline and to caisson wall

Given the results in figure 7.18 it was deemed necessary to further investigate the vertical placement of the padeye (which was set to 2/3 L in earlier calculations) due to the major influence it exerts on anchor capacity.

If the soil strength is isotropic the optimal placement will be at 1/2 L for a load angle of 0 degrees. However, because of the linear strength increase assumed in the applied soil model this will result in a forward tilt of the caisson, see figure 7.19. The optimum vertical padeye location for the soil model discussed in chapter 5 was found by applying a large number of loads to the caisson along the vertical centreline. Load angles of 20 degrees and 40 degrees were investigated, and the results can be seen in figure 7.20.

It can be observed from the results in figure 7.20 that maximum capacity can be achieved when padeye is located between 0,6 L and 0,7 L when small load angles are applied. As the load angle increases the optimum load angle will be higher up on the caisson. It can be seen that there is a larger reduction in capacity when the padeye is placed above the optimum location than when it is placed below. Due to this it was decided to continue using 2/3 L

as vertical padeye location when investigating incline loads on various aspect ratios with load angles ranging from 0 degrees to 90 degrees. Figure 7.21, 7.22, 7.23, and 7.24 shows the effect of loading a suction anchor with aspect ratio 3 above, at, and below the optimum padeye location.

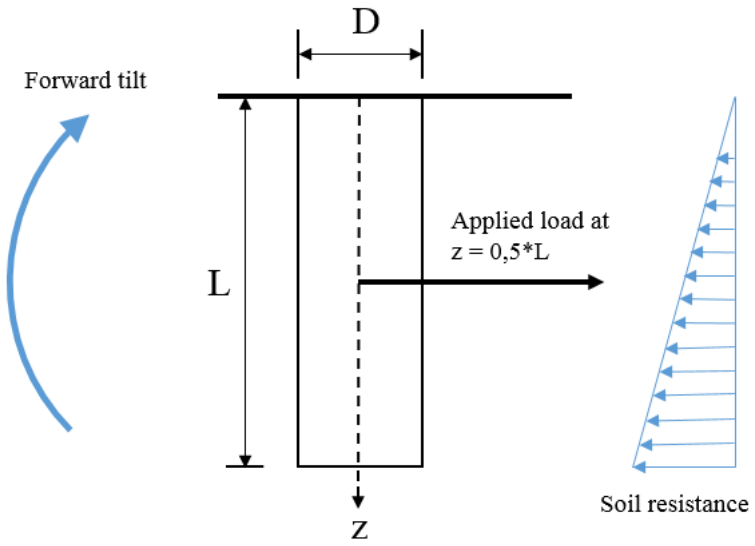

Fig. 7.19 Load applied at the wrong location may result in caisson rotation

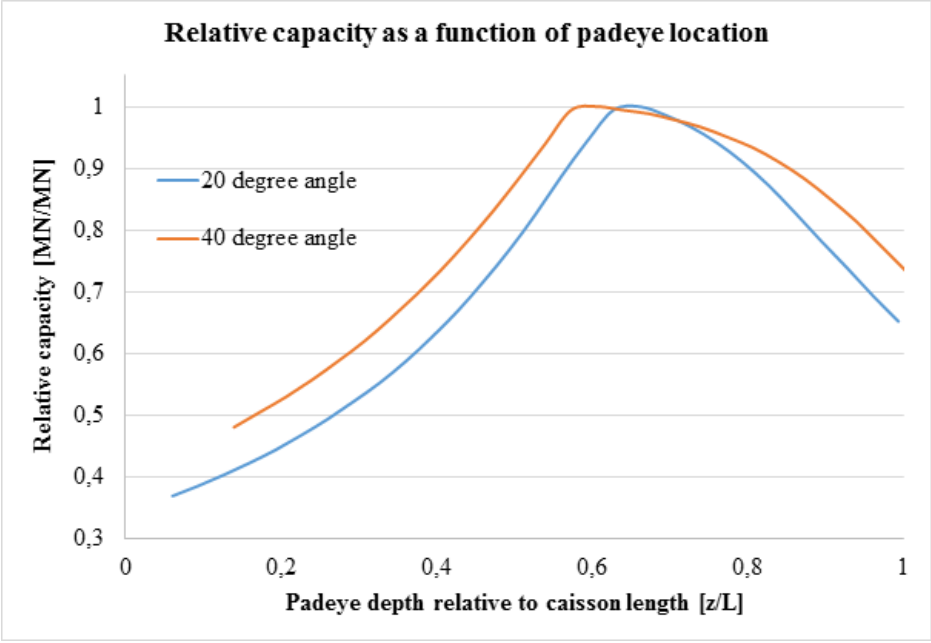

Fig. 7.20 Capacity of the anchor as a function of padeye location. Capacities are given as fractions of the largest capacity obtained

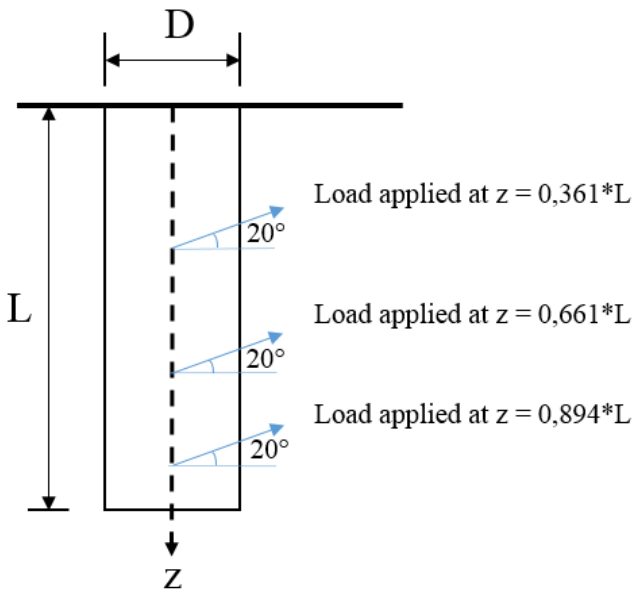

Fig. 7.21 Method used to determine which padeye location yields the largest capacity

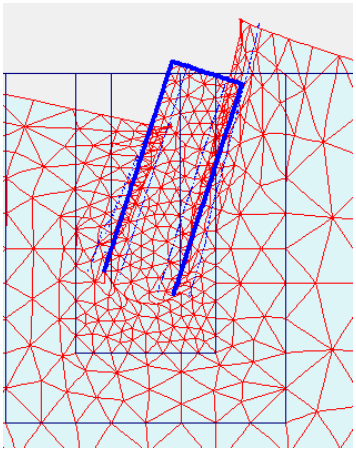

Fig. 7.22 Load applied at $z = 0,361 * L$

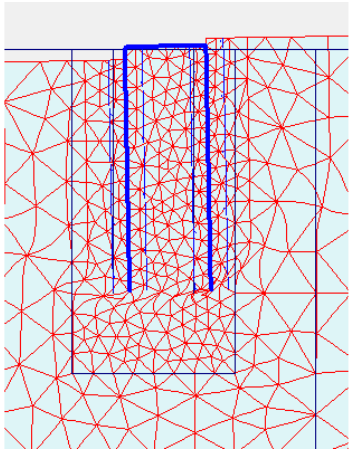

Fig. 7.23 Load applied at $z = 0,661 * L$

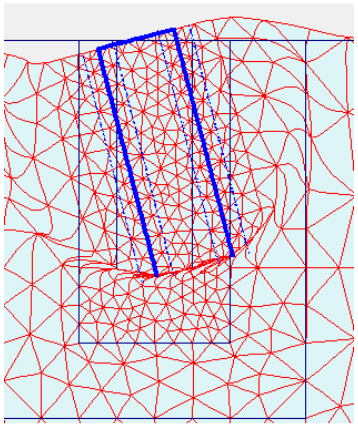

Fig. 7.24 Load applied at $z = 0,894 * L$

Simulations were subsequently done to investigate incline capacities of suction anchors with aspect ratio 3,4,5, and 6 (constant diameter 5 m) subjected to loads with inclination angle 0,10,20,30,40,50,60,70, and 90 degrees from the horizontal. The results are first presented with the values unaltered. Figure 7.25 show the results plotted in a horizontal-vertical load space. It also shows the analytical predictions obtained with equation 5.12. Figure 7.26 show the incline capacity, P as a function of load angle. P is found using equation 7.1.

$$P = \sqrt{F_h^2 + F_v^2} \tag{7.1}$$

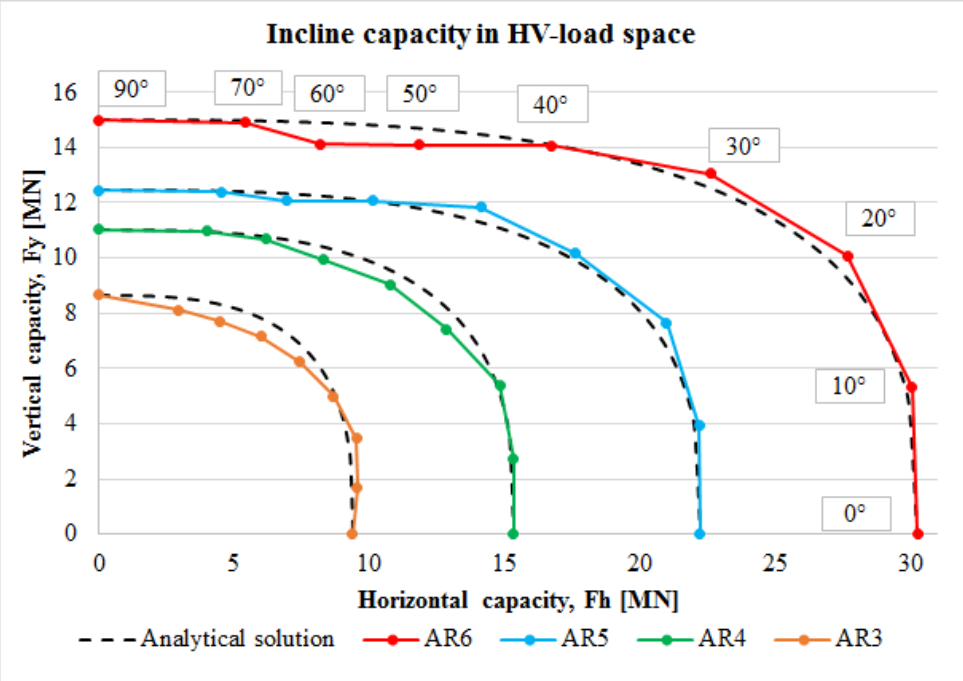

Fig. 7.25 Loads with load angles of 0,10,20,30,40,50,60,70, and 90 degrees from the horizontal are applied to the caisson at 2/3 L (with respect to the caisson vertical centreline) until maximum capacity is reached. The maximum capacity is plotted in a horizontal-vertical load space where they are compared with analytical solutions obtained through equation 5.12

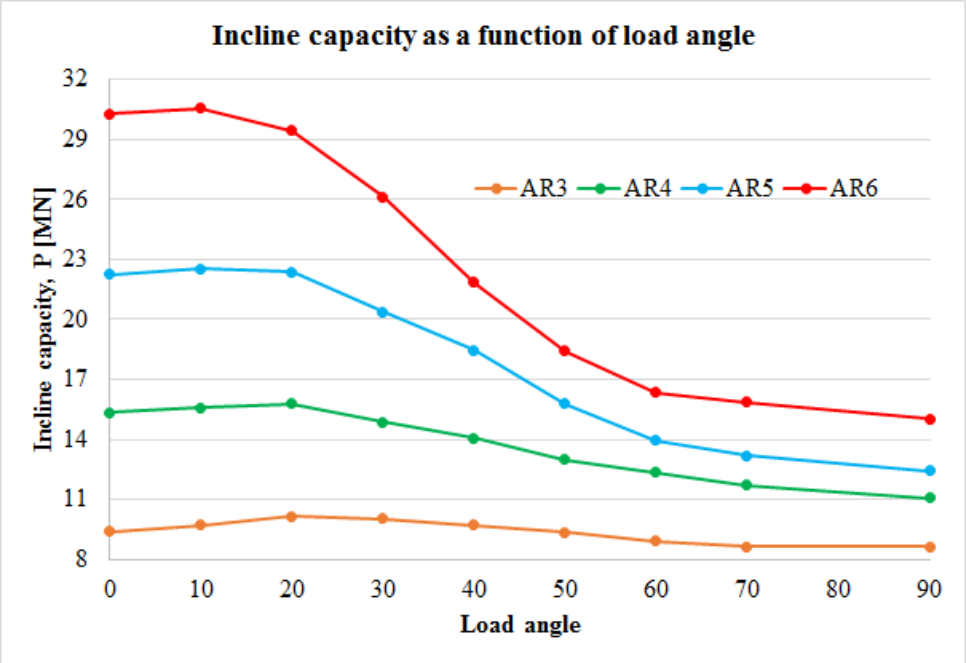

Fig. 7.26 The incline capacity value, P obtained with equation 7.1 is plotted against load angles between 0 degrees and 90 degrees from the horizontal

To simplify and parametrize the problem it was decided to normalize the results. Figure 7.27 and 7.28 presents the results from figure 7.25 and 7.26 normalized with respect to caisson diameter, caisson length, and average undrained shear strength, using equation 7.2 and 7.3.

$$N_v = \frac{F_v}{LD_0 s_{u,avg}} \tag{7.2}$$

$$N_h = \frac{F_h}{LD_0 s_{u,avg}} \tag{7.3}$$

where:

$$s_{u,avg} = \frac{s_u(L) + s_u(0)}{2}$$

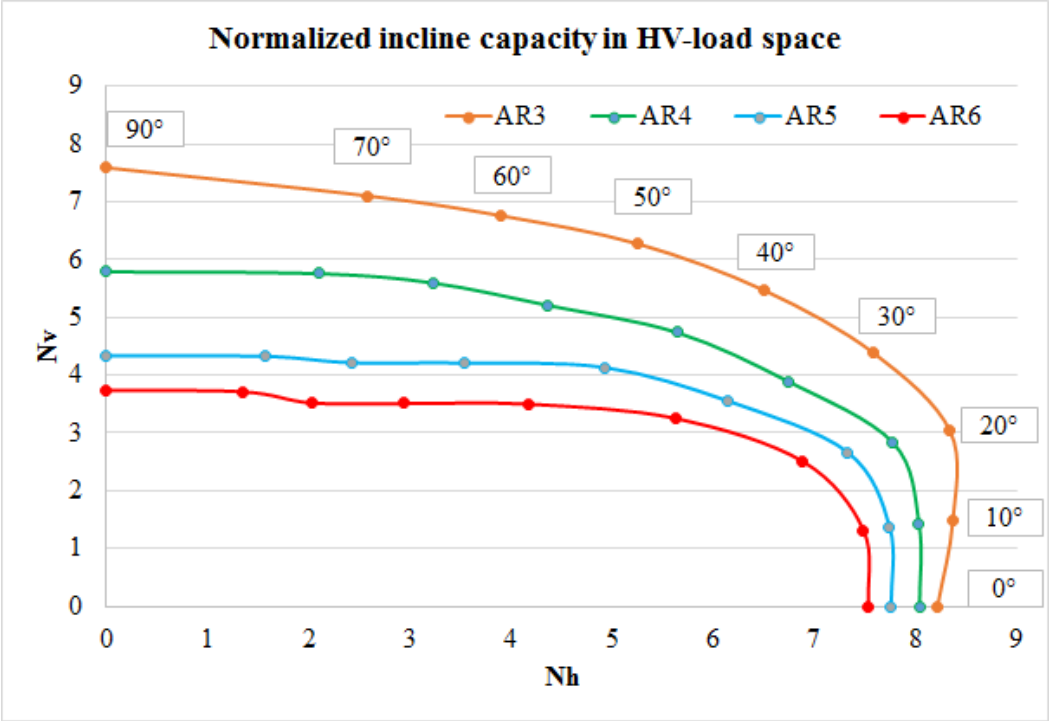

Fig. 7.27 The results shown in figure 7.25 are normalized using equation 7.2 and 7.3

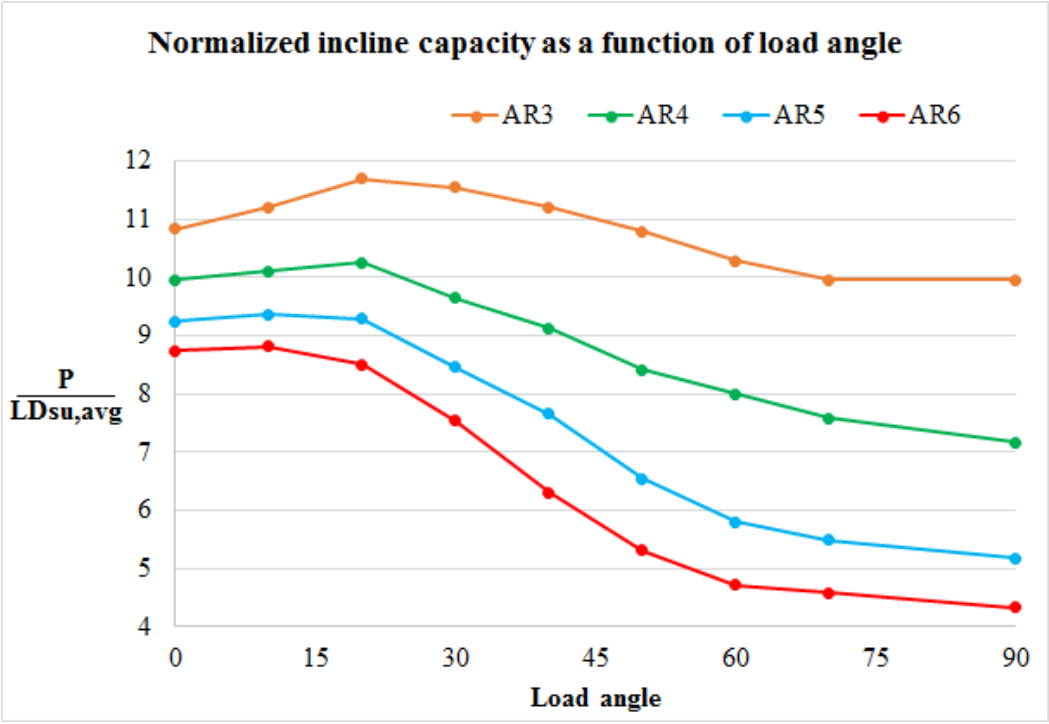

Fig. 7.28 The results shown in figure 7.26 are normalized with respect to soil strength, caisson length and caisson diameter

Chapter 8

Discussion

8.1 Vertical uplift capacity evaluation

From figure 7.5 it can be seen that the capacity of suction anchors subjected to vertical loading in undrained soil appears to be limited by reverse end bearing failure. When diameter is held constant the FEA results correspond quite well with analytical solutions for small to medium aspect ratios. It matches the solution from equation 5.7 especially well up to an aspect ratio of 2,5. From 2,5 the FEA results retain a linear increase in capacity, while the solution from equation 5.7 show exponential growth. This exponential growth is largely attributed to the applied embedment factor ($\zeta_{ce} = 1 + 0,4\left(\frac{L}{d}\right)$). It is also of interest that this is a semi-empirical equation derived through FEA with a Modified Cam-Clay model. Deviations in results from the Modified Cam-Clay model and Mohr-Coulomb model may be attributed to how these models estimate friction and magnitude of passive suction. A parameter analysis is done in section 8.4 where the objective is to further investigate the FEA results.

8.2 Horizontal capacity evaluation

Horizontal capacity shown in figure 7.10 predicted by FEA exceeds that predicted by equation 5.11 with a fully rough caisson when aspect ratios are in the 0,2 to 2,5 range. For aspect ratios between 2,5 and 5 the FEA give an almost linear increase in capacity, while the analytical solution tends to grow exponentially.

From figure 7.12, 7.13, 7.14, and 7.15 it can be seen that the Mohr-Coulomb points do not extend much below the caisson tip. Instead, the large stresses (and eventually soil failure)

can be found in front of the caisson where soil is being compressed, behind the caisson where soil is subject to tension, and just beneath the caisson where there is "soil flow". From the lack of failure points beneath the caisson, as well as the relatively small total displacement ($10^{-3}m$) it is reasonable to suggest that horizontal capacity depends little on passive suction, but rather on cross-sectional area and soil strength. This is supported by figure 8.1 which show the normalized horizontal capacity as a function of aspect ratio. Note that diameter is held constant (5 m) so the normalized capacity is in reality shown as a function of embedment depth. It can be seen that from aspect ratio 1,5 (corresponding to 7,5 m embedment) and up to 5 the normalized capacity approaches a constant value. The large initial values is likely to be because the contribution from passive suction is added almost immediately upon soil contact (and stays approximately constant) while the cross-sectional area is very small. The contribution from passive suction gradually becomes small compared to the contribution from the vertical cross-sectional area which is why the normalized horizontal capacity approaches a constant value.

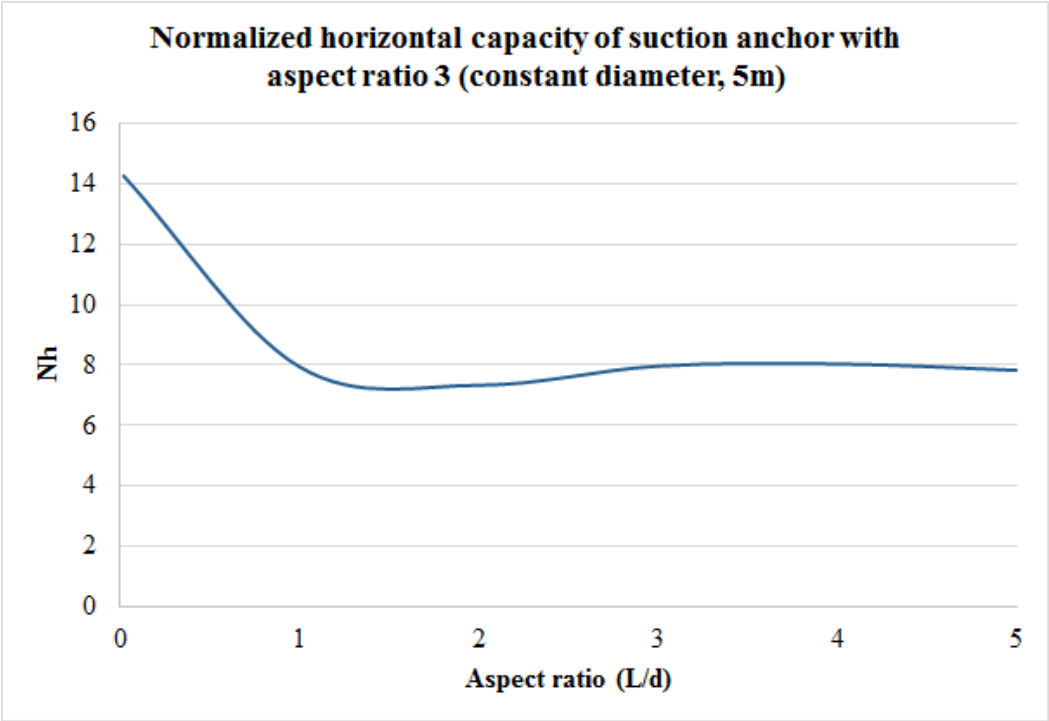

Fig. 8.1 The horizontal capacity shown in figure 7.10 is normalized using equation 7.3

8.3 Incline capacity evaluation

Optimum padeye location was investigated. The results confirmed what was presented in chapter 3 section 3.5. However, to reduce computation time the optimum location was taken as 2/3 of caisson length regardless of load angle. This does not result in maximum capacity for all load angles as can be seen from figure 7.20. If the padeye location was to be adjusted for each load angle then there would be some increase in the capacities. From figure 7.25 and 7.26 it can be seen that an increase in aspect ratio results in a greater increment in horizontal capacity than in vertical capacity. The largest values are obtained with load angles between 10 degrees and 20 degrees. FEA results correspond nicely with the failure envelope given by equation 5.12 for all aspect ratios analysed.

Failure mechanisms for a suction anchor subjected to a range of load angles between 0 degrees and 90 degrees can be found in appendix A.

8.4 Parameter analysis

Because soil shear strength was defined as a function of depth only ($3,68 + 1,54z$) and not as a function of effective cohesion, effective normal stress, and effective friction angle (equation 6.3) it is impossible to test how the latter parameters influence the pullout capacity in the constitutive model. The pullout capacity (and installation resistance) will increase if the shear strength increase given that the ratio between undrained stiffness and undrained shear strength remains the same or increases.

Strength reduction factor, R_{inter}

As discussed in chapter 6 section 6.1.1 a strength reduction factor, R_{inter} is used which relates the interface strength to the soil strength. More specifically it specified the magnitude of soil cohesion and friction force which is transferred to the caisson. From figure 8.2 we can see that for $R_{inter} = 0,4$ to $R_{inter} = 1$ there is an approximately linear increase in the capacity of the anchor. R_{inter} values below 0,4 cause a large reduction in capacity.

The applied value for R_{inter} was 0,5 which is typical for a steel-clay interaction. However, the exact value for this parameters should be investigated at location as relatively small deviations from this value cause severely impacts the capacity. This value will naturally also impact the soil resistance during installation.

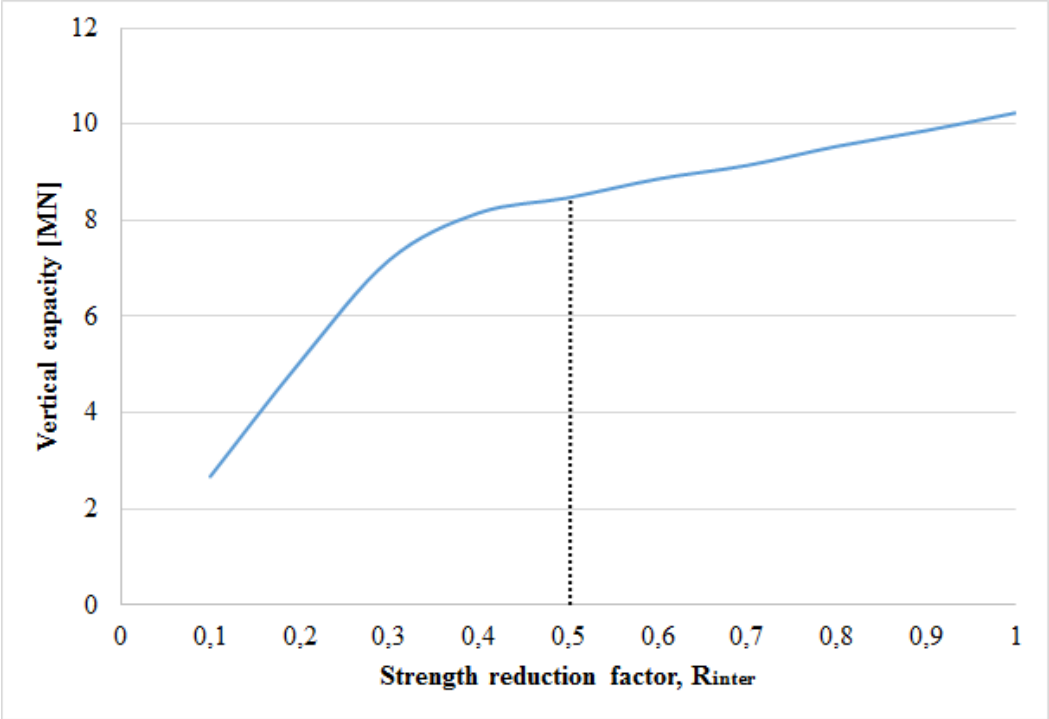

Fig. 8.2 Effect of interface strength reduction factor, R_{inter} on vertical capacity of a caisson with aspect ratio 3. The remaining soil parameters are as given in table 6.3

Poisson's ratio

It has been stated that the Mohr-Coulomb model assumes elastic-perfectly plastic behaviour where no volumetric change is allowed during loading in undrained conditions. From elasticity theory of isotropic materials the Poisson's ratio can only be 0,5 if the criteria of no volumetric change is to be upheld, see equation 8.1. This parameter is therefore not subject to further investigation. The applied value of Poisson's ratio in the FEA was 0,495 because 0,5 caused a singularity in the stiffness matrix.

$$\frac{\Delta V}{V} = (1-2\nu)\frac{\Delta L}{L} \tag{8.1}$$

Undrained stiffness to undrained shear strength ratio

The applied value for E_u/s_u during the calculations was 600. The reasoning for this value was explained in chapter 6 subsection 6.1.1. Increasing the E_u/s_u ratio above that of 600 will according to figure 8.3 cause a small reduction in capacity. E_u/s_u values of 200 or less cause a major reduction in capacity.

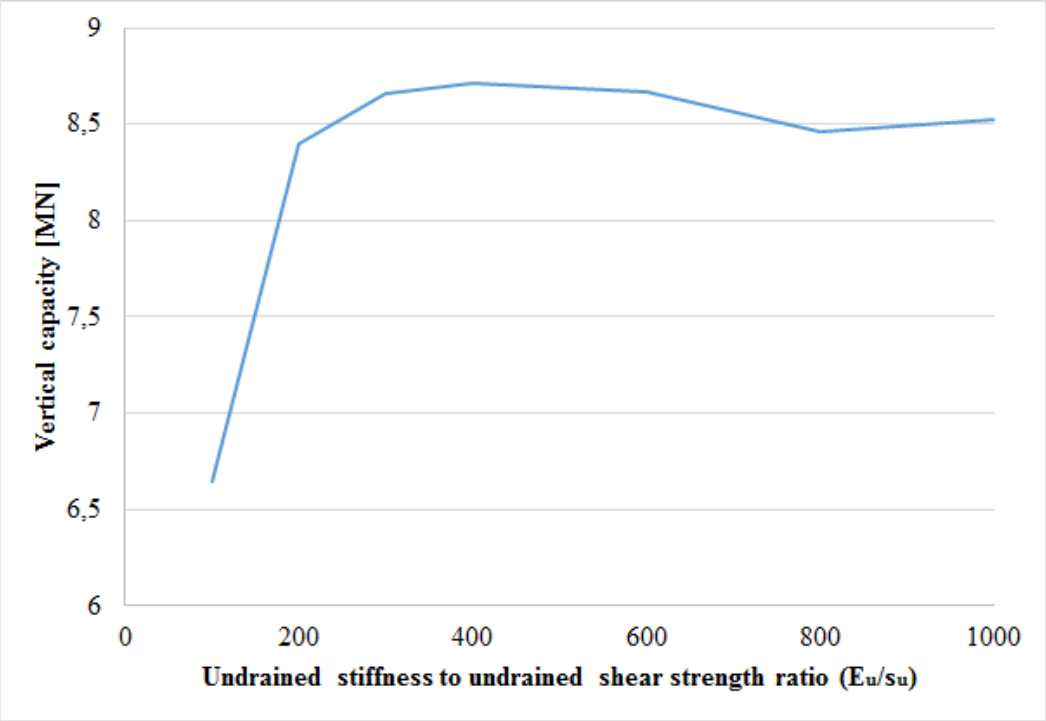

Fig. 8.3 Effect of undrained stiffness to shear strength ratio on the vertical capacity of a caisson with aspect ratio 3. Undrained stiffness is altered, and the remaining soil parameters are as given in table 6.3

Modelling considerations

The caisson geometry used in the calculations is idealized. In a real case there are padeyes, stiffeners, and other protrusion which affect the installation and operation. The results do not take into account the caisson self-weight and overburden water pressure. This was done mainly to simplify the model and reduce computation time.

Chapter 9

Conclusion and further work

Load capacity and failure modes of suction anchors subjected to vertical, horizontal, and incline loading was investigated in this thesis. The thesis is limited to loading conditions in undrained soil with linear strength development. Finite element analyses (FEA) was conducted based on a Mohr-Coulomb failure envelope defined through undrained total stress parameters.

In all studied cases it was found that the capacity of a suction anchor increases when the volume of the caisson increases.

From FEA it was found that the pullout capacity of a suction anchor subjected to vertical loading increases approximately linearly with increments in caisson length (constant caisson diameter) in the specified soil conditions. The most critical point on the caisson geometry with respect to stress developments during loading was found to be the caisson tip. This is also a critical point for suction anchors subjected to horizontal or incline loads. The cause is attributed to soil flow.

Suction anchors in undrained soil subjected to vertical pullout loads develop a reverse bearing mechanism as the applied load approaches the maximum capacity.

The development of Mohr-Coulomb points (failure points) in simulations, and study of normalized capacity graphs indicate that the horizontal capacity of a suction anchor (no rotation) is primarily a function of caisson vertical cross-sectional area and soil strength profile once the embedment has reached a certain depth. Little to no passive suction was observed to develop beneath the caisson.

Optimum padeye location (mooring line attachment point) for incline loads was investigated for load angles of 20 degrees and 40 degrees. Load angles are measured relative to the horizontal. For a load angle of 20 degrees the optimum location was at 0,66 L (two thirds) of total caisson length along the vertical centreline. Placing the padeye at 0,56 L resulted in a reduction in capacity of 11,3 percent. For a 40 degree load angle the optimum padeye location was at 0,61 L.

Suction anchor capacity was investigated for a load angles between 0 degrees and 90 degrees when the load is applied at the optimal padeye location. It was found that the largest capacities is achieved with load angles between 10 degrees and 20 degrees to the horizontal. The failure envelope formed by plotting the horizontal capacity component against the vertical capacity component fit nicely with the elliptical equation 9.1 (Supachawarote et al., 2004)

$$\left(\frac{H}{H_{ult}}\right)^{a} + \left(\frac{V}{V_{ult}}\right)^{b} = 1 \tag{9.1}$$

where:

$H =$ Horizontal load component
$V =$ Vertical load component
$a = 3$
$b = 3$

Further work could investigate soil drainage conditions when a static load is applied to the suction anchor for a long period of time, e.g. TLP mooring system. It would also be of interest to study how cyclic loading on the anchor affects the soil strength.

References

Ahn, J., Lee, H., Choi, B., and Kim, Y. (2013). Holding capacity of suction caisson anchor in uniform clays based on finite element analysis. The Twenty-third International Offshore and Polar Engineering Conference, 30 June-5 July, Anchorage, Alaska.

Andersen, K. H. and Jostad, H. P. (1999). Foundation design of skirted foundations and anchors in clay. Offshore Technology Conference, 3rd June, Houston, Texas.

Andersen, K. H. and Jostad, H. P. (2004). Shear strength along inside of suction anchor skirt wall in clay. Offshore Technology Conference, 3rd May, Houston, Texas.

Aubeny, C. and Murff, J. D. (2005). Simplified limit solutions for the capacity of suction anchors under undrained conditions. *Ocean engineering*, 32(7):864–877.

Bai, Y. and Bai, Q. (2010). *Subsea structural engineering handbook*. Gulf Professional, Burlington, Mass.

Beardmore, R. (2011). Stress & strain. Online; accessed 23rd April 2015 from http://www.roymech.co.uk/Useful_Tables/Mechanics/Strain.html.

Benz, T. and Nordal, S. (2000). *Numerical Methods in Geotechnical Engineering: (NUMGE 2010)*. Taylor & Francis.

Broms, B. B. (1964). Lateral resistance of piles in cohesive soils. *Journal of the Soil Mechanics and Foundations Division*, 90(2):27–64.

Cao, J., Audibert, J. M. E., Al-Khafaji, Z., Phillips, R., and Popescu, R. (2002). Penetration resistance of suction caissons in clay. The Twelfth International Offshore and Polar Engineering Conference, 26-31 May, Kitakyushu, Japan.

Clukey, E.C., B. H. K. F. (2000). Reliability assessment of deepwater suction caissons. Offshore Technology Conference, 1-4 May, Houston, Texas.

Clukey, E. C., Morrison, M. J., Gamier, J., and Corte, J. F. (1995). The response of suction caissons in normally consolidated tlp loading conditions. Offshore Technology Conference, 1st May, Houston, Texas.

Colliat, J. L., Boisard, P., Gramet, J. C., and Sparrevik, P. (1996). Design and installation of suction anchor piles at a soft clay site in the gulf of guinea. Offshore Technology Conference, 6-9 May, Houston, Texas.

Cotter, O. (2009). *The installation of suction caisson foundation for offshore renewable energy structures*. PhD thesis, Oxford University Press.

Craig, R. (2004). *Craig's Soil Mechanics, Seventh Edition*. CRC Press.

Deng, W. and Carter, J. P. (2000). A theoretical study of the vertical uplift capacity of suction caissons. The Tenth International Offshore and Polar Engineering Conference, 28 May-2 June, Seattle, Washington, USA.

DNV (1992). Classification notes no 30.4 foundations. Oslo, Norway. Det Norske Veritas Classification AS.

DNV (2005). Dnv recommended practice rp-e303: Geotechnical design and installation of suction anchors in clay. Hovik, Norway. Det Norske Veritas Classification AS.

ExxonMobil Development Company (2000). Suction pile design specification, emdc-bre-c-js-0332.1001.

Fines, S., Stole, O. J., and Guldberg, F. (1991). Snorre tlp tethers and foundation. Offshore Technology Conference, 6th May, Houston, Texas.

Goodman, L., Lee, C., and Walker, F. (1961). The feasibility of vacuum anchorage in soil. *Geotechnique*, 1(3):356–359.

Hogervorst, J. R. (1980). Field trails with large diameter suction piles. Offshore Technology Conference, 5th May, Houston, Texas.

Houlsby, G. and Byrne, B. (2004). *Calculation Procedures for Installation of Suction Caissons*. University of Oxford: Department of Engineering-Science.

Huang, J., Cao, J., and Audibert, J. M. E. (2003). Geotechnical design of suction caisson in clay. The Thirteenth International Offshore and Polar Engineering Conference, 25-30 May, Honolulu, Hawaii, USA.

Iskander, M., El-Gharbawy, S., and Olson, R. (2002). Performance of suction caissons in sand and clay. *Canadian geotechnical journal*, 39(3):576–584.

Lambe, T. and Whitman, R. (1969). *Soil Mechanics*. Wiley.

Leeder, M. and Arlucea, M. (2009). *Physical Processes in Earth and Environmental Sciences*. John Wiley & Sons.

Mayne, P. (2008). Piezocone profiling of clays for maritime site investigations. 11th Baltic Sea Geotechnical Conference, Geotechnics in Maritime Engineering, Gdansk, Poland, 15-18 September.

Mitchell, James, K. (1981). *Thixotropy*, chapter 143, pages 507–509. Encyclopedia of Earth Science. Springer US.

Neubecker, S. R. and Randolph, M. F. (1995). Performance of embedded anchor chains and consequences for anchor design. Offshore Technology Conference, 1st May, Houston, Texas.

Newcomb, D. and Birgisson, B. (1999). *Measuring in Situ Mechanical Properties of Pavement Subgrade Soils*. National Academy Press.

Ou, C. (2006). *Deep Excavation: Theory and Practice*. Taylor & Francis.

PLAXIS (2008). *Plaxis 2D Version 8.6 Reference Manual*. Plaxis bv.

Puzrin, A., Alonso, E., and Pinyol, N. (2010). *Geomechanics of Failures*. Springer Netherlands.

Rahman, M., Wang, J., Deng, W., and Carter, J. (2001). A neural network model for the uplift capacity of suction caissons. *Computers and Geotechnics*, 28(4):269–287.

Randolph, M. F. (2002). Analysis of suction anchor capacity in clay. Offshore Technology Conference, 6-9 May, Houston, Texas.

Randolph, M. F. and Gourvenec, S. (2009). *Offshore Geotechnical Engineering*. Spon (E & F).

Robertson, P. and Mayne, P. (1998). *Geotechnical Site Characterization*. Taylor & Francis.

Schmid, W. E. (1969). *Penetration of objects into the ocean bottom (the state of the art)*. Clearinghouse for Federal Scientific and Technical Information.

Senpere, D. and Auvergne, G. A. (1982). Suction anchor piles - a proven alternative to driving or drilling. Offshore Technology Conference, 3rd May, Houston, Texas.

Supachawarote, C., Randolph, M., and Gourvenec, S. (2004). Inclined pull-out capacity of suction caissons. The Fourteenth International Offshore and Polar Engineering Conference, 23-28 May, Toulon, France.

Tjelta, T. I. (2001). Suction piles: Their position and application today. The Eleventh International Offshore and Polar Engineering Conference, 17-22 June, Stavanger, Norway.

Tjelta, T. I., Guttormsen, T. R., and Hermstad, J. (1986). Large-scale penetration test at a deepwater site. Offshore Technology Conference, 5th May, Houston, Texas.

Tjelta, T. l. (1994). Geotechnical aspects of bucket foundations replacing piles for the europipe 16/11-e jacket. Offshore Technology Conference, 2nd May, Houston, Texas.

United States Naval Facilities Engineering Command (1982). Soil mechanics: Design manual 7.01. Revalidated by change 1st September 1986. Naval Facilities Engineering Command, 200 Stovall Street, Alexandria, Virginia 22322-2300.

Vryhof Anchors B.V. (2010). Anchor manual 2010. Online; accessed 10th February 2015 from http://www.vryhof.com/anchor_manual.pdf.

Yang, S. L., Grande, L. O., Qi, J. F., and Feng, X. L. (2003). Excessive soil plug and anti-failure mechanism of bucket foundation during penetration by suction. The Thirteenth International Offshore and Polar Engineering Conference, 25-30 May, Honolulu, Hawaii, USA.

Appendix A

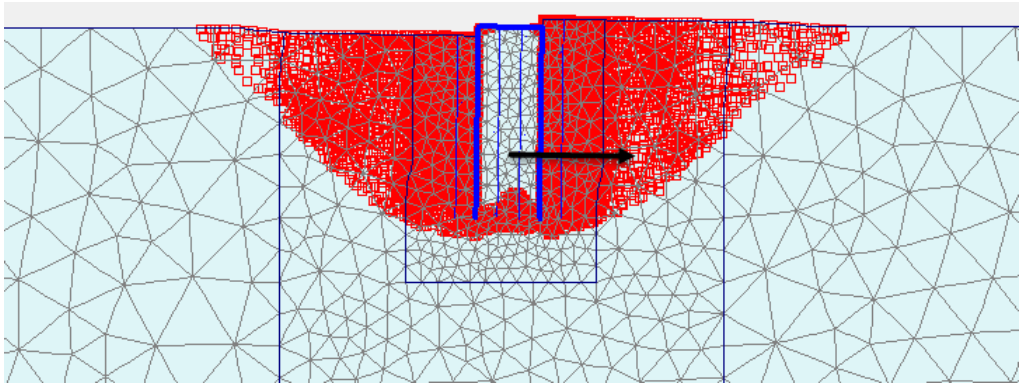

Fig. A.1 Failure mechanism when load angle is 0 degrees

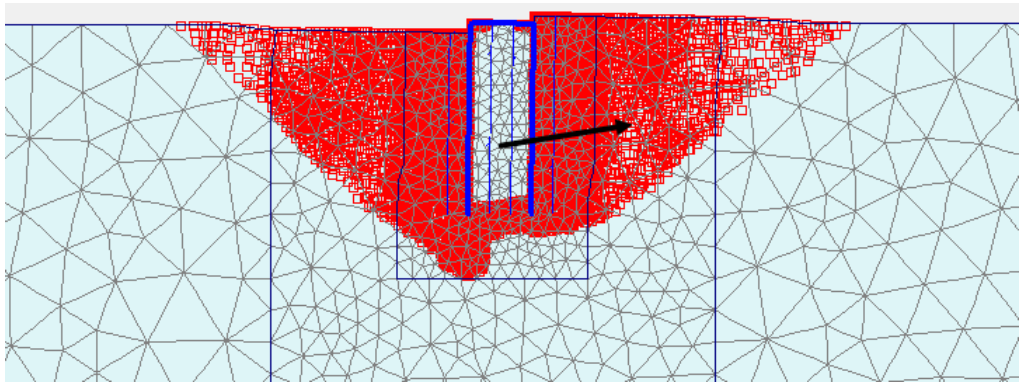

Fig. A.2 Failure mechanism when load angle is 10 degrees

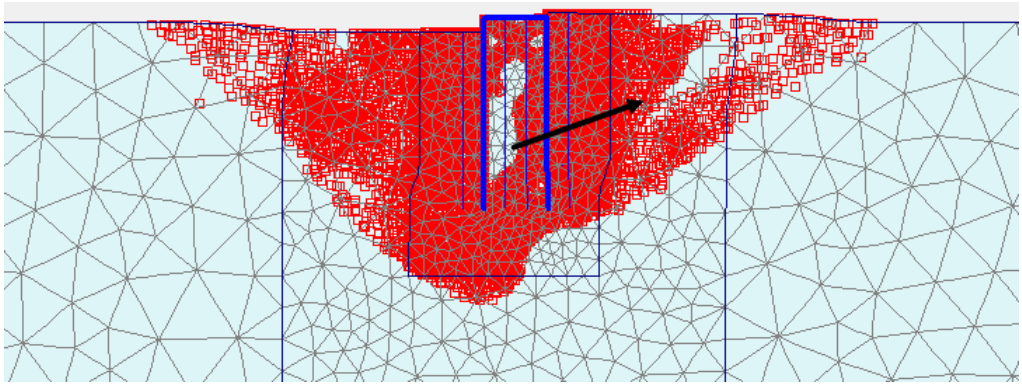

Fig. A.3 Failure mechanism when load angle is 20 degrees

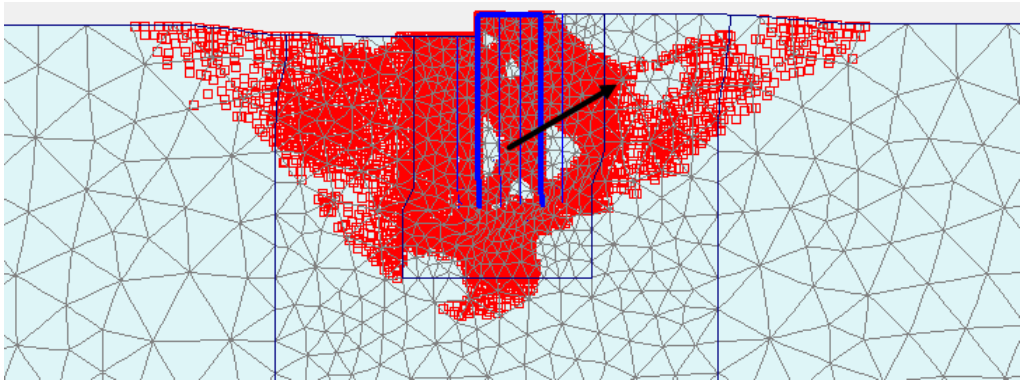

Fig. A.4 Failure mechanism when load angle is 30 degrees

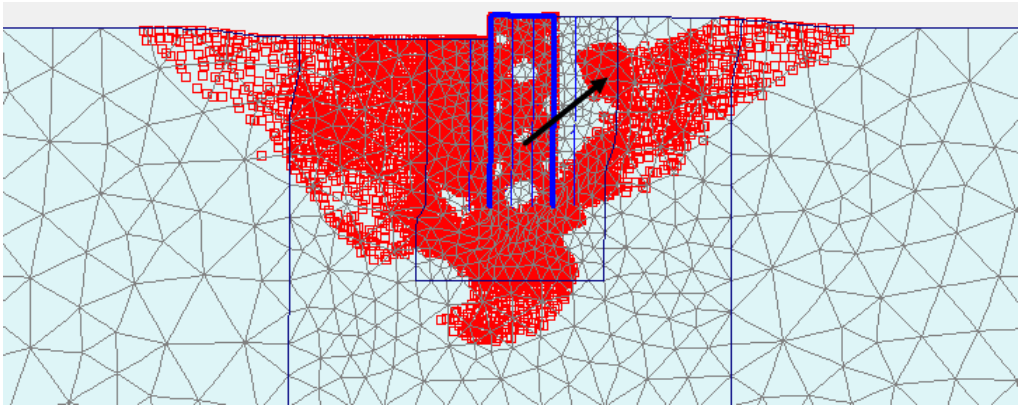

Fig. A.5 Failure mechanism when load angle is 40 degrees

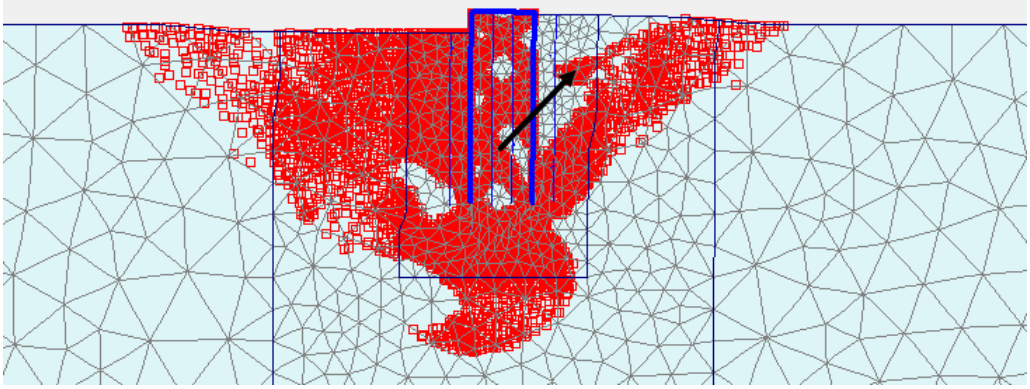

Fig. A.6 Failure mechanism when load angle is 50 degrees

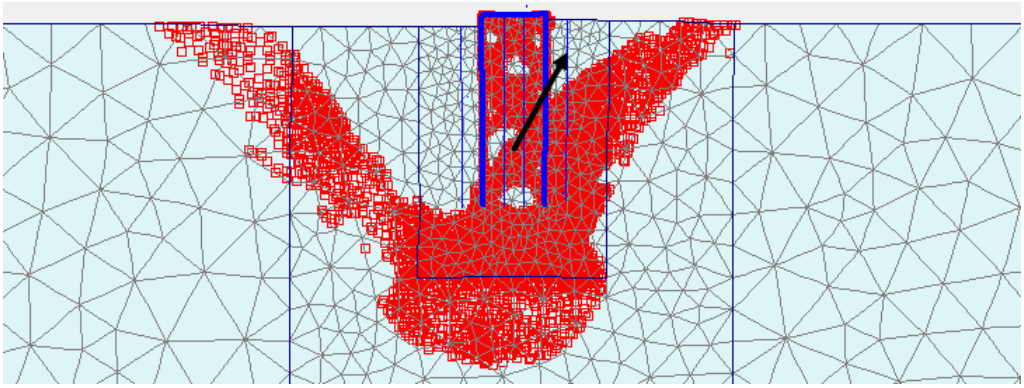

Fig. A.7 Failure mechanism when load angle is 60 degrees

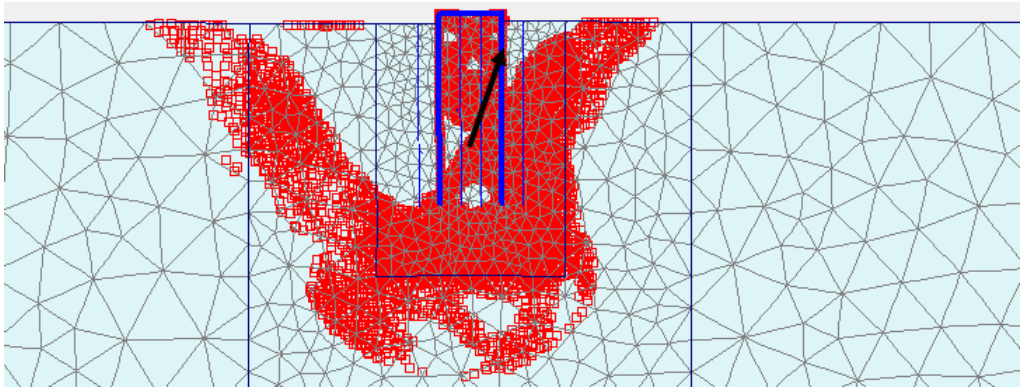

Fig. A.8 Failure mechanism when load angle is 70 degrees

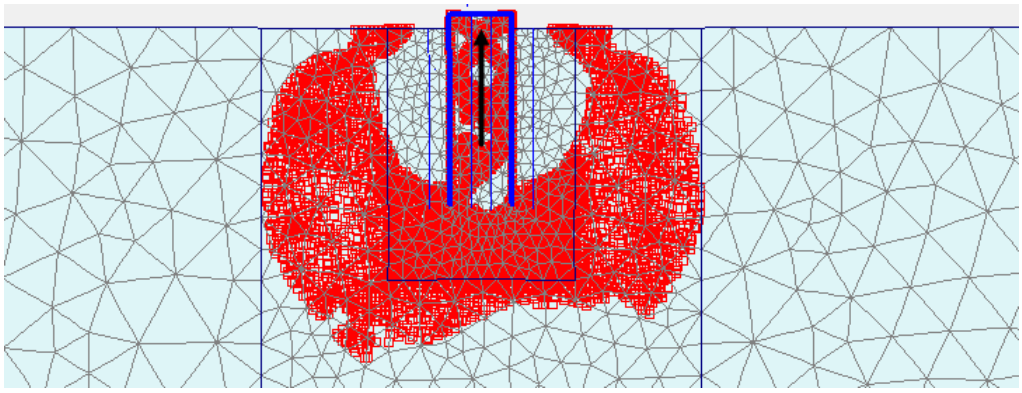

Fig. A.9 Failure mechanism when load angle is 90 degrees